Abstract

Title of Dissertation: Investigating Aerosol Effects on Clouds, Precipitation and Regional Climate in US and China by Means of Ground-based and Satellite Observations and a Global Climate Model

Feng Niu, Doctor of Philosophy, 2011

Directed by: Dr. Zhanqing Li
Department of Atmospheric and Oceanic Science/ Earth System Science Interdisciplinary Center

Aerosols affect climate by scattering/absorbing radiation and by acting as cloud condensation nuclei (CCN) or ice nuclei (IN). One of the least understood but most significant aspects of climate change is the aerosol effect on cloud and precipitation. A hypothesis has recently been proposed that, in addition to reducing cloud effective radius and suppressing precipitation, aerosols may also modify the thermodynamic structure of deep convective clouds and lead to enhanced precipitation when complex thermodynamic processes are involved. Taking advantage of the long-term and extensive ground-based observations at the US Department of Energy's Atmospheric Radiation Measurement (ARM) Southern Great Plains (SGP) site, we thoroughly tested such a hypothesis and provide direct evidence of it. Moreover, the hypothesis is also supported by analysis of

satellite-based observations over tropical regions from multiple sensors in the A-Train satellites constellation. Extensive analyses of the long-term ground-based and large-scale data reveal significant increases in rain rate or frequency and cloud top heights with increasing aerosol loading for mix-phase deep convective clouds, decreases rain frequency for low liquid clouds, but little impact on cloud height for liquid clouds. Rigorous tests are conducted to investigate any potential artifacts and influences of meteorological conditions.

Large-scale circulation patterns and monsoon systems can be changed by scattering and absorption of solar radiation by aerosols. By means of model simulations with the National Center for Atmospheric Research Community Climate Model (NCAR/CCM3), we found that the increase of aerosol loading in China contributes to circulation changes, leading to more frequent occurrence of fog events in winter as observed from meteorological records. The increase in atmospheric aerosols over China heats the atmosphere and generates a cyclonic circulation anomaly over eastern-central China. This circulation anomaly leads to a reduction in the influx of dry and cold air over that area during winter. Weakening of the East Asian winter monsoon system may also contribute to these changes. All these changes favor the formation and maintenance of fog over this region.

The MODerate resolution Imaging Spectroradiometer (MODIS) aerosol products used in the above studies are validated using ground-based measurements from the Chinese Sun Hazemeter Network (CSHNET). Overall, substantial improvement was found in the current version of aerosol products relative to the previous one. At individual sites, the improvement varies with surface and atmospheric conditions.

INVESTIGATING AEROSOL EFFECTS ON CLOUDS, PRECIPITATION AND REGIONAL CLIMATE IN US AND CHINA BY MEANS OF GROUND-BASED AND SATELLITE OBSERVATIONS AND A GLOBAL CLIMATE MODEL

By

Feng Niu

Dissertation submitted to the Faculty of the Graduate School of the
University of Maryland, College Park, in partial fulfillment
of the requirements for the degree of
Doctor of Philosophy
2011

Advisory Committee:
Professor Zhanqing Li, Chair
Professor Russell Dickerson
Professor Robert Hudson
Professor Rachel Pinker
Professor Sumant Nigam

Acknowledgements

I would like to express my sincerest gratitude to Prof. Zhanqing Li for his unending patience, support, guidance and advice. He grants me enormous freedom to explore my own research interest. His insightful guidance leads me to the right way. In addition, he provides me various and abundant opportunities to prepare myself for future career, such as attending conferences, giving presentations, reviewing journal papers. These experiences cannot be learned in any classroom. I am sincerely thankful to Prof. Daniel Rosenfeld, Dr. Jiwen Fan and Dr. Yangang Liu for invaluable and heuristic suggestions on my work. I am also indebted to Prof. Kwon-Ho Lee, Dr. Can Li, Maureen Cribb and Pat Kablick for their kindly help.

I would like to thank Prof. Russell Dickerson, Prof. Robert Hudson, Prof. Sumant Nigam and Prof Rachel Pinker for agreeing to serve as my committee member.

My thank goes out to all the faculty and staff of AOSC and ESSIC for their help. I also need to thank my friends at the University of Maryland, especially Haifeng Qian, Xiaolei Niu and Tianle Yuan for five delightful years of my life.

I would like to thank my parents and my sister from the bottom of my heart. They are an unending source of love, encouragement and support. I owe a great deal to my wife, Fei, whose understanding and support allow me fully dedicated in my research.

I appreciate the Atmospheric System Research (ASR) program for providing data used in Chapter 2. The computing resources supporting the work in Chapter 5 are provided by the NCAR Computer & Information Systems Laboratory.

Table of Contents

List of Tables

List of Figures

List of Abbreviations

AOT – Aerosol Optical Thickness

ARM – Atmospheric Radiation Measurement (now ASR program)

ASR – Atmospheric System Research

CBH – Cloud Base Height

CBT – Cloud Base Temperature

CN – Condensation Nuclei

CCN – Cloud Condensation Nuclei

CTH – Cloud Top Height

CTT – Cloud Top Temperature

CWV – Column Water Vapor

GCM – Global Circulation Model

IN – Ice Nuclei

LWP – Liquid Water Path

LTSS – Lower Tropospheric Static Stability

P – Surface Pressure

SGP – Southern Great Plains

T – Surface Temperature

Chapter 1 : Introduction

1.1 General Overview

Aerosols play important roles in the atmospheric hydrological cycle and the Earth's radiation budget, with many possible mechanisms that are not yet fully understood. The most direct interaction between aerosol and climate occurs through scattering and absorption of shortwave and thermal radiation in the atmosphere, referred to the "aerosol direct effect." This effect could change the radiation budget at the surface or top of atmosphere (TOA), atmospheric stability, convection, and the large-scale circulation pattern [*Ramanathan et al*., 2001].

Aerosols also affect clouds and precipitation in other ways. By acting as cloud condensation nuclei, they influence cloud albedo, convective energy, lifetime and precipitation efficiency. They are often referred to as "aerosol indirect effects." These effects could enhance cloud albedo by reducing cloud particle size (Twomey effect), reduce precipitation by further suppressing collision and coalescence processes, and increase cloud life time by suppressing precipitation [*Twomey*, 1959; *Albrecht*, 1989]. Absorbing aerosols may heat the air, resulting in the evaporation of cloud particles (semi-direct effect) [*Graßl*, 1979; *Hansen et al*., 1997; *Ackerman et al*., 2000].

These effects remain poorly understood. In this chapter, we will discuss some of these important aerosols effects.

1.2 Aerosol Direct Effects

1.2.1 Aerosol Effects on Radiation

The direct effects of aerosols reduce the amount of solar radiation reaching the surface, and therefore lead to less heat available for evaporating water and energizing convection [*Ramanathan et al*., 2001]. The global mean surface direct radiative forcing is approximately -4 ~ -2W m^{-2}. This value is much higher over the tropical Indian Ocean region (Fig. 1.1). Even larger reduction was found over the tropical biomass burning regions (~100 Wm^{-2}) [*Li*, 1998], and heavy polluted regions in China (Fig. 1.2) [*Li et al*., 2007a; 2010; *Xia et al*., 2007]. Overall, the reduced surface radiation must be balanced by the reduction in surface evaporation and therefore reduce rainfall. The increase in aerosol loading will eventually spin down the hydrological cycle [*Ramanathan et al*., 2001].

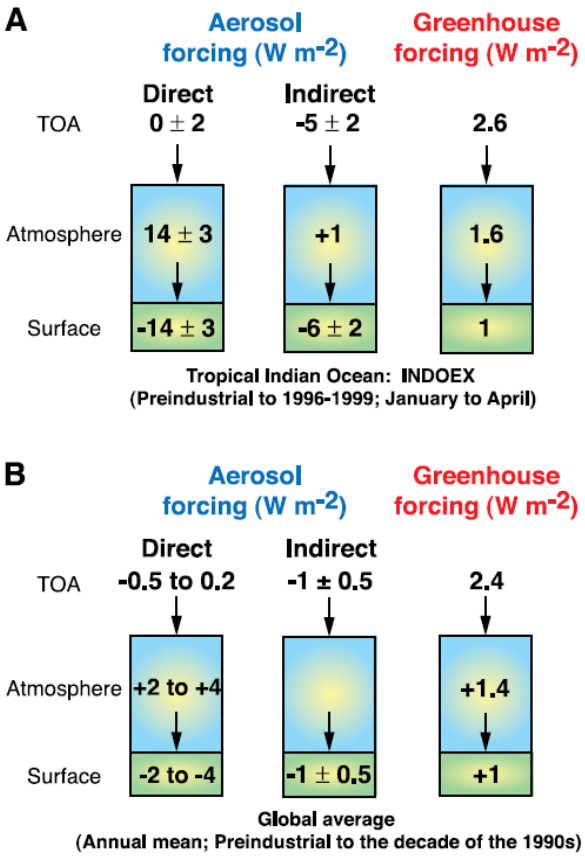

Fig. 1.1. Comparison of anthropogenic aerosol forcing with greenhouse forcing. (A) The indo-Asian region. The greenhouse forcing was estimated from the NCAR community climate model with an uncertainty of 20%. (B) Same as above, but for global and annual average conditions. [*Ramanathan et al.*, 2001].

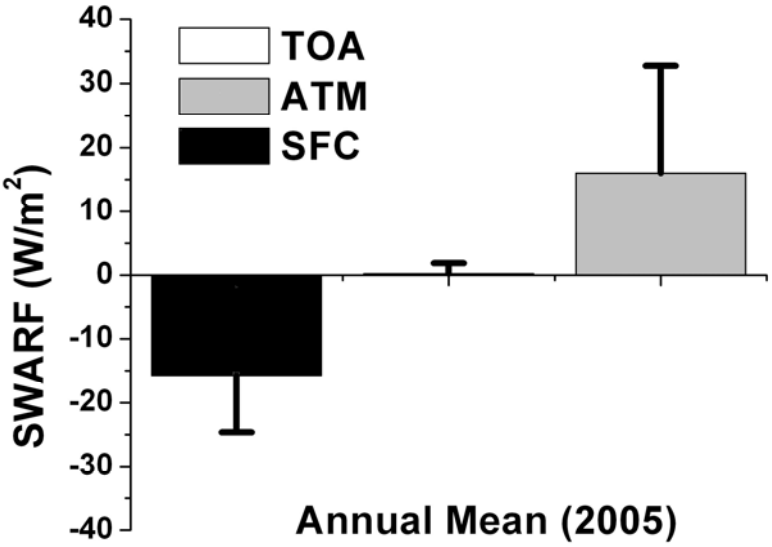

Fig. 1.2. Annual mean shortwave aerosol radiative forcing (SWARF) over China. [*Li et al*., 2010].

A fraction of radiation is absorbed by aerosols, mainly carbonaceous and mineral aerosols, leading to heating of the air above the surface. This changes the atmospheric lapse rate, stabilizes the low atmosphere and suppresses the generation of convective clouds [*Koren et al*., 2004]. Heating due to absorbing aerosols may even evaporate cloud particles, further reducing cloud cover. *Koren et al*. [2004] showed that for scattered cumulus, the cloud cover was reduced from 38% in clean conditions to 0% during the presence of heavy smoke (optical depth of 1.3) over the Amazon region during the biomass burning season. Large precipitation reductions of 10 to 50% in the Mediterranean region, the Middle East, and the eastern Sahel were found to be caused by reduction of evaporation from the Mediterranean Sea by pollution from northern and eastern Europe using model simulations [*Lelieveld et al*., 2002].

1.2.2 Aerosol Effects on Atmospheric Circulation

An increase in atmospheric aerosol loading can also affect atmospheric circulation, and influence global and regional climate. Recent simulations using global circulation models (GCMs) [*Held et al*., 2005; *Paeth and Feichter*, 2006] found a substantial cooling that was strongest in the NH, with a consequent southward shift of the Inter-Tropical Convergence Zone (ITCZ) and the associated tropical rainfall belt. *Rotstayn and Lohmann* [2002] even suggested that aerosol effects might have contributed to the Sahelian droughts of the 1970s and 1980s. *Ramanathan et al*. [2005] found that convection was suppressed due to increased stability resulting from black carbon heating. However, heating of lofted absorbing aerosols could strengthen the Asian summer monsoon circulation and cause a local increase in precipitation [*Lau et al.*, 2006b], although the global reduction of evaporation is needed to compensate for aerosol radiative cooling at the surface [*Miller et al*., 2004b]. Estimates of dust inputs to the Chinese Loess Plateau indicate that higher and more variable dust concentrations occurred during glacial periods compared with interglacial, and high dust loadings frequently preceded decreases in winter sea surface temperature of the North Pacific Ocean during glacial periods [*Zhang et al*., 2002]. The dust-induced thermal contrast changes between the Eurasian continent and the surrounding oceans were proposed to trigger or modulate a rapidly varying or unstable Asian winter monsoon circulation, with a feedback to reduce the dust emission from its sources. These results indicate that aerosols could greatly impact regional and global climate on a variety of time scales, from decadal to millennial.

High aerosol loadings are found over China due to increased industrial emissions as a result of the economic growth in recent decades, which may have great impacts on climate. Many associated phenomena have been observed. For example, both solar radiation and evaporation have decreased in China, with solar radiation decreasing by 3.1 W/m^2 and evaporation decreasing by 39 mm per decade. This finding implies that aerosol loading has increased drastically, as inferred from surface radiation measurements [*Luo et al*., 2002]. This may attribute to the finding by *Xu et al*., [2006] that the summer air temperature in Southern central China has significantly decreased, particularly in terms of daily maximum temperature. Meanwhile, the rainfall in this area has increased but decreased in northern China. The surface wind speed associated with the East Asian monsoon has significantly weakened in both winter and summer in the recent three decades [*Xu et al*., 2006].

Several investigators have studied the potential impacts of aerosols on these changes in recent several decades. *Menon et al.* [2002] found that adding aerosols with strong absorption (SSA=0.85) causes a cooling of the surface and warming of the atmosphere. The warmer air strengthened the convection over southern China, resulting in increased rainfall over the south but reduced rainfall over the north. Studies using regional climate models [*Giorgi et al.*, 2002, *Qian et al*., 2003] showed that aerosols induce a negative TOA radiative forcing. For example for anthropogenic sulfate, the forcing varies spatially from -1 to $-8W/m^2$ in the winter to -1 to $-15W/m^2$ in the summer, inducing a surface cooling in the range of -0.1 to -0.7 K. *Xu et al*. [2006] proposed that cooling of the land due to the increase of aerosols reduces the temperature difference between the land and ocean, and decreases the strength of the summer monsoon.

Therefore, less water vapor can be transported to the north of China, which causes decreased cloud cover and rainfall there. These studies indicate that aerosol radiative effects over Asian regions are so large that they could greatly impact the regional climate.

1.3 Aerosol Effects on Clouds and Precipitation

1.3.1 Important Aerosol Indirect effects

1) Twomey effect

The Twomey effect refers to enhanced cloud albedo due to more but smaller cloud particles in a cloud with constant liquid water path [*Twomey*, 1959]. However, the cloud liquid water path may also be affected by aerosols. For example, large amount of pollution entrained into clouds was found to decrease liquid water path (LWP) and cause a reduction in the observed cloud reflectance [*Jiang et al.*, 2002; *Brenguier et al*., 2003; *Twohy et al*., 2005]. Since the cloud albedo depends on both the cloud particle size and cloud LWP, the Twomey effect may be enhanced or partially cancelled by the change of LWP caused by pollution. The studies above highlight the difficulty of devising observational studies that can isolate the albedo effect from other effects (e.g., meteorological variability, cloud dynamics) that influence LWP and therefore cloud radiative forcing.

One example of observational evidence of the Twomey effect is ship tracks [*Ferek et al*., 1998]. It has also been supported with ample evidence from satellite [*Nakajima et al.*, 2001; *Liu et al.*, 2003], ground and in-situ observations [*Feingold et al.*, 2003; *Penner et al.*, 2004]. *Nakajima et al*. [2001] found a positive correlation between

column aerosol number concentration and column cloud droplet concentration over oceans from the Advanced Very High Resolution Spectro-Radiometer (AVHRR) instrument. They also found an increase in shortwave reflectance of low-level, warm clouds with increasing column aerosol number concentration, while LWP remained unmodified. The positive correlation between an increase in cloud reflectance and an enhanced ambient aerosol concentration has been confirmed by other studies [*Brenguier et al*., 2000a,b; *Rosenfeld et al*., 2002]. The radiative forcing due to the Twomey effect in the context of liquid water clouds, is estimated to be –0.7 [–1.1, +0.4] Wm^{-2} [*IPCC 2007*] (Table 1.1).

On the other hand, *Yuan et al*. [2007] surveyed the relationship between MODIS-derived cloud droplet size and aerosol optical depth over many parts of the world. While the vast majority show negative correlations, positive relations were found over the coasts of the Gulf of Mexico and South China Sea during summer when a plentiful water supply combined with strong convection provide a more favorable condition for droplets to grow.

2) Lifetime effect

Aerosols are hypothesized to increase cloud life time since increased concentrations of smaller cloud droplets lead to decreased drizzle production and reduced precipitation efficiency [*Albrecht*, 1989]. However, fully explaining this effect turns out to be a great challenge due to the influence of other factors.

Delays in the onset of precipitation can increase the cloud lifetime and thereby increase cloud cover. *Kaufman et al*. [2005] conclude from satellite observations that the

aerosol indirect effect is likely primarily due to an increase in cloud cover, rather than an increase in cloud albedo. Using solar measurements from Aerosol Robotic Network sites around the globe, *Kaufman and Koren* [2006] showed an increase in cloud cover with increasing aerosol column concentration. In contrast, model results of *Lohmann et al*. [2006] associate the increase in cloud cover with differing dynamic regimes and higher relative humidities that maintain higher aerosol optical depths.

The suppression of precipitation does not necessarily lead to the increase of cloud lifetime. A study using a two-dimensional single cloud model and three-dimensional large eddy simulations (LES) showed that a change in aerosol concentration from very clean to very polluted conditions does not lead to an increase in cloud lifetime, even though precipitation is suppressed [*Jiang et al*., 2006]. They proposed that the small changes in cloud lifetime are due to competing effects of precipitation suppression and enhanced evaporation of more and smaller cloud droplets, with the latter tending to dominate in these shallow clouds.

Aerosol size concentration or composition may also play a very important role in determining whether precipitation is suppressed or not. *Feingold et al*. [1998] and *Wurzler et al*. [2000] showed that cloud processing could either lead to an increase or decrease in precipitation, depending on the size and concentration of activated CCN. Giant sea salt nuclei may override the precipitation suppression effect of the large number of small pollution nuclei [*Feingold et al*., 1999; *Rosenfeld et al*., 2002]. A reduction of 20 to 60% in marine cloud droplet number concentrations and an increase in precipitation were predicted because of the present of sea salt [*Gong and Barrie*, 2003].

The scientific understanding of the aerosol lifetime effect is inadequate. The simulated cloud lifetime effect in a subset of models used in the IPCC report varies between -0.3 and -1.4Wm^{-2} [*IPCC 2007*].

3) Semi-direct effect

Absorbing aerosols have drawn increasing attention in recent years. The semi-direct effect refers to the absorption of solar radiation by soot, hence heating the air mass, increasing static stability relative to the surface [*IPCC 2007*], and causing evaporation of cloud droplets. Recent observations in the Amazon [*Koren et al*., 2004] provide the first observational support for a reduction in cloud fraction due to smoke (absorbing) aerosol at a continental site. *Feingold et al*. [2005] used large eddy simulations of smoke-cloud interactions to demonstrate the relative importance of various factors responsible for cloud suppression in the biomass burning regions of the Amazonia. The study showed that the vertical distribution of smoke aerosol in the convective boundary layer is crucial to determining whether cloudiness is reduced; smoke aerosol emitted at the surface in a daytime convective boundary layer may reduce or increase cloudiness, whereas smoke aerosol residing in the layer where clouds tend to form will reduce cloudiness. On the other hand, the reduction in surface latent and sensible heat fluxes associated with biomass burning is sufficient by itself to substantially reduce cloudiness. Studies over South Asia [*Bollasina et al.*, 2008; *Bollasina and Nigam*, 2009] suggested more complex effects of aerosols on the Indian summer monsoon system. Absorbing aerosols were found responsible in May for a decrease of cloudiness over India, which leads, above all, to reduced precipitation, increased shortwave radiation at the surface, and heating of the

dry ground. The anomalous heating of the land-surface in May increases thermal contrast between land and ocean, leading to enhanced monsoon rainfall in June and July over both local and remote regions.

The semi-direct effect of aerosols could be superimposed on other aerosol effects, and have much more complex impacts on clouds. *Koren et al*. [2008] showed that clouds will be strongly invigorated in the low aerosol optical thickness (AOT) range due to the invigoration effect (discuss later), but inhibited again in the high AOT range due to the semi-direct effect of absorbing aerosols. *Kaufman and Koren* [2006] showed that when aerosol absorption is strong, cloud cover does not increase much with increasing AOD, though a general increase in cloud cover with an increase in the aerosol column concentration was found.

4) Other aerosol effects

Other aerosol effects include the thermodynamic effect and the glacial effect. The thermodynamic effect refers to a delay in freezing by the smaller droplets causing super-cooled clouds to extend to colder temperatures. The glaciation effect refers to an increase in ice nuclei resulting in a rapid glaciation of a super-cooled liquid water cloud due to the difference in vapor pressure over ice and water [*IPCC 2007*].

The radiative forcing of these effects and their influence on precipitation are summarized in Table 1.1. We can see that our understanding of these indirect effects is generally very low, leading to substantial uncertainties in our study of climate change.

Table 1.1. a) Overview of the different aerosol indirect effects and their sign of the net radiative flux change at the top of the atmosphere (TOA); b) Overview of the different aerosol indirect effects and their implications for the global mean net shortwave radiation at the surface, F_{sfc} (Columns 2-4) and for precipitation (Columns 5-7). [*IPCC 2007*].

Effect	Cloud Types Affected	Process	Sign of Change in TOA Radiation	Potential Magnitude	Scientific Understanding
Cloud albedo effect	All clouds	For the same cloud water or ice content more but smaller cloud particles reflect more solar radiation	Negative	Medium	Low
Cloud lifetime effect	All clouds	Smaller cloud particles decrease the precipitation efficiency thereby presumably prolonging cloud lifetime	Negative	Medium	Very low
Semi-direct effect	All clouds	Absorption of solar radiation by absorbing aerosols affects static stability and the surface energy budget, and may lead to an evaporation of cloud particles	Positive or negative	Small	Very low
Glaciation indirect effect	Mixed-phase clouds	An increase in IN increases the precipitation efficiency	Positive	Medium	Very low
Thermodynamic effect	Mixed-phase clouds	Smaller cloud droplets delay freezing causing super-cooled clouds to extend to colder temperatures	Positive or negative	Medium	Very low

Effect	Sign of Change in F_{sfc}	Potential Magnitude	Scientific Understanding	Sign of Change in Precipitation	Potential Magnitude	Scientific Understanding
Cloud albedo effect	Negative	Medium	Low	n.a.	n.a.	n.a.
Cloud lifetime effect	Negative	Medium	Very low	Negative	Small	Very low
Semi-direct effect	Negative	Large	Very low	Negative	Large	Very low
Glaciation indirect effect	Positive	Medium	Very low	Positive	Medium	Very low
Thermodynamic effect	Positive or negative	Medium	Very low	Positive or negative	Medium	Very low

1.3.2 How can Aerosols Suppress Rainfall

Aerosols also suppress precipitation through indirect effects [*Albrecht*, 1989]. Direct evidence demonstrates that urban and industrial air pollution can completely shut off precipitation from clouds over large areas as shown in Fig. 1.3 [*Rosenfeld*, 2000]. The study revealed reduced cloud particle size and suppressed precipitation originating from major urban areas and from industrial facilities (black lines in Fig.1.3). However, cloud particle sizes of clouds forming in clean regions increase gradually with height and exceed the precipitation threshold to generate rain (red lines). The reduced cloud particle

size due to high aerosol loading is also confirmed by in-situ observations from airplanes [*Andreae*, 2004].

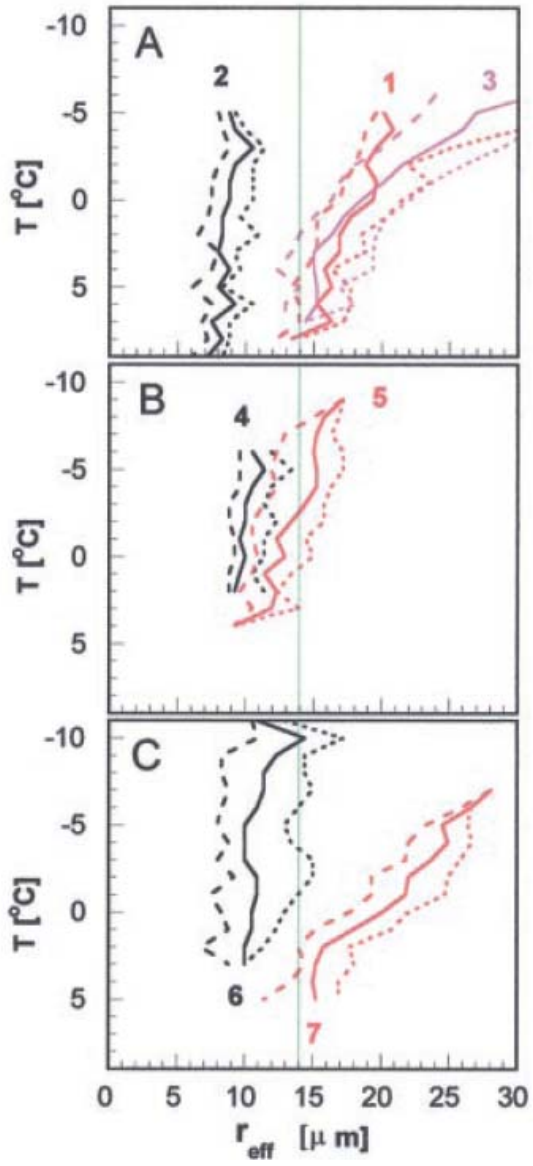

Fig. 1.3. Satellite-retrieved effective radius of particles near the top of deep convective clouds at various stages of their vertical development, as a function of the cloud top temperature. Red and black lines are for clouds forming in clean and polluted regions, respectively. The vertical green line is the 14μm precipitation threshold. The numbers along the red and black lines indicate different regions over southeastern Australia. Please refer to [*Rosenfeld et al*., 2000] for more details.

1.3.3 How can Delayed Warm Rain Processes Enhance Rainfall

In clean conditions, cloud particles may grow large enough to start raining before reaching the freezing level through diffusion, collision and coalescence processes. However, in polluted conditions, the warm rain process may be completely shut down by suppressing collision and coalescence. Without the downdraft of rainfall, smaller cloud particles may reach to higher levels to start ice processes, leading to more latent heat released aloft and stronger convection as demonstrated in Fig. 1.4.

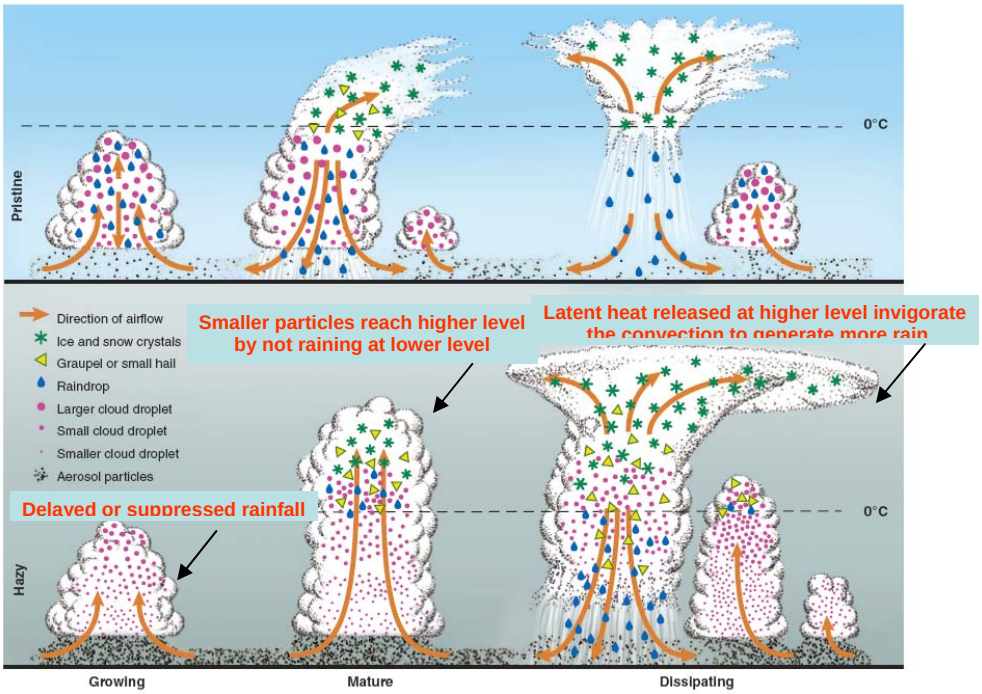

Fig. 1.4. Evolution of deep convective clouds developing in the pristine (top) and polluted (bottom) atmosphere. [*Rosenfeld et al.*, 2008].

An in-situ observation of such an effect is provided by *Andreae et al*. [2004] (Fig. 1.5). The cases “Blue” and “Green” in Fig. 1.5 are clean clouds over the ocean and the Amazon. Two Pyro cases are the most extreme form of smoky clouds. The others except

for two Thai cases are the clouds with moderate concentrations of smoke. Substantial differences in the cloud drop size D_L appear in the clouds. D_L at 1000m above cloud base is only 10 μm for extremely polluted cases, compared to 25 μm for clean cases. Precipitation occurs at 1000-1500m above cloud base for clean cases. But the precipitation threshold is over 6000m for pyro-clouds. The observation in Thailand on 2 May 1998 shows that the cloud has to exceed 6400m to produce warm rain under smoky conditions. It is also found that once clouds reach above the freezing level, they become quiet vigorous and intensive showers, thunderstorms, and sometimes hail occurs. These observations indicate that the shift of onset of precipitation to a higher level under polluted conditions leads to formation of ice hydrometers and more vigorous convection.

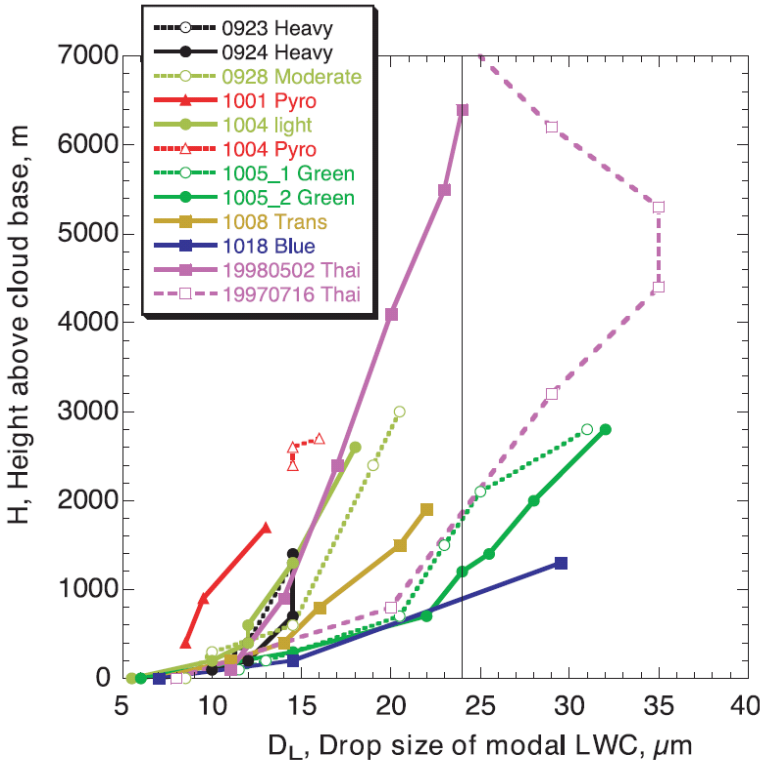

Fig. 1.5. The dependence of drop diameter on distance above cloud base for different regimes. The vertical line at D_L = 24 μm denotes the onset of warm rain. [*Andreae et al.*, 2004].

A theoretical explanation of such effect is provided by [*Rosenfeld et al.*, 2008]. This was done by using a parcel model to demonstrate the buoyancy changes for different conditions. The effect was shown to greatly increase the buoyancy of air parcels as shown in Fig. 1.6. The cloud base is at 22°C and 960hPa. The zero buoyancy reference is the standard parcel: liquid water saturation, immediately precipitating all condensates without freezing (vertical line b). The buoyancy of the following scenarios is shown: (a) suppressing rainfall and keeping all condensed water load, without freezing; (b) precipitating all condensed water, without freezing; (c) precipitating all condensates, with freezing at T < –4°C; (d) Suppressing precipitation until T = –4°C, and then freezing and precipitating all condensed water above that temperature. The released static energy (J /kg) with respect to reference line b is denoted by the numbers. In scenario d, when not allowing precipitation, the condensed water needs about 415J/kg to reach to the freezing level (d1). Freezing all the cloud water would warm the air and add thermal buoyancy by an amount that would almost exactly balance the condensate load (d2). When the ice hydrometeors precipitate from a parcel, it becomes more positively buoyant because of its reduced weight (d3), so that the released convective energy at the top of the cloud (d4) is the largest in the four scenarios. It is about 1000 J/kg larger than the case that cloud water is precipitated as rain below the –4°C isotherm and as ice above that level. This model result suggests that the suppression of warm rain but enhancement of cold rain processes can greatly invigorate the convection.

The importance of cloud top and base heights in determining the strength of the invigoration effect can also be seen in this figure. If cloud particles never reach above the freezing level, there will be no invigoration effect. If the cloud base is high, for

example, very close to the freezing level, there will not be very much liquid water to release latent heat since the distance for cloud particles to grow before reaching the freezing level is too short.

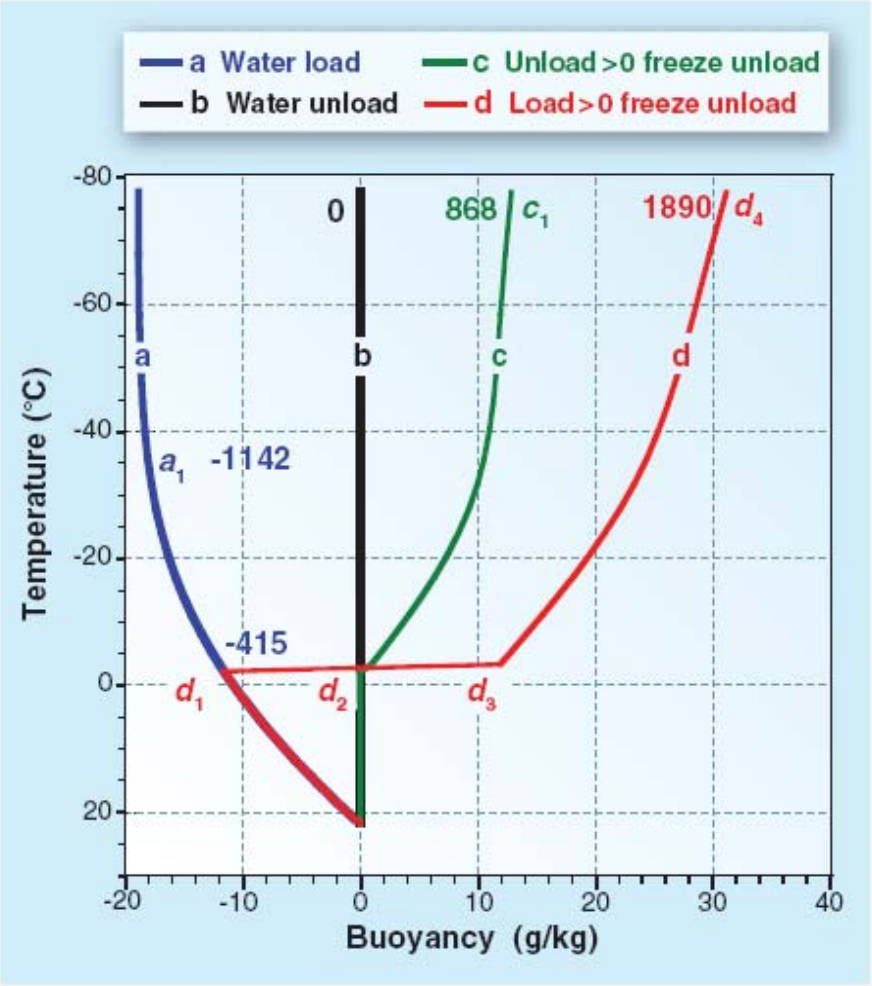

Fig. 1.6. The buoyancy of an unmixed adiabatically raising air parcel. Numbers near lines show the released static energy (J/kg). [*Rosenfeld et al*., 2008].

Satellite observations provide some evidence of such an effect. *Koren et al.* [2005, 2008] examined cloud top heights derived from MODIS, and found they are systematically increased by aerosols over the Atlantic Ocean and Amazon basin region. *Lin et al.* [2006] employed multiplatform satellite data over the Amazon basin, and found

that aerosol optical thickness from MODIS is positively correlated with the cloud top height, cloud fraction and rainfall amount. A midweek increase of afternoon convective rainfall during summer over the southeast U.S. was found using long-term TRMM-derived precipitation data [*Bell et al.*, 2007], and is considered to be associated with the weekly cycle of the aerosol concentration.

These observational results are supported by many cloud-resolving model studies [*Khain et al.*, 2005; *Fan et al.*, 2007; *Van den Heever and Cotton*, 2007; *Wang*, 2005]. The studies also showed that precipitation may be enhanced. *Tao et al.* [2007] and *Khain et al*. [2008] summarized these modeling studies. They found relative humidity, wind shear, and radiative cooling may play important roles in the process.

1.4 Three Pathways by Which Aerosols Influence Climate

The above mentioned complex aerosol effects are summarized as three pathways by which aerosols impact climate: radiative, microphysical, and thermodynamic (Fig.1.7). Through the radiative pathway, aerosols redistribute solar energy within the atmosphere. For example, sulfate aerosols mostly scatter solar radiation back to the space, cool the surface, increase atmospheric stability, and suppress precipitation. However, absorbing aerosols, such as black carbon, may heat the atmosphere, strengthen the local convection, and enhance precipitation, or stabilize the atmosphere and suppress precipitation, depending on aerosol layer height. Absorbing aerosols are also found to be able to evaporate clouds particles, reduce cloud fraction, and suppress precipitation. Through the microphysical pathway, aerosols reduce cloud particle size and enhance cloud albedo,

which is the well-known Twomey effect. The thermodynamic pathway is more complicated. Aerosols suppress warm rain processes but enhance cold rain processes, leading to more latent heat released a loft and stronger convection. However, much smaller cloud particles may also delay freezing, resulting in more super-cooled water at higher altitude. These three pathways may occur simultaneously, making aerosol effects too complicated to predict their net effect. Understanding how aerosols influence radiation, clouds and climate through these three pathways and how they interact with each other will greatly advance our understanding of the human impact on climate.

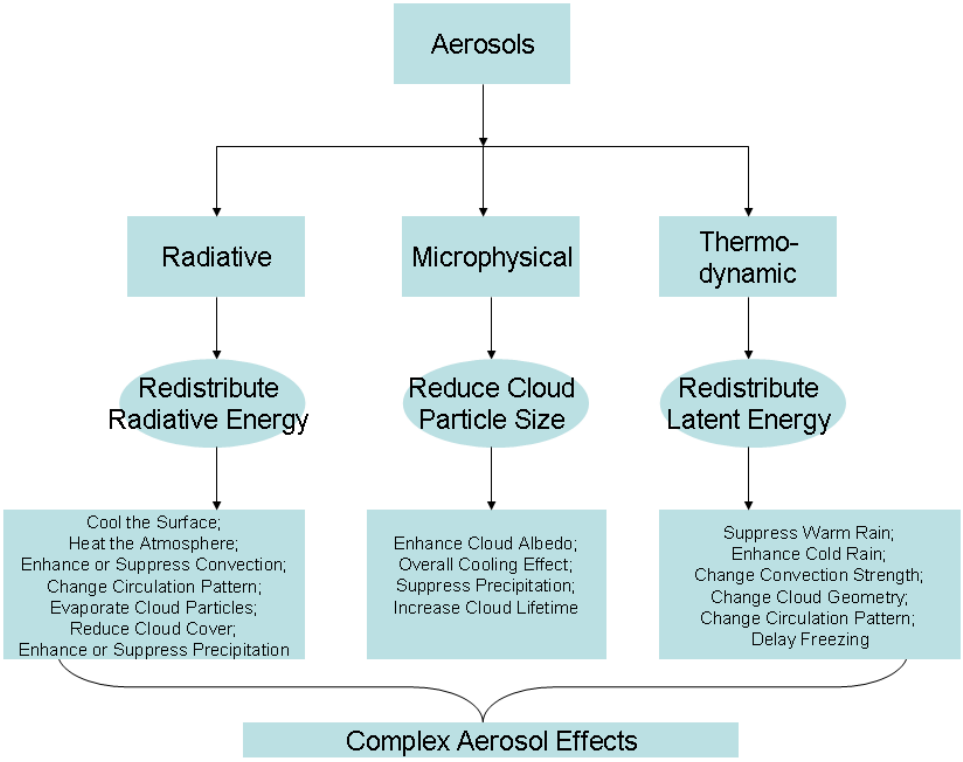

Fig. 1.7. Three major pathways by which aerosols influence climate.

1.5 Objective of Current Study

One of the objectives of this study is to investigate how aerosols influence clouds and precipitation. We want to examine whether the invigoration effect of aerosols has significant and systematical influences on clouds and precipitation. Impacts of aerosols on regional climate by changing circulation patterns are also an important aspect of this study, especially focusing on the region encompassing China. Validation of the aerosol products used in the above two studies is also necessary. The following methods are used:

a) Ground based observations

Ground-based observations have great advantages for studying aerosol indirect effects. Aerosols beneath clouds are most likely to be transported into clouds to serve as CCN or IN, making ground-based observations useful for the studies of aerosols-cloud interactions. Ground-based observations usually have long records of meteorological conditions, important to sort out conditions that may influence cloud development differently.

Unlike satellite observations which can only observe aerosols in cloud-free regions in the daytime, ground-based observations can be conducted continuously. For example, *Feingold et al.* [2003] used ground-based remote sensors to measure the aerosol indirect effect. They measured cloud droplet size with cloud radar, aerosol extinction at 355nm under clouds using Raman Lidar and LWP using a microwave radiometer. Results suggest that aerosols associated with maritime sources tend to have a stronger effect on clouds than aerosols associated with northwesterly trajectories. This kind of work can not be done without simultaneous ground-based observations of aerosols and clouds.

b) Satellite remote sensing

Satellite remote sensing plays an important role in the study of aerosol indirect effects, especially for studies covering a large land region or oceans. However, studies using satellite data face several challenges, such as uncertainties from retrievals and cloud contaminations. To gain more confidence in the data we used, validation of the aerosol products from MODIS will also be conducted in our study. Satellites measure aerosol (represented by optical thickness or other aerosol indices) in cloud-free regions and the cloud droplet size or reflectance in adjacent cloudy regions. It is unclear to what extent the path-integrated aerosol is representative of the aerosol entering the clouds. Meteorological variables are not easy to get from satellite data, which may obscure the evidence of aerosol effects, because of potential correlations between meteorological conditions and aerosols. Therefore, in the study of aerosol indirect effects using satellite data, the main efforts will be devoted to eliminate possible influences other than those of aerosols.

c) Climate modeling

Aerosol effects on regional and global circulations are mainly examined by modeling studies. Over the Asian region, local weather is largely controlled by large scale monsoon systems, including East Asian summer and winter monsoons. Therefore, a global circulation model is used to study how aerosols may influence these systems. We will focus on aerosol direct effect on large scale circulations although these effects may also impact circulations by changing cloud reflectance or other feedbacks. Some findings from observations will be explained using model results or reanalysis data.

We will use the above methods to study aerosol effects on clouds, precipitation and regional climate in the following chapters. Chapter 2 will focus on the study of

aerosol effects on clouds and precipitation using ground-based observations, while Chapter 3 will focus on the same topic but using satellite observations. Validation of the latest MODIS aerosol product over China will be provided in Chapter 4. Aerosol effects on the East Asian winter monsoon system will be discussed in Chapter 5. Chapter 6 will summarize the results and conclusions.

Chapter 2 : Long-term Impacts of Aerosols on Cloud and Precipitation at the SGP Site

2.1 Introduction

Many observations of the invigoration effect, which is hypothesized to suppress warm rain processes, invigorate convection, and enhance ice rain processes [*Andreae et al*., 2004; *Rosenfeld et al*., 2008], have been reported [*Koren et al*., 2005,2008; *Lin et al*., 2006]. However, most of the studies only provided indirect evidence of the effect instead of in-depth analysis of the processes involved and evidence of such processes. For instance, in most of the studies, increases of cloud top heights were considered as evidence of the invigoration effect. However, cloud top heights were not constrained in these studies, making it unclear if the increases of cloud top heights were caused by ice processes. Cloud base temperature was not considered either although it is also an important factor determining if clouds are invigorated. These limitations stem from the dearth of cloud geometry information, that weaken their findings as the evidence of the aerosol invigoration effect. Furthermore, in most studies using satellite observations, multi-layer clouds were not excluded. Such clouds would have much less connection with aerosols than single-layer clouds developed from the boundary layer. For example, for convective clouds with separate cirrus on the top of them, changes of cloud top heights cannot be considered as evidence of the invigoration effect.

Here, we report results from 10-year ground-based observations of aerosols, clouds, precipitation, and other important meteorological variables at the central observation facility of the Department of Energy's Atmospheric Radiation Measurements (ARM, now the Atmospheric Science Research) program. Using these extensive data sets,

we will try to tackle these problems and provide much more convincing evidence of the aerosol invigoration effect.

2.2 Ten-year Data Sets at the SGP Site

Since its inception in late 1980s [*Stokes and Schwartz*, 1994; *Ackerman and Stokes*, 2003], ARM has provided the most extensive, accurate and long-term observations attempting to understand and parameterize atmospheric processes in climate models. ARM has developed and operated a suite of state-of-the-art passive and active instruments measuring cloud hydrometeors and geometry [*Liljegren*, 1994; *Clothiaux et al*., 2000].

Continuous observations are conducted at the Central Facility site over the SGP, the largest and most extensive climate research field site in the world. It consists of in-situ and remote-sensing instrument clusters arrayed across approximately 55,000 square miles (143,000 square kilometers) in north-central Oklahoma. The heart of the SGP site is the heavily instrumented central facility located on 160 acres of cattle pasture and wheat fields southeast of Lamont, Oklahoma (Fig. 2.1). The instruments throughout the site automatically collect data on surface and atmospheric properties, routinely providing data to the Site Data System, linked by high-speed communications to the ARM Archive and Data Center. The SGP was chosen as the first ARM field measurement site for several reasons including its relatively homogeneous geography and easy accessibility, wide variability of climate cloud type and surface flux properties, and large seasonal variation in temperature and specific humidity. In fiscal year 2003, DOE designated all ARM sites to be a national user facility known as the ARM Climate Research Facility.

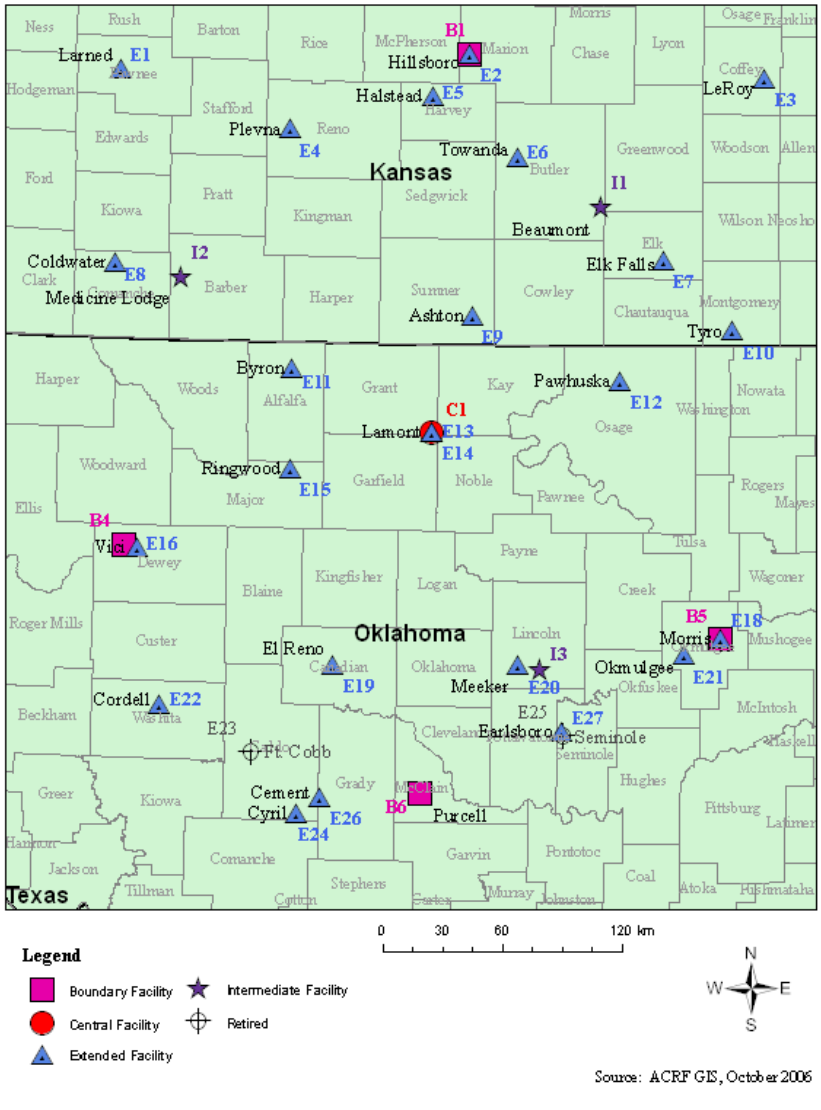

Fig. 2.1. Location of the Central Facility site over the SGP (red dot C1). The map is from the ARM website (www. Arm.gov).

Employed in this study are the continuous observations of cloud, precipitation and atmospheric variables acquired at the Central Facility site over the SGP. They include aerosol number concentration (CN), LWP, cloud top and base heights, precipitation and meteorological variables. The most unusual data that are rarely available elsewhere are the cloud boundaries obtained from the ARSCL (Active Remote Sensing of Clouds).

ARSCL is a value-added product derived for the period from 1999 to the present by combining data from millimeter cloud radars, laser ceilometers, microwave radiometers, and micropulse lidars [*Clothiaux et al*., 2000]. LWP is obtained from a microwave radiometer that measures column-integrated liquid water based on the microwave emissions of liquid water molecules at specific frequencies [*Liljegren*, 1994]. The CN number concentration is provided by TSI condensation particle counter. And meteorological data are provided by a surface meteorological observation station. Two sets of precipitation data of complimentary merits are utilized that were acquired by the Surface Meteorological Observation System Instruments (SMOS) and the Carbon dioxide Flux Measurement System (CO2FLX). Both use a tipping bucket rain gauge. SMOS data are available over the 10-y period, while the CO2FLX data are from 2003 to 2008. The minimum value in the 30-min data used in this study is 0.254 mm from the SMOS, and 0.1 mm from the CO2FLX. Because of the higher initial detection value, the SMOS only detected 58% of rain events that the CO2FLX did, and often also was delayed by 1.5 hours on average, if a rain event lasted 1.5 hours or longer. As such, we matched the rain data from the CO2FLX with CN measurements made just prior to rain onset, while the CN data are 1.5 hours earlier for the SMOS. To get profiles of vertical velocity and air temperature, the analysis data specifically generated for ARM SGP site from the European Centre for Medium-range Weather Forecasting (ECMWF) model are used. These data consist of hourly profiles of atmospheric variables calculated on a 60-level grid ranging from the surface to 10hPa. The hourly data are interpolated to a half hour resolution to match the observational data. Table 2.1 summarizes these data and associated instruments or data sources.

Both the height and temperature of cloud base and top are employed. The two are related to each other using atmosphere temperature profiles form ECMWF data. Cloud top temperature (CTT) helps identify the phase of a cloud, while cloud base height indicates the likelihood of interaction between cloud and aerosol measured near the ground. If CTT is below -4°C, it is considered as having the potential to be a mix-phase cloud. To better identify the aerosol effect, only single-layer clouds are considered, as multi-layer clouds are often associated with more complex weather systems.

Table 2.1. Data used in the study and associated instruments or data sources.

Instruments or data sources	**Variables**
Microwave radiometer	Liquid water path Column water vapor
SMOS[1]	Rain rate in 30 minutes Surface temperature Surface pressure Surface wind speed and directions
Rain gauge from CO2FLX[2]	Rain amount in 30 minutes
ARSCL[3]	Cloud top and base heights
TSI condensation particle counter	CN number concentration CCN over a limited period
ECMWF[4]	Atmosphere temperature profile Vertical velocity profiles

[1]*Surface Meteorological Observation System, ten years of data*
[2]*Carbon Dioxide Flux Measurement System, six years of data*
[3]*Active Remote Sensing of Clouds*
[4]*European Centre for Medium-range Weather Forecasting*

2.3 Analysis and Results

2.3.1 CN as a Proxy of CCN

Aerosols near the surface are quantified as CN number concentrations in this study. The number concentration, size distribution and composition of the CN determine the CCN number concentration as a function of supersatuation. The CCN number concentration is an important factor determining the cloud droplet size distribution at cloud base, which controls most of the evolution of cloud droplet size distribution and thus the onset of precipitation. Since there is no long-term observation of CCN, CN is used as a proxy of CCN. In a statistical study, CN has been used as a proxy of CCN at a certain supersaturation value. *Andreae et al*., [2009] showed a very good correlation between CN and $CCN_{0.4}$ obtained at different locations. Using three years of CN and CCN data acquired at the SGP site from 2006 to 2008, we correlate CN number concentrations with CCN number concentrations at supersaturation in the range of 0.35%-0.45% and superimpose the result on the Andreae's plot [*Andreae et al.*, 2009] as shown in Fig. 2.2. Note that CCN are measured at several discrete supersaturation levels, instead of a fixed supersaturation level in the data set. The data are grouped in six bins with an interval of $1000/cm^3$ based on the CN number concentration. The CCN number concentration is averaged in each bin. The bars denote the standard deviation (STD) of the CN and CCN number concentrations in each bin. The relative large STD of the CCN number concentration are partly due to the coarse bin of the CN number concentration ($1000/cm^3$) and the large range of supersaturation (0.35%-0.45%). A good correlation with R^2=0.96 is found and it is consistent with the Andreae's result. Therefore, CN

number concentrations are used as proxies of CCN number concentrations in the study. To avoid the influence of precipitation scavenging, CN measurements made 1.5 hours prior to the onset of rain are employed.

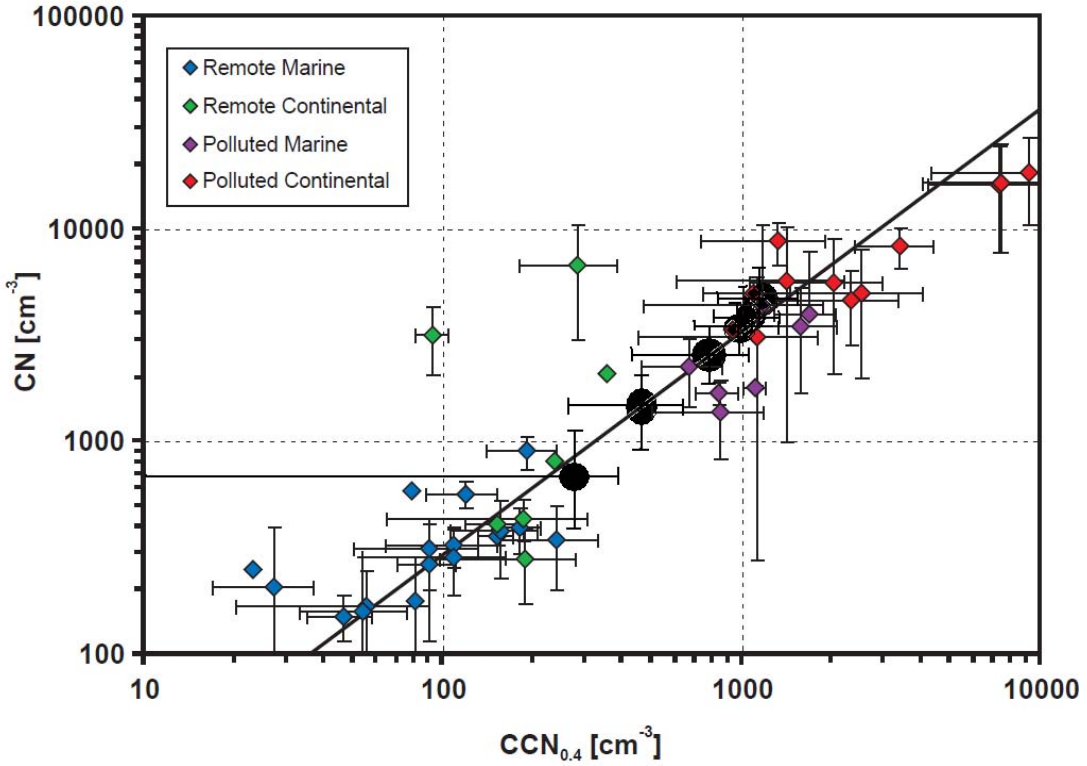

Fig. 2.2. Relation between observed CN and CCN number concentrations superimposed on the Andreae's plot [*Andreae et al*., 2009] (black dots, R^2=0.96). CN and CCN number concentrations are measured at the SGP site from 2006 to 2008.

2.3.2 Significant Impacts of Aerosols on Clouds and Precipitation

We focus on the deep convective clouds with warm bases and with tops reaching the freezing level, because these clouds were found to be the most sensitive to aerosol effects on their invigoration [*Rosenfeld et al*., 2008; *Lee et al*., 2010]. Respectively, our analyses were carried out by differentiating clouds according to their base and top temperatures, phase, and season. To warrant statistical significance, all cloud events

occurred over the 10-year period are analyzed. We divide clouds into six bins based on CN, and the averaged CTT is calculated in each bin. Fig. 2.3 shows the CTT as a function of the CN for mix-phase and liquid clouds for all-season and summer-only. Note that convective clouds are dominant in the summer and much more frequent than in the other seasons. For mix-phase clouds, CTT decreases significantly with increasing CN. The rate of decrease is much greater in summer than in all seasons, presumably because of prevailing convective clouds during the summer. Both trends are statistically significant at the 95% confidence level. By stark contrast, the cloud top temperature for liquid clouds is virtually invariant at all with the CN for both all-season and summer-only measurements.

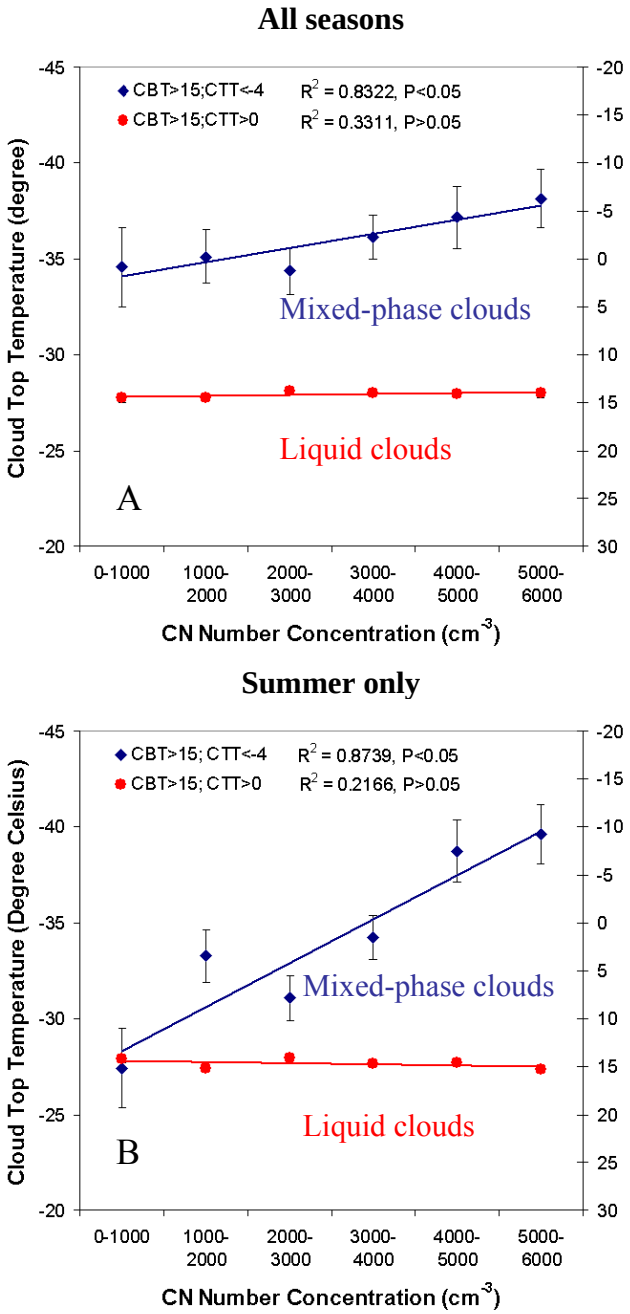

Fig. 2.3. Cloud top temperature as a function of CN for single layer clouds with base temperature higher than 15°C in all seasons (A) and summer (B). Clouds with CTT<-4°C (blue) and >0°C (red) are shown separately. The right y-axes are for clouds with CTT>0°C. The CTT is in a reverse order. The standard errors are too small to be shown as error bars for clouds with CCT>0°C (red). There are totally 3545 and 1567 samples in all seasons and summer, respectively.

With ample measurements, the finding confirms the theory of the aerosol invigoration effect:

1) *aerosol fuels the vertical development of clouds;*

2) *the effect is only significant for mixed-phase clouds, not for water clouds*.

The first is not only supported by the decreasing trend of CTT with CN, but also by the fact that the effect only occurs for clouds of low bases for which aerosols in the boundary layer have a chance to interact with clouds. Fig. 2.4 shows the dependence of cloud thickness on the CN for three ranges of cloud base height (CBH) in summer and all seasons. Clouds with lower bases tend to be more strongly invigorated, due to not only the fact that aerosols in the boundary layer have higher chance to interact with these clouds, but also the longer distance for cloud particles to grow before freezing, leading to more latent heat released. As the CBH increases, cloud development is gradually decoupled from the influence of ground-level CN, as one would expect. For CBH greater than 2km, the dependence disappeared virtually completely. Since the measurements were taken under exactly the same conditions except for different CBH, no other factor than the aerosol invigoration can explain the dependence of cloud thickness on the CN.

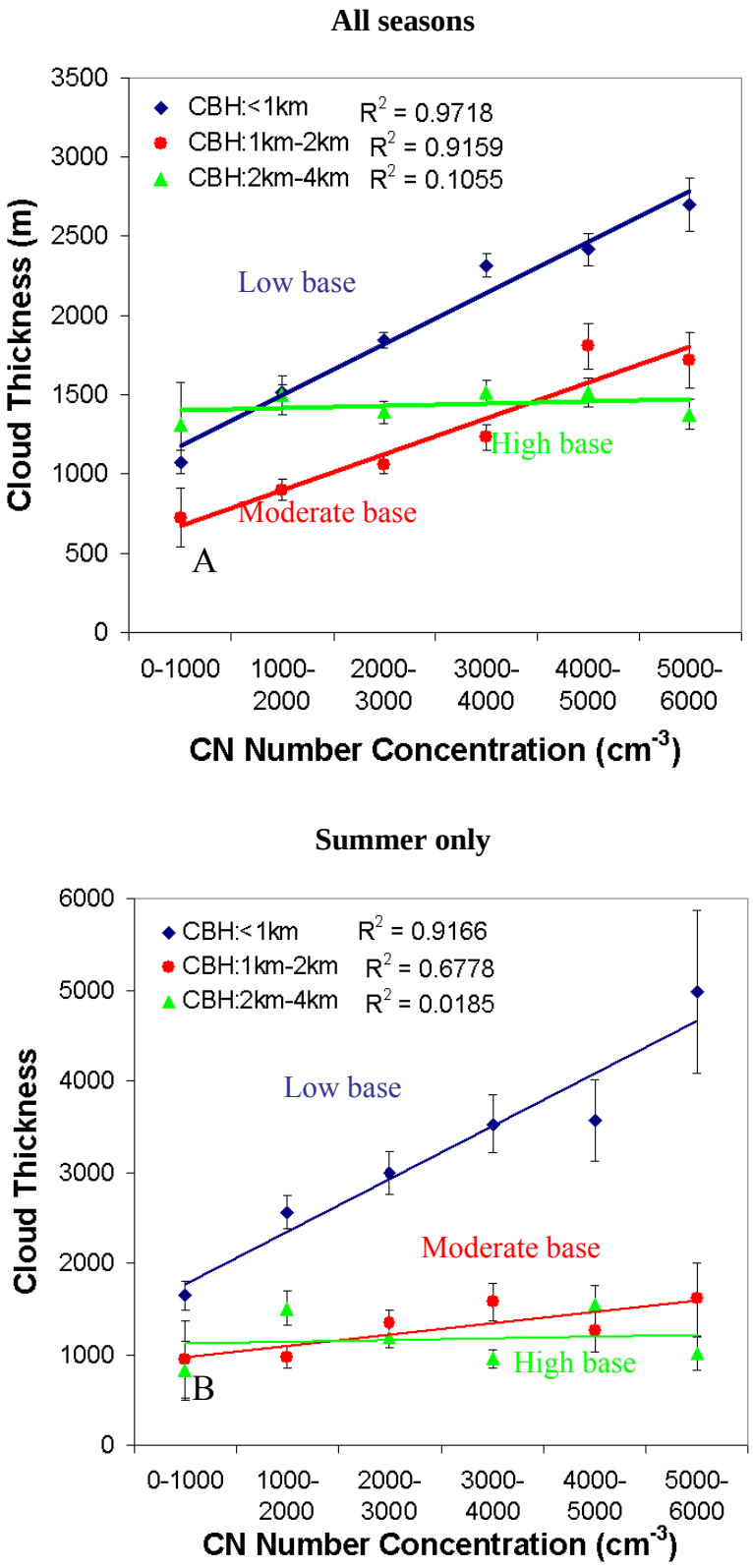

Fig. 2.4. Changes in cloud thickness with the CN for single-layer clouds with different cloud base heights in all seasons (A) and summer (B).

The finding that the invigoration effect deepens clouds is further reinforced by an analysis of cloud height frequency for clouds with base height <1km. Clouds in all seasons are divided into six bins based on cloud top heights. In each bin, clouds are further divided into six subsets based on CN. The frequency of occurrence of different cloud top heights under different CN conditions is calculated in each subset. As shown in Fig. 2.5, as the CN increases, deep clouds occurred more frequently but shallow clouds occurred less frequently. The transition took place right around the freezing level of 3.3km as determined from the 10-y ARM data.

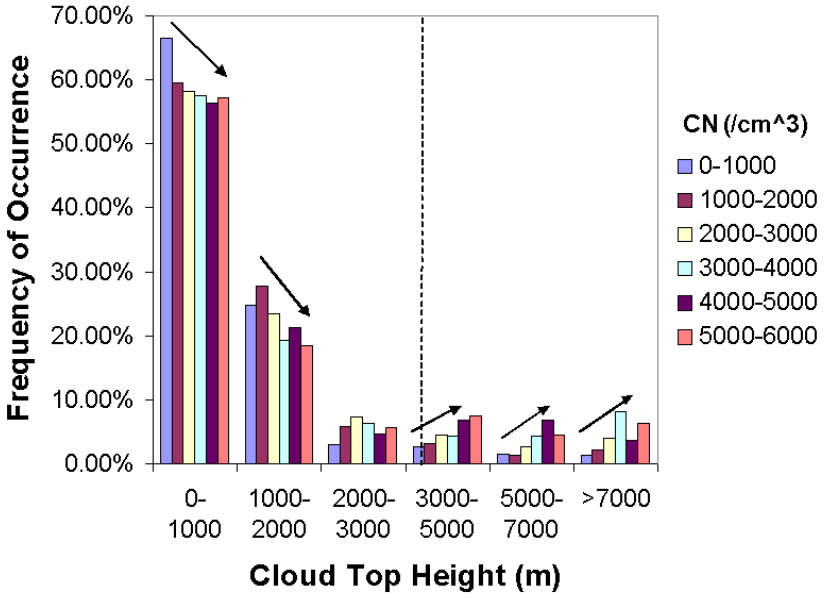

Fig. 2.5. Frequency of occurrence of cloud top heights for cloud with base height<1km in all seasons.

The importance of ice processes in the invigoration effect as hypothesized in [*Rosenfeld et al*., 2008] is also supported by observations as shown in Fig. 2.6. This figure was generated under the constraints: CBH <1km and Cloud top height (CTH) >3.3 km to assure interaction with aerosols and ice processes are involved. Rainy and non-

rainy conditions were separated. Cloud top heights in rainy conditions were measured in the first half hour of rain. Note that the CTH increases only in rainy conditions but decreases in non-rainy conditions (Fig. 2.6). This is because the unloaded water (no rain occurrences) needs extra buoyancy to be held inside clouds (Fig. 1.6). The latent heat release can just balance the weight of crystals when they reach above the freezing level. After that, only if ice particles precipitate, the clouds will be invigorated due to reduced weights and melting cooling below the freezing level [*Rosenfeld et al*., 2008].

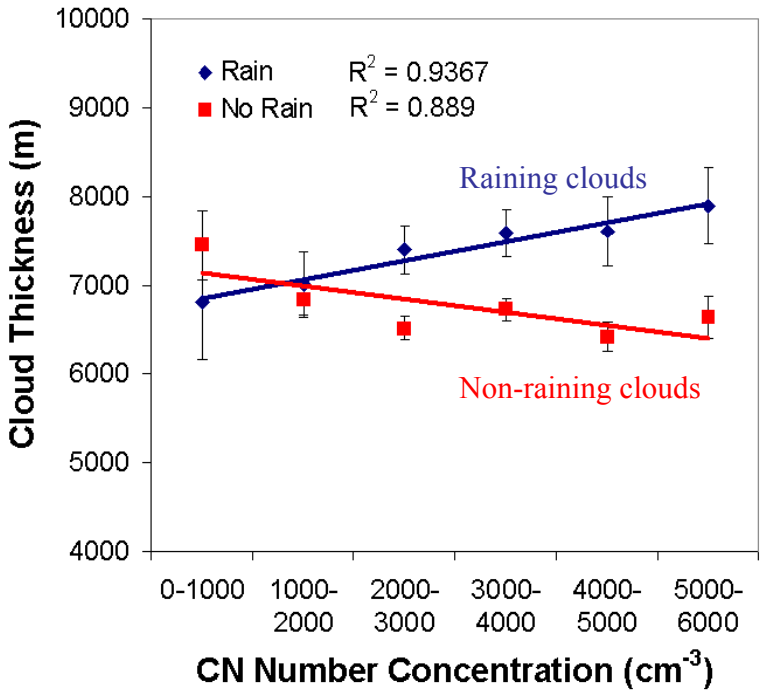

Fig. 2.6. Changes in cloud thickness under rainy (blue) and non-rainy (red) conditions for clouds with CTH>3.3km and CBH<1km.

The significant impact of aerosols on cloud vertical development is likely to induce changes of precipitation with aerosol loading as well. To test this, we examine the influence of aerosols on rainfall frequency by counting all individual raining events occurred over the 10-y period and associate them with CN measured 1.5 hours prior to

the onset of rain. Rainfall frequency is calculated as the ratio of the number of rain events divided by the total number of observations, regardless of rain duration. Since rainfall frequency is highly influenced by meteorological conditions, we correlate several important meteorological variables with rainfall frequency as shown in Fig. 2.7. These meteorological variables include LWP, column water vapor, surface temperature, surface pressure, wind speed, and LTSS. Rainfall frequency is highly correlated with LWP and column water vapor but has no significant correlation with other meteorological conditions. LWP and column water vapor are actually correlated with each other too. These results indicate the primary driving force in rainfall is column water vapor and LWP (as a consequence). Therefore, we group the data into three categories based on LWP to constrain the influence of liquid water and also to roughly define three cloud types: deep, moderate and shallow. The constraint in LWP (LWP<0.4mm, 0.4mm<LWP<0.8mm, and LWP>0.8mm) as shown in Fig. 2.8 therefore defines three regimes. The rainfall frequency in these regimes agrees with expectation that rainfall frequency is highest for clouds with LWP>0.8mm and lowest for clouds with LWP<0.4mm. In each regime, there exists the aerosol effect on rainfall frequency. The rainfall frequency increases with increasing CN for high LWP, but decreases for low LWP. Both regression relations are statistically significant at a 95% confidence level. For moderate LWP, their relation appears to be neutral.

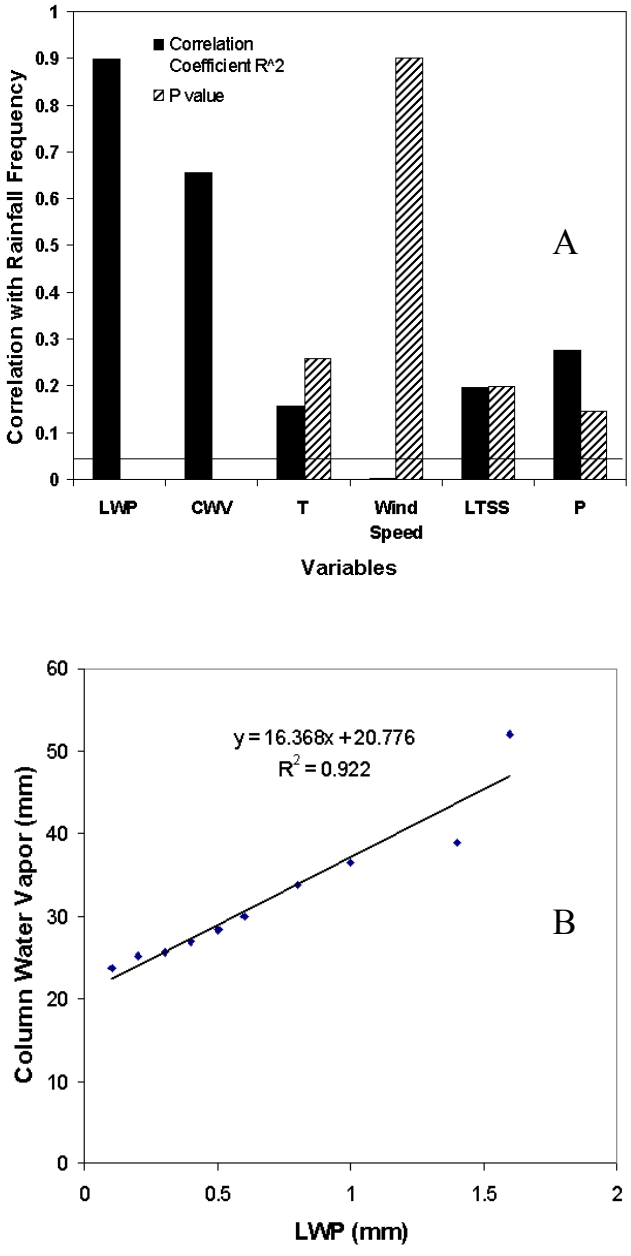

Fig. 2.7. A) Correlation coefficient R^2 and P value between rainfall frequency, several meteorological conditions and cloud properties (liquid water path, column water vapor (CWV), surface temperature (T), wind speed, low-troposphere static stability (LTSS), and surface pressure(P)). B) Correlation between LWP and column water vapor.

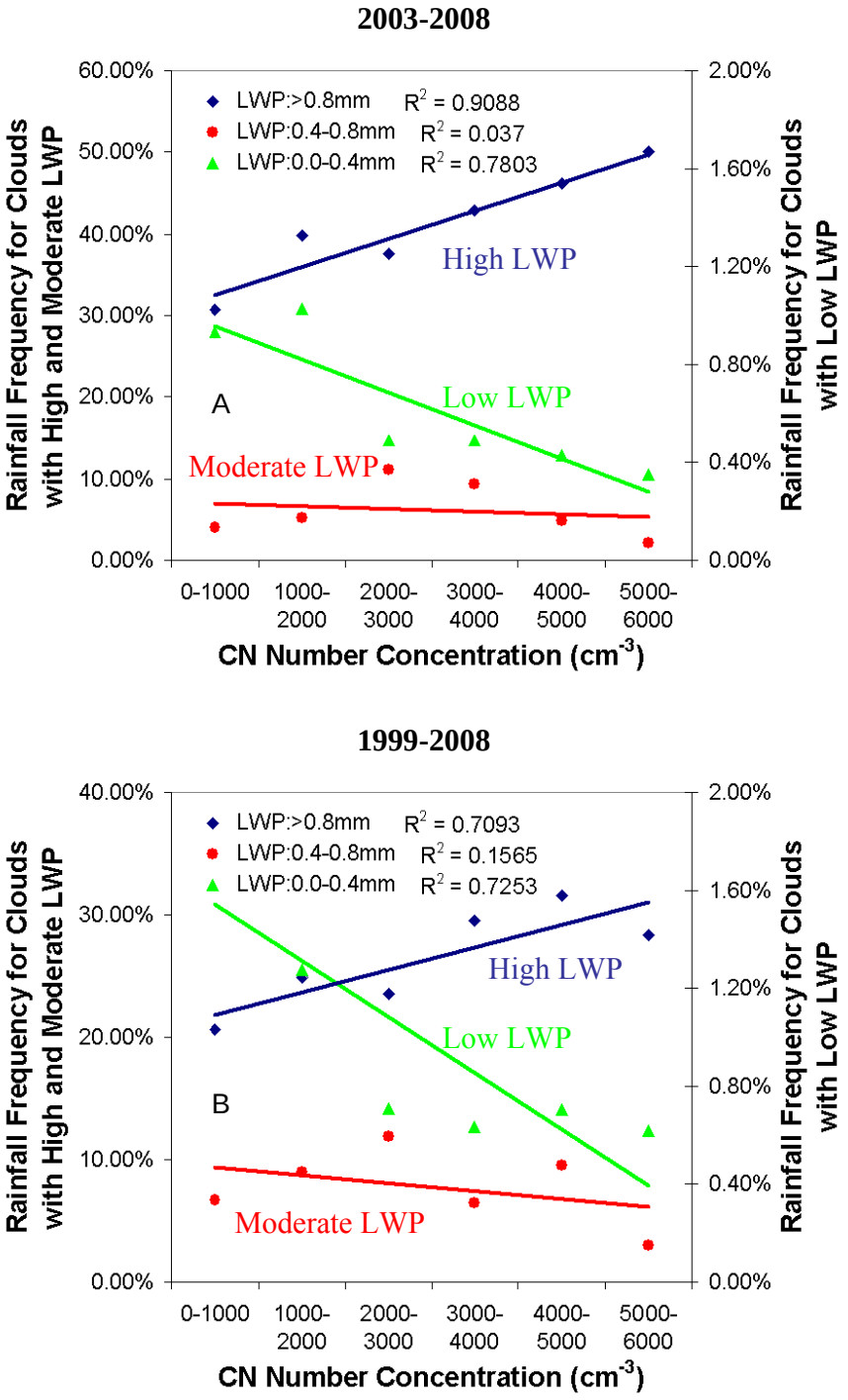

Fig. 2.8. Rainfall frequency as a function of CN for different LWP bins at the SGP site during (A) 2003-2008 and (B) 1999-2008. About 20,000 and 32,000 total data points are used in the calculation of A and B, respectively. For clouds with LWP smaller than 0.4mm (green), the right Y axis is used to more clearly show the changes. Please note that error bars cannot be shown as the rainfall frequency is a ratio.

The importance of cloud base heights is also observed from the relationship between rainfall frequency and CN number concentration. Fig. 2.9 presents relationships for two distinct ranges of cloud base heights: CBH < 1km and between 1-4km. Rain frequency increases sharply with the CN for low CBH, but decreases for high CBH. As elaborated before, the increase is caused by the invigoration effect whose strength is dictated strongly by cloud base height. The correlation coefficient R^2 is as large as 0.982 for the CO2FLX rain data, and 0.715 for the SMOS. Apparently, the low data resolution degrades the correlation.

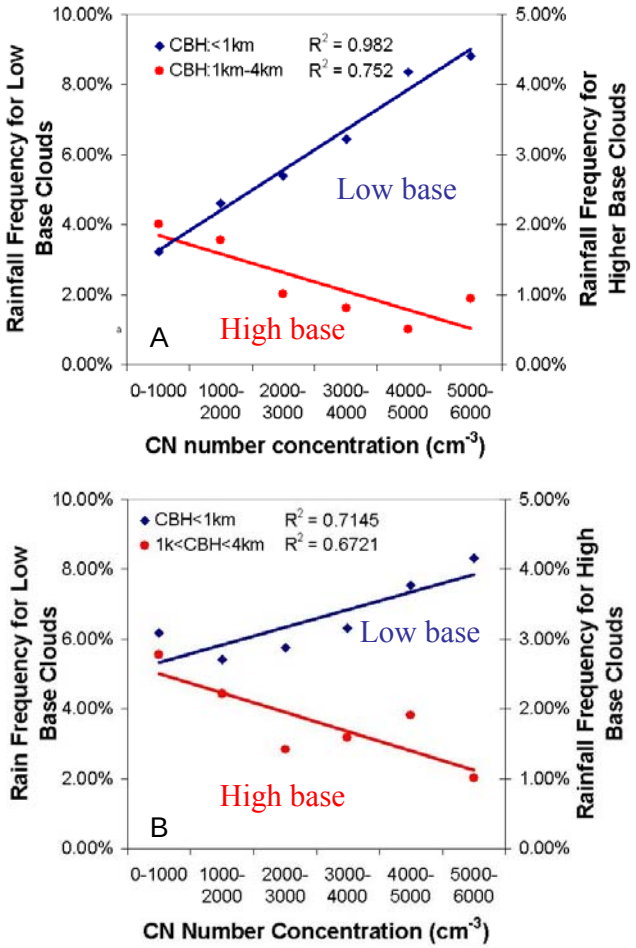

Fig. 2.9. Rainfall frequency as a function of CN for clouds of different cloud base heights during (A) 2003-2008 and (B) 1999-2008. The right Y-axes are for high base clouds (red).

Aerosols also alter the rainfall regime, as revealed by the contrast in the frequency distribution of rain amount per rain event between clean ($CN<2000cm^{-3}$) and dirty ($4000<CN<6000cm^{-3}$) conditions shown in Fig. 2.10. Overall, more than 50% rain events precipitate less than 1mm per rain event. The two curves cross at a rain amount slightly less than than 1 mm/event indicating that heavy rains (rain amount ≥ 2mm) occur more frequently and light rains (rain amount ≤ 1mm) occur less frequently under polluted conditions than under clean conditions. This is testimony to the effect that aerosols suppress warm rain processes but invigorate ice precipitation processes.

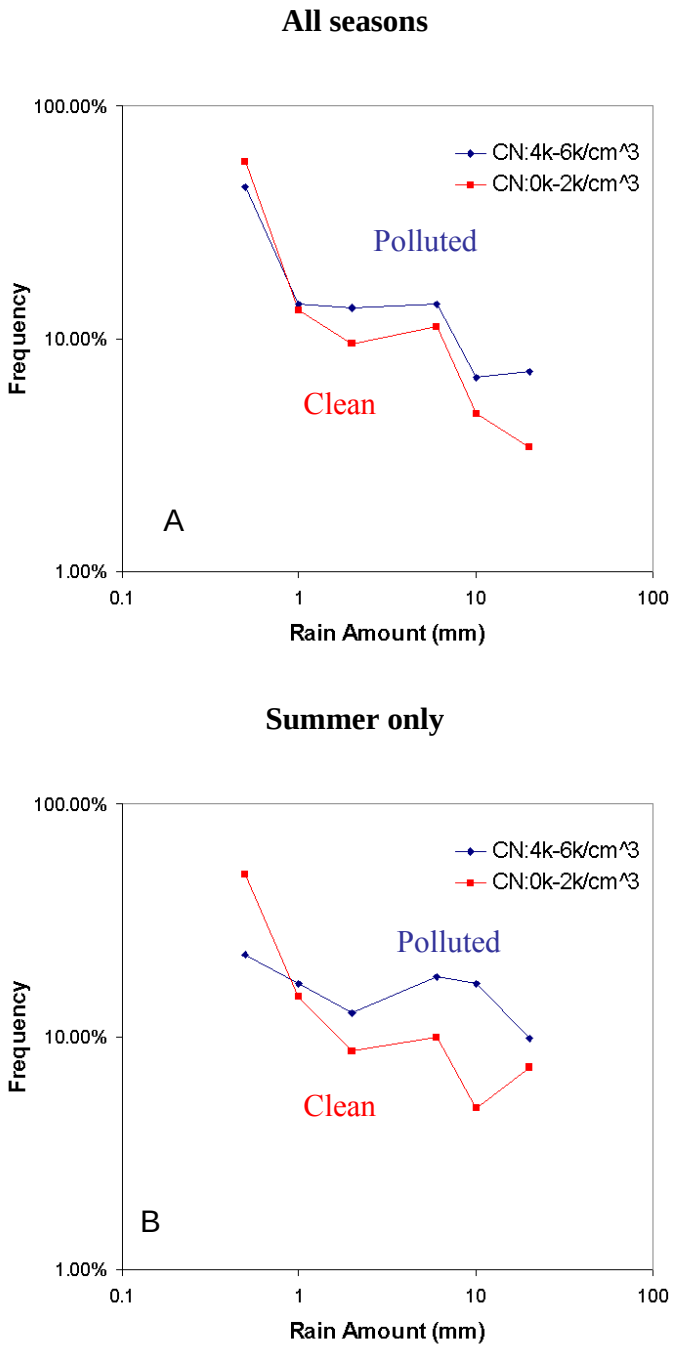

Fig. 2.10. Frequency of occurrence of rain amount per rain event under clean (red, CN: 0-2000cm^{-3}) and polluted conditions (blue, CN: 4000-6000cm^{-3}) in all seasons (A) and summer only (B).

2.3.3 The Causes

These observation-based findings provide solid evidence to support the influence of aerosol on cloud and precipitation. Of no doubt, for each individual cloud and rain event, the influence of meteorology may mask any potential impact of aerosols on an event base. On the other hand, their influences are expected to be smoothed out, insofar as the derivate changes (not the absolute magnitude) with respect to changes in aerosol loading are of concern. However, if the CN is correlated with a meteorological variable, it may render a false relation. To test if this is the case, we conducted painstaking investigations into any possible links that may exist and the available data can be brought to bear. They include surface meteorological variables, atmospheric profiles, stability and thermodynamics.

As the proxy variables of weather system, surface pressure, temperature and wind are examined with respect to changes in the CN to test the dependences of rainfall frequency on CN (Fig.2. 11). No dependence is found at all for surface temperature and pressure, except a weak dependence on wind speed as shown in Fig. 2.11. More CN is accumulated under calm conditions than under windy conditions, but this does not help explain the above finding on the invigoration effect. To some extent, it is opposite to what would be expected, as a calm condition is more likely to occur under stable atmosphere. Tests on the dependence of rainfall frequency on wind directions are also conducted as shown in Fig. 2.12. One issue is that the sample size is not large enough for clouds with LWP>0.8mm, so only two categories are examined: LWP<0.4mm and LWP>0.4mm. The rainfall frequency decreases with increasing CN for all wind directions when cloud LWP is less than 0.4mm. For clouds with LWP>0.4mm, the

rainfall frequency shows no significant correlation with CN for all directions. These results indicate that wind directions may not cause the dependence of rainfall frequency on the CN.

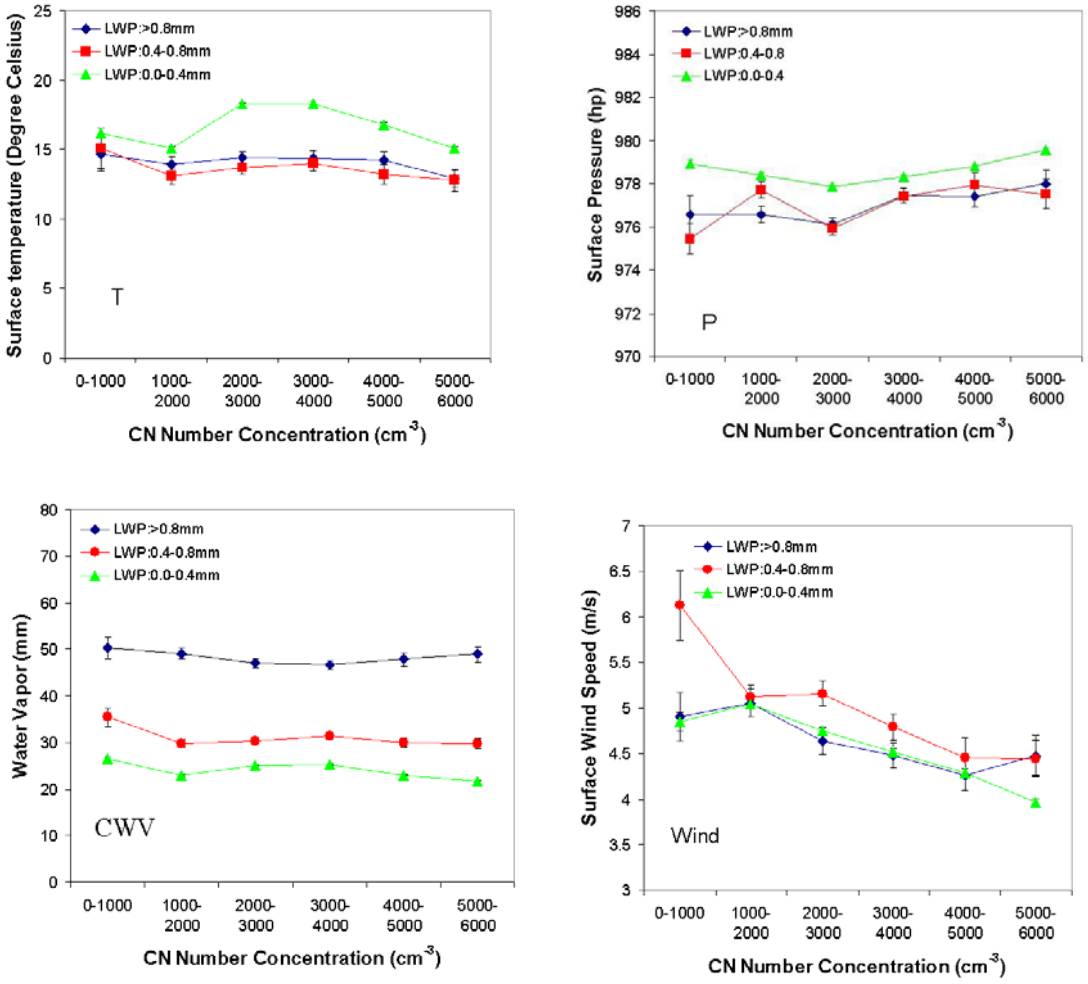

Fig. 2.11. Meteorological variables including surface temperature (T), pressure (P), and wind speed (Wind) and column water vapor (CWV) as functions of CN number concentration from 10-year observations.

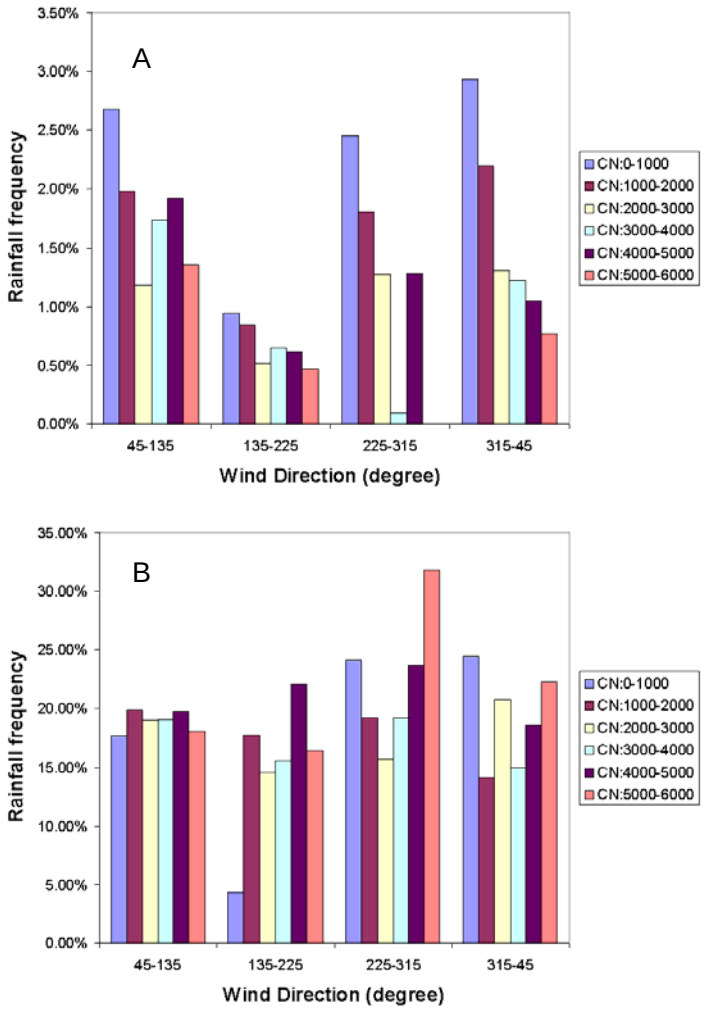

Fig. 2.12. Dependence of rainfall frequency on wind directions for clouds with LWP<0.4mm (A) and LWP>0.4mm (B) in all seasons.

As precipitation washes out aerosols, we may get a false "rain suppression effect" due to cleaner atmosphere under higher rainfall frequency. Therefore, the CN number concentration measured before rain events instead of during rain events was used to avoid the washout effect. However, the washout effect cannot explain any positive correlation between aerosol loading and rainfall frequency. Conversely, it could mask the invigoration effect. To test the influence of this effect, we calculated the ratio between the number of observations with rain and the total number of observations from raw data, and

then correlated it with CN measured simultaneously, instead of before rain. Results from both six-year and ten-year data sets show that the ratio generally decreases with CN number concentration, even for clouds with high LWP (Fig. 2.13). This result indicates that if we simply use the raw data, the washing-out effect may mask the invigoration effect, leaving us the only "rain suppression effect".

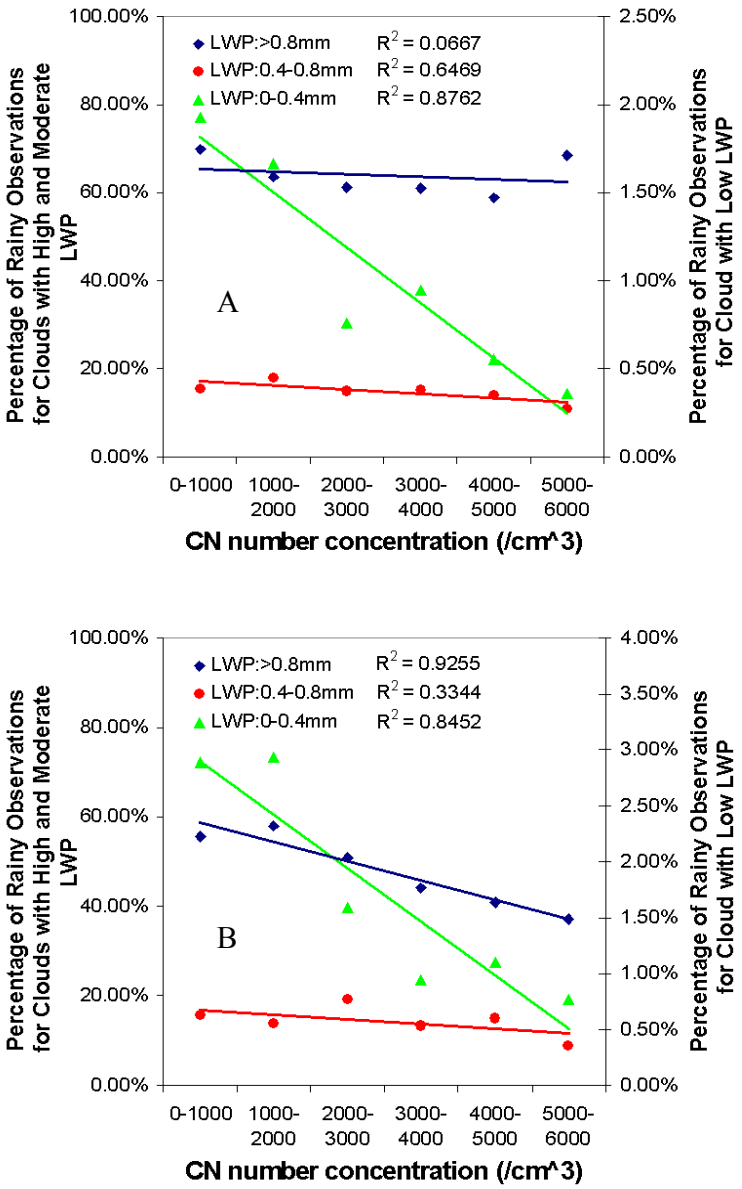

Fig. 2.13. The percentage of rainy observations from raw data during (A) 2003-2008 and (B) 1999-2008.

To investigate if atmospheric thermodynamic condition plays any role in the relation between CTT and CN for clouds with cloud base temperature (CBT)>15^{o}C and CTT<-4^{o}C (blue lines) as shown in Fig. 2.3, the column water vapor (CWV) and lower tropospheric static stability (LTSS) are derived from profiles of atmospheric temperature and humidity from ECMWF to check if they have any correlation with the CN. The LTSS is defined as the potential temperature difference between the surface and the 700 hPa pressure level [*Klein and Hartmann*, 1993]. A lower value of LTSS mean more unstable atmosphere. Here, we do not use the convective available potential energy (CAPE) because the aerosol invigoration effect could also increase CAPE due to the increased buoyancy as shown in a conceptual model [*Rosenfeld et al*., 2008]. The LTSS, however, is more related to large scale thermodynamic conditions [*Klein and Hartmann*, 1993]. Therefore, we use LTSS instead of CAPE to represent the stability of the atmosphere. Both LTSS and CWV for clouds with CBT>15^{o}C and CTT<-4^{o}C in summer show no dependence on CN as shown in Fig. 2.13, in stark contrast with the steady decrease in the CTT with CN as shown in Fig. 2.3. The CWV shows a negative correlation with CN for all seasons, which cannot explain the decrease in CTT with CN, because clouds are likely to be lower in relatively dry conditions. CBH measures overall atmospheric thermodynamic conditions. Therefore, the constraints on CBH (CBT<1km) in Fig. 2.4 also make sure that those clouds have similar thermodynamic conditions, and the increases in cloud thickness are not caused by their changes. It is thus safe to conclude that the CN is neither an agent of the meteorological variables nor atmospheric thermodynamics. The dependences revealed in Fig. 2.3 and 2.4 are thus unlikely the manifestations of any false relations.

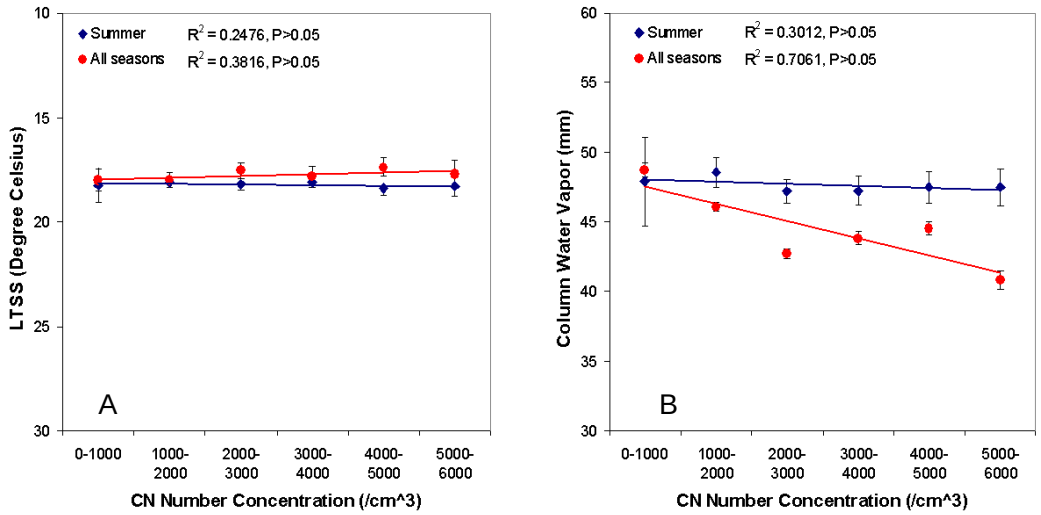

Fig. 2.14. Dependence of the lower tropospheric static stability (LTSS) (A) and column water vapor (B) on the CN for clouds with CBT>15^{o}C and CTT<-4^{o}C in summer and all seasons.

To reduce statistical uncertainties, we also use the same two categories of samples (clean and dirty) as in Fig. 2.9. Likewise, we computed the LTSS for the two categories. The mean LTSS before rain under clean and polluted conditions are 14.71^{o}C and 14.93^{o}C in all seasons and 18.31^{o}C and 18.21^{o}C in summer, respectively. Statistical tests show these numbers are not significantly different under clean and polluted conditions, considering their sample sizes and standard errors (Table 2.2). This result indicates the difference in rain amount distribution is not caused by the variability of atmospheric stabilities.

Table 2.2. Mean, standard error and sample size of LTSS before rain in each condition (unit: ^{o}C).

Conditions	Mean LTSS	Standard Error	Sample Size
Clean (Summer)	14.71	0.34	92
Polluted (Summer)	14.93	0.41	79
Clean (All Seasons)	18.31	0.29	290
Polluted (All Seasons)	18.21	0.31	310

If the increase of CTH with the CN is indeed caused by the invigoration effect, vertical wind velocity is expected to differ between clean and dirty conditions. Fig. 2.14 presents comparisons of vertical velocity for two distinct CN concentrations, for all-year (left panels) and summer-only (right panels), and for mix-phase clouds (top panels) and water clouds (lower panels). Note that all clouds have warm base (>15^{o}C). The contrasts are striking. Above the freezing level, the upward motion is much stronger under dirty conditions than under clean conditions for mix-phase clouds. For water clouds, the two curves are tangled together with little systematic difference. Moreover, the contrasts are much more in summer than other seasons for the mix-phase clouds above freezing level, implying the stronger enhancement of convection for the deep convective clouds since it is the major cloud type in the summer, which is consistent with many observational and cloud-resolving modeling studies [*Andreae et al*., 2004; *Khain et al*., 2005; *Fan et al*., 2009; *Zhang et al*., 2007]. On the other hand, the findings of this study also indicate the general dynamic and thermodynamic conditions in the summer at the SGP are favorable for the aerosol invigoration effects.

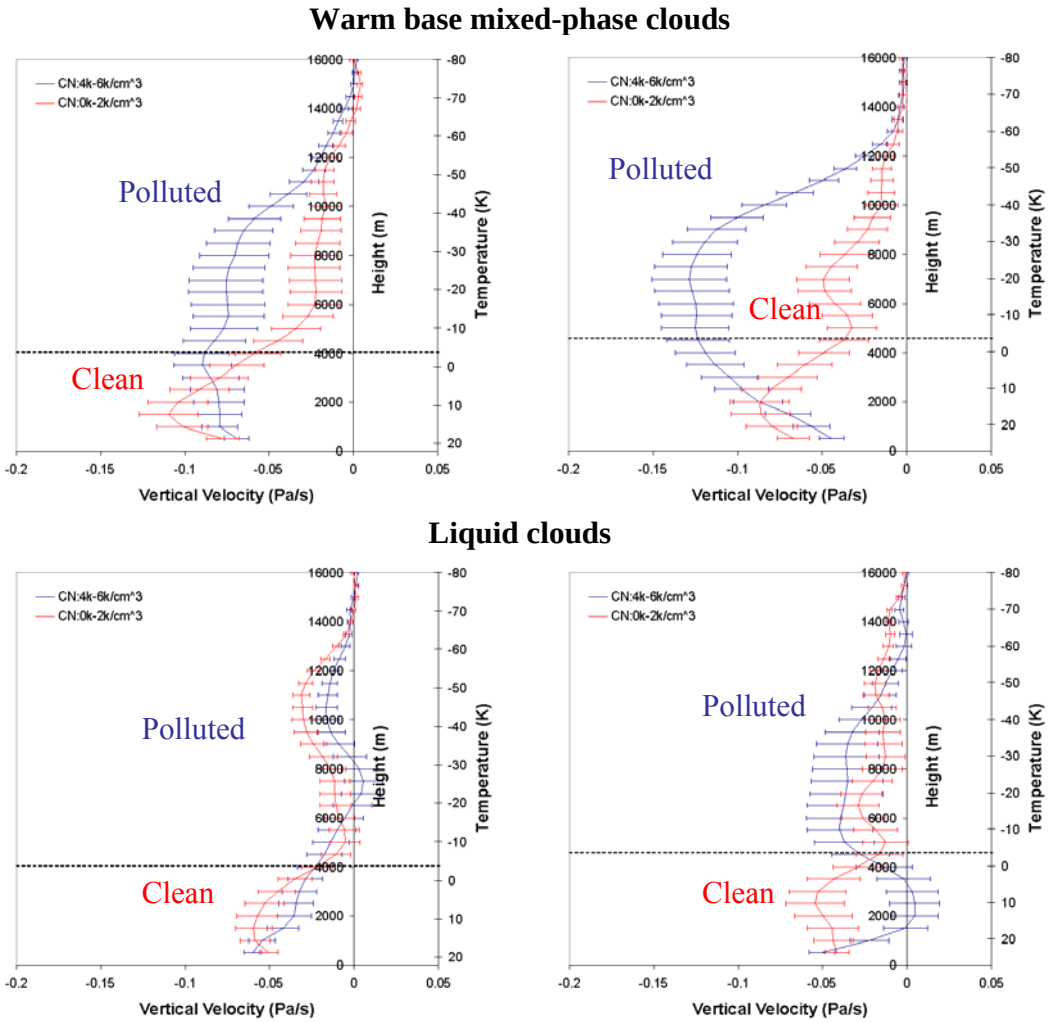

Fig. 2.15. Vertical velocity profiles for clouds with base temperature higher than 15°C and cloud top temperature lower than -4°C under relatively clean (CN:0-2000/cm^3) and dirty (CN:4000-6000/cm^3) conditions. The left two panels are all seasons and the right two panels are summer only. The top panels are for clouds with tops colder than -4°C, whereas the low panels are for liquid water clouds only.

Stronger atmospheric instability can induce effects on clouds similar to those from the addition of aerosols, i.e., increasing updraft strength [*Roberts et al.*, 2001]. Separating the two effects represents a major challenge. To eliminate this factor as a major source of variability, we compared the average temperature profiles under clean and polluted conditions to make sure that they had similar thermodynamic structure of the atmosphere. Results show the vertical temperature profiles under clean and polluted

conditions are almost identical for warm base mixed-phase clouds (Fig. 2.15). Note that error bars of the mean temperature profiles are not drawn in Fig. 2.15 in order to clearly see the lines.

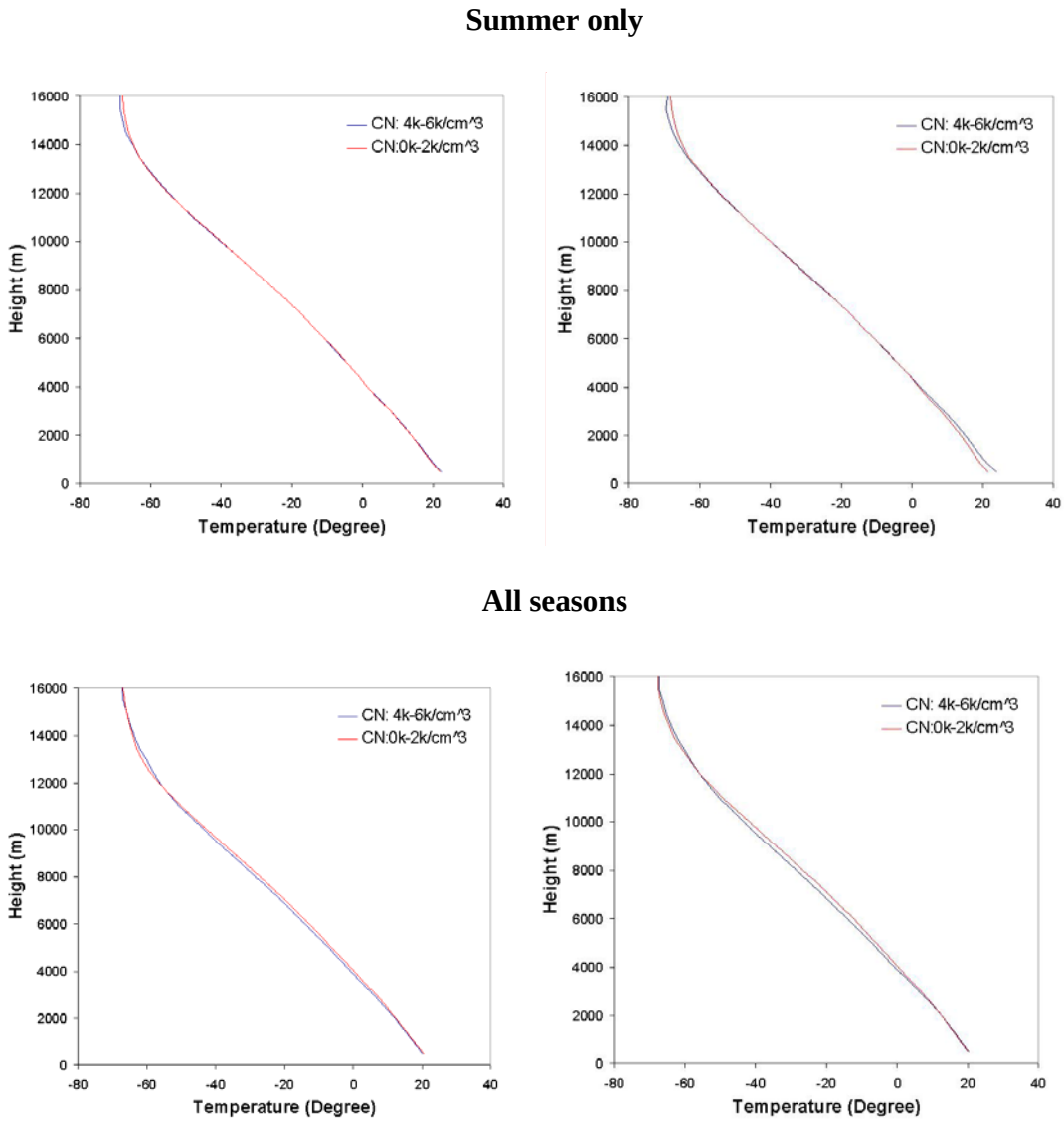

Fig. 2.16. Mean vertical temperature profiles under clean and polluted conditions for warm base mixed-phase clouds (left) and liquid clouds (right) in summer-only (upper) and all seasons (lower).

2.4 Theoretical Explanation

To understand the observed dependence of cloud thickness and rain frequency on aerosol concentration, we use a simple conceptual model to try to explain the observational findings.

As stated earlier, the rain suppression effect and the invigoration effect are, among others, key to the onset of precipitation. The height for the onset of precipitation (H^*) determines partially how deep a cloud can develop. H^* is reached when cloud top effective radius (R_e) exceeds a critical size R_e^* of 12 – 14 μm [*Andreae et al*., 2004; *Rosenfeld and Gutman*, 1994] to generate rain. For liquid clouds, R_e can be parameterized as below [*Brenguier et al.*, 2003]:

$$R_e = \alpha (L / N)^{1/3} \qquad (1)$$

where L and N are cloud liquid water content and the cloud drop concentration respectively. Note that L generally increases with height for H<H*. N depends mainly on the CCN concentrations. Below the convective cloud base, CCN can be parameterized as a power function of aerosol number concentration (N_a) [*Nakajima et al*., 2001]. L can be parameterized as a function of H by a power law function [*Brenguie et al*., 2003; *Shao and Liu*, 2005], we have

$$\mathrm{R}_e = \sigma N_a^{-\alpha} H^{\beta}, \qquad (2)$$

The two exponents, α and β, denote the influence of aerosol number concentration and cloud thickness on cloud drop size. α is positive and β is equal to 1/3 for an adiabatic cloud. When cloud top effective radius (R_e) reaches a critical size R_e^*, H^* can be expressed as:

$$H^* = \left(R_e^* N_a^{\alpha} / \sigma \right)^{1/\beta} \qquad (3)$$

R_e*, α, β, and σ are all constant. Therefore, we can clearly see that H* increases with N_a. This result indicates that as aerosol number concentration increases, cloud particle size decreases, and clouds must reach a higher level to grow larger enough to precipitate. For mixed-phase convective clouds, in-situ measurements over the Amazon basin also found that H* generally increase with $CCN_{0.5}$ [*Freud et al*., 2008].

If cloud top height (H) is less than H*, rain is unlikely. But, if $H > H$* and cloud is above the freezing level (H_0), there would be an invigoration effect by freezing super-cooled cloud water. If $H^* >> H_0$ the suppression of ice hydrometeors to greater heights would decrease the invigoration or may even lead to a suppression.

Fig. 2.16 demonstrates the processes involved in the aerosol suppression or invigoration effects. For warm base clouds, in clean conditions, H* is low and clouds are easy to reach above it to generate precipitation. However, in polluted conditions, clouds are hard to reach above H*, because H* is higher in polluted conditions (H* increases with CN). This leads to the rain suppression effect by aerosols. However, rain can also be enhanced in polluted conditions under some circumstances. It happens when H* is higher than the freezing level, and clouds manage to reach above it to generate precipitation. In this case, the clouds are mostly deep convective clouds and precipitation is generated from ice processes. Latent heat released during ice processes can further invigorate the convection and enhance rainfall.

For cold base clouds, in polluted conditions, H* is higher than that for warm base clouds due to higher cloud bases. Therefore, clouds are much harder to ascend above H*

to generate precipitation compared to those in clean conditions. As a result, precipitation is mostly suppressed in polluted conditions for cold base clouds.

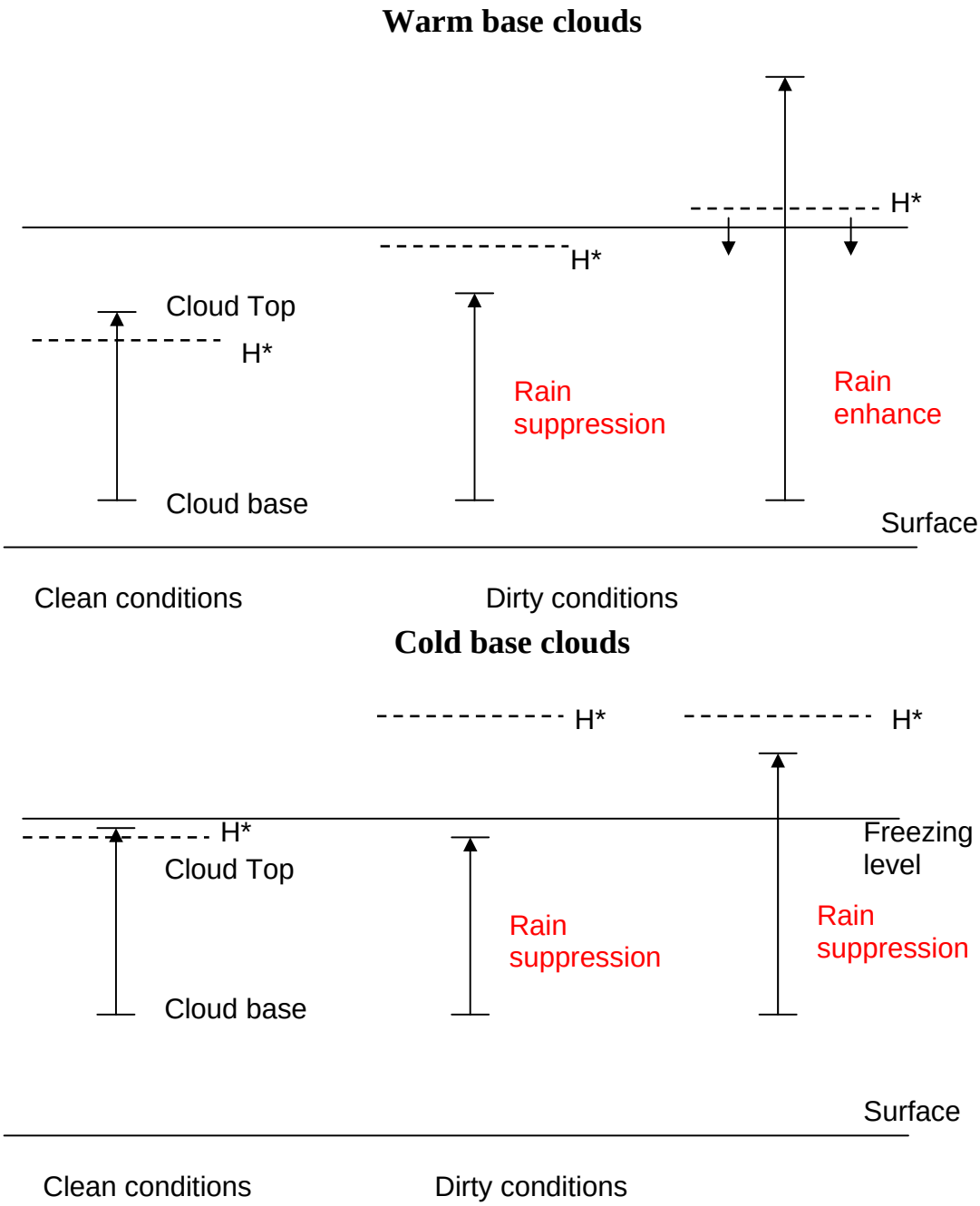

Fig. 2.17. Diagram showing the concept how aerosols suppress or invigorate warm base and cold base clouds. *H** is the height for the onset of precipitation. The surface and the freezing level are marked on the diagram as horizontal lines.

2.4. Conclusions

2.4.1 Summary of Results

Using 10 years of the US Atmospheric Radiation Measurement (ARM) measurements, strong aerosol effects of climatological significance are detected. With increasing total CN measured near the ground, both cloud top height and precipitation change systematically for low-base clouds with tops reaching freezing levels, but not for high-base clouds and ice-free clouds of any cloud base. For the clouds with bases lower than 1km, cloud thickness increases systematically with the CN concentration by up to a factor of 2. The response of precipitation depends on cloud LWP. As CN increases, rain occurs more frequently for high LWP but less frequently for low LWP. The overall distributions of cloud top heights and rain rates are also changed with CN. In conditions with higher CN, clouds with high tops occur more frequently and there tends to be heavier rain events than in conditions with lower CN. These observations are in agreement with previous theoretical considerations and model simulations [*Khain et al*., 2005; *Fan et al*., 2009; *van den Heever et al*., 2006; *Tao et al*., 2007]. Rigorous tests on the above results are conducted by using meteorological variables observed at the same location. None of the results can be explained as caused by systematic changes in meteorological conditions.

The findings from the long-term statistics reveal a strong signal of human impact on precipitation, which have significant implications for climate change studies, especially concerning regional and global climate change induced by pollution.

2.4.2 Limitations of the Study at the SGP Site

Though the ground-based observations at the SGP site have great advantages for studying of aerosols indirect effects with extensive and continuous measurements of aerosols, clouds, and meteorological variables, the SGP site is actually not a perfect location to study the effect of aerosols on precipitation for the following reasons:

1) The ARM SGP site is located in the central US, where it is relatively dry and does not rain frequently. Deep clouds rarely occur, leading to small sample sizes and relatively large variability for warm base mixed-phase clouds (Fig. 2.3). The small sample of deep clouds prevents us from doing more detailed analyses, such as the influence of wind directions as shown in Fig. 2.12 (In this figure, we have to use a broader constraint LWP>0.4mm instead of LWP>0.8mm to increase the sample size).

2) The SGP site has large seasonal variation in temperature and specific humidity, which imposes a great challenge for us to eliminate the influences of them on the effects of aerosols. A site located in tropical regions is ideal for our study because of the relatively uniform meteorological conditions and frequent occurrence of convective clouds. However, existing sites in the tropical region, such as the ARM Darwin site, do not have long enough measurements of aerosols, clouds, and other important variables.

3) The fundamental reason for the invigoration effect is the more latent heat released due to enhanced ice processes. Though increases in cloud top heights (or decreases in cloud top temperature) provide a clue, a more direct way to support this effect is to examine if the ice water content (or ice water path) changes with aerosol loading. Unfortunately, there is no long-term dataset of it at the SGP site.

Satellite instruments such as MODIS and the CloudSat Radar have some advantages that can overcome the above limitations. Focusing on the tropical region, we may have more uniform meteorological conditions and a larger number of deep clouds, compared with at the SGP site. The ice water path can also be retrieved from CloudSat to provide more direct evidence of the enhanced ice processes. Our studies using satellite observations will be discussed in the next chapter.

Chapter 3 : Satellite-based Studies of the aerosol effects on Clouds and Precipitation

3.1 Introduction on Satellite-based Studies of Aerosol Indirect Effects

3.1.1 Previous Satellite-based Studies

Large-scale satellite surveys provide a detailed view of the aerosol–cloud–precipitation system. Correlative studies based on satellite records have found intriguing relationships between aerosols and clouds. Such relationships have been considered as evidence in support of strong aerosol effects.

The "Twomey effect" has been observed from many satellite-based studies [*Kaufman and Nakajima*, 1993; *Kaufman and Fraser*, 1997; *Han et al*., 1998; *Nakajima et al*., 2001; *Bréon et al*., 2002; *Yuan et al*., 2007; *Jiang et al*., 2009]. *Han et al*. [1998] found that the cloud albedo increases with decreasing droplet size for optically thicker clouds, but not for thinner clouds, because the liquid water content may not remain constant if the cloud droplet number concentration changes. *Nakajima et al*. [2001] used AVHRR to demonstrate a negative correlation between the column CCN concentration and the effective radius and a positive correlation with cloud optical thickness over the ocean. *Bréon et al*. [2002] expanded on this analysis and demonstrated that negative correlations between cloud effective radius and aerosol index (defined as the multiple of the aerosol optical thickness and Angstrom exponent) exists over both land and ocean, using the POLarization and Directionality of the Earth's Reflectance (POLDER) instrument. On the other hand, *Yuan et al*. [2007] found positive relations between

MODIS-derived cloud droplet size and aerosol optical depth over the coasts of the Gulf and South China Sea during summer when plentiful of water supply combined with strong convection provide a more favorable condition for droplets to grow. *Jiang et al*. [2009] examined the same relations for ice clouds and they found suppressed precipitation and reduced r_e associated with polluted clouds in the dry season in South America. However, little difference in ice particle size was found in the wet season. These results suggest that the impact of aerosols on cloud microphysics is global and could be strongly influenced by meteorological conditions. Note that the satellite measurements of aerosol loading and cloud droplet size are not coincident, because sensors such as MODIS cannot detect AOD beneath optically thick clouds, and there is a lack of simultaneous measurements of LWP, which makes assessment of the cloud albedo radiative forcing difficult. With an assumption of 15% to 40% increase in the aerosol number after the industrial revolution *Nakajiam et al*. [2001] estimated the albedo and lifetime radiative forcing (hard to separate using only satellite observations) ranges from -0.7 to -1.7Wm^{-2} over the global ocean.

The expected effects on cloud lifetime are more difficult to observe with current satellite observations. However it is commonly assumed that cloud fraction and cloud lifetime are related. Therefore analysis of the lifetime effect using satellite observations tends to focus on changes in the cloud fraction by aerosols. Cloud fraction tends to be larger, on average, in the presence of more aerosols [*Sekiguchi et al*., 2003; *Loeb and Schuster*, 2008; *Kaufman et al*., 2005; *Matheson et al*., 2005]. For example, *Sekiguchi et al*. [2003] show a correlation between AI and cloud fraction on the global scale using data from both AVHRR and POLDER. *Kaufman et al*. [2005] also found that the

coverage of shallow clouds increases over the Atlantic Ocean from clean to polluted, smoky, or dusty conditions using the Moderate Resolution Imaging Spectroradiometer (MODIS) data. Such correlations have been taken as evidence of a strong cloud lifetime effect. Global surveys suggest a radiative forcing of between 0 and -1Wm^{-2} [*Sekiguchi et al*., 2003; *Nakajima et al*., 2001].

Along with the progress in understanding the radiative forcing of the aerosol indirect effect, the aerosol effect on the hydrological cycle, through modification of the microphysical and thermodynamic processes of clouds, has recently received much attention. Some examples of aerosol-induced suppression of the development of precipitation have also been reported [*Rosenfeld and Lensky*, 1998; *Lebsock et al*., 2008; *L'Ecuyer et al*., 2009 ; *Jiang et al*., 2008]. However, most of these studies focus on warm clouds. For example, a technique combining cloud top temperature and effective radius, retrieved from AVHRR, has been used to show the suppression of coalescence processes [*Rosenfeld and Lensky*, 1998]. Recent studies using CloudSat and MODIS data by *Lebsock et al.* [2008] showed the global conditional probability of warm cloud precipitation generally decrease with the increase of aerosol index for various column water vapor regimes. For mixed-phase convective clouds, aerosols are hypothesized to invigorate convection and enhance rainfall through the invigoration effect [*Rosenfeld et al*., 2008]. However, only a handful of satellite studies provided demonstrations of the enhancement of precipitation by aerosols [*Lin et al*., 2006; *Bell et al*., 2007]. For example, *Lin et al*. [2006] found that aerosols optical thickness from MODIS is positively correlated with rainfall amount by examining multiplatform satellite data over the Amazon basin. Many other studies such as [*Koren et al*., 2005, 2008], however, just

reported the increase of cloud top heights with aerosol loading as evidence of the invigoration effect, and no precipitation was observed. Further more, there is still a lack of process-level evidence of the invigoration effect from observations.

3.1.2 Objectives

In this chapter, we will report satellite observations of aerosol-induced effects on clouds and precipitation. Satellite-based observations provide important alternative data sources for extending our study to a much larger spatial domain. We choose the tropical regions to have more samples of deep convective clouds and relatively uniform cloud types and meteorological conditions. However, satellite-based studies of aerosol indirect effects face their own challenges, discussed later (Section 3.3).

Here we use the combination of the CloudSat 94GHz nadir looking Cloud Profiling Radar (CPR) data and the MODIS imagery data. The CloudSat, can determine cloud geometry, including cloud top and base heights, and if a cloud is raining or non-raining cloud. MODIS can determine aerosols properties, such as aerosols optical thickness and with less precision angstrom exponent. Combining the two datasets makes it possible to study the aerosol effects on both clouds and precipitation.

The objectives of our satellite-based analyses are to examine aerosol effects on different clouds, including liquid and mixed-phase clouds. With the cloud geometry information, clouds can be classified based on their tops and bases. We will try to examine how aerosols influence cloud top temperature (or heights) and ice water path retrieved from satellites, which is not available from the ground-based observations. Aerosol effects on the rain rate from the CloudSat precipitation radar will also be examined.

3.2 Satellite Products Used in This Study

The main satellite products used in the study include cloud and rain retrievals from CloudSat/CALIPSO (Cloud-Aerosol Lidar and Infrared Pathfinder Satellite Observation) and aerosols retrievals from the MODIS (aboard Aqua). Table 3.1 summarizes these products.

MODIS is a key instrument aboard the Terra and Aqua satellites. The MODIS aerosol products are generated by two different algorithms applied to ocean and land, which were originally documented by *Tanre et al.* [1997] and *Kaufman et al*. [1997a]. The products provide the aerosol optical thickness over land and ocean globally. The aerosol size distribution is also derived over oceans, and the aerosol type is derived over land. Daily level 2 aerosol optical thickness data are produced at the spatial resolution of as tight as 10 x 10 km. The aerosol products over ocean are retrieved through an inversion method, which is aptly described by *Tanré et al*. [1997] and *Levy et al*. [2003]. The retrieval algorithm over land has been revised a few times [*Levy et al*. 2007a]. To obtain the surface reflectance, the ratios of surface reflectance at red and blue channels versus that at 2.12 μm are originally considered fixed values of ½ and ¼. In the latest collection, the ratios are considered as functions of the scattering angle and the normalized difference vegetation index in the last version. Together with the modification of the aerosol model, a large improvement was made compared with previous collections. The validation of the aerosol land products with ground-based observations shows good agreement [*Li et al*., 2007c; *Mi et al*., 2007; *Levy et al*., 2007a; 2010].

The CALIPSO mission provides crucial data on aerosol and cloud vertical structure and optical properties. CALIPSO consists of three co-aligned, near-nadir

viewing instruments: a 2-wavelength polarization-sensitive lidar, an imaging infrared radiometer, and a high-resolution wide field camera. The lidar profiles provide information on the vertical distribution of aerosols and clouds, cloud particle phase, and classification of aerosol size using measurements at two wavelengths at 532nm and 1064nm [*Winker et al*, 2003].

CloudSat provides information of cloud structure, microphysical and radiative properties. The main instrument on CloudSat is the Cloud Profiling Radar (CPR), which is a 94-GHz nadir-looking radar measuring the power backscattered by clouds as a function of distance from the radar. The CloudSat data footprint is approximately 1.7km along-track by 1.3km across-track. For each radar profile, there are 125 vertical bins, and each one is approximately 240m thick. CloudSat standard data products include cloud geometrical profile, cloud classification, cloud water content, cloud optical depth and fluxes and heating Rates.

The cloud products to be used in the study include:

2B-GEOPROF-LIDAR: The geometrical profile product is derived by identifying the levels (bins) in the vertical column, which contain a significant echo [*Stephens et al*., 2002]. The Cloud Geometrical Profile from combined CPR and the CALIPSO Lidar provides a more complete picture of the cloud structure. These two are flying in close coordination with each other. With the ability of the CPR to probe optically thick layers and the ability of the Lidar to sense optically thin layers and tenuous cloud tops, the two instruments provide significant observational capabilities. We will use this product to study the influence of aerosols on cloud geometry.

2C-PRECIP-COLUMN: The rain detection of CloudSat is achieved by combining path-integrated attenuation and high sensitivity radar reflectivity observations from the 94-GHz nadir-looking radar (CPR) [*Haynes et al*., 2009]. The approach makes use of sea surface wind speed, surface temperature, and atmospheric temperature and moisture profiles over the oceans from the European Centre for Medium-range Weather Forecasting (ECMWF) to determine the theoretical backscatter cross section of the surface in the absence of hydrometeors. By comparing the radar observed backscatter cross section against the theoretical calculation, the presence and intensity of precipitation can be determined. The comparison of the frequency of precipitation with those ship-based and island-based results shows excellent agreement [*Ellis*, 2009]. The dataset will be used to study the aerosol effect on the precipitation rate.

ECMWF-AUX: The ECMWF-AUX data set is an intermediate product that contains the set of ancillary ECMWF state variable data interpolated to each CloudSat cloud profiling radar (CPR) bin. The variables include atmospheric pressure, temperature, and specific humidity at each level. These data can be used to covert cloud top and base heights into top and base temperature. The column water vapor and LTSS can also be calculated from the dataset to constrain meteorological conditions.

Table 3.1. Summary of the MODIS and CloudSat/CALIPSO products used in the study.

Geophysical Parameter	Product	Sensor	Spatial Resolution
AOT	MOD08	MODIS	1×1 Degree
Cloud Geometry	2B-GEOPROF-LIDAR	CloudSat and CALIPSO	Horizontal: 1.4×2.5 km Vertical: ~250m
Cloud Ice Water	2B-CWC	CloudSat	1.4×2.5 km
Column Water Vapor	ECMWF-AUX	N/A	1.4×2.5 km
Atmospheric Temperature Profiles	ECMWF-AUX	N/A	1.4×2.5 km

CloudSat and CALIPSO lag Aqua by 1 or 2 minutes, so the AOT and cloud properties at a specific location can be obtained almost simultaneously. The CloudSat products have been validated through the Canadian CloudSat and CALIPSO Validation Project (C3AP) [*Hudak et al*., 2006a, 2007]. The precipitation detection was compared with the ground occurrence of rain detected by several types of ground-based rain sensors. The results showed very good agreement and no overall bias. The cloud geometry products were compared with cloud boundaries detected by ground radar or aircraft *in-situ* measurements. The general agreement of these geometric cloud profiles lends confidence to the products, although there are some discrepancies for very high or low clouds [*Hudak et al*., 2009]. The cloud top heights detected by CPR are lower for high clouds due to CPR sensitivity. And the cloud base heights are higher compared to ground radar retrievals. The averaged biases from cases used to compare are about 0.5km. A good agreement has been found for middle clouds.

3.3 Challenges and Methodologies

The study of aerosol indirect effects using satellite data faces several challenges and also received some criticisms [*Stevens and Feingold*, 2009]. They include:

1) It is unclear to what extent the path-integrated aerosol is representative of the aerosol entering the clouds, because satellites measure aerosols in cloud-free regions and cloud properties in adjacent cloudy regions.
2) Uncertainties of satellite retrievals and other artifacts, such as cloud contamination, may incur false relationships between clouds and aerosols.
3) Meteorological conditions, affecting both aerosols and clouds, must be carefully examined to reduce the possibility that aerosol optical thickness acts as a proxy of one or more meteorological variables such as available water vapor.

Last, but probably the most serious is the lack of simultaneous measurements of aerosol and cloud properties, as aerosol quantities can only be retrieved under cloud-free condition. One must thus assume that any aerosol retrieval within the proximity of cloudy pixels is representative of the aerosol inside cloud. We are not going to solve all these problems in this study, as some of them are really inherent weaknesses of satellite observations. However, knowing how these problems may affect our results will be helpful to find ways to reduce their influences.

The first problem leads to the fundamental method of this study. Generally, observational studies can be done through two commonly used methods: a case study and a statistical study. For case studies, we need to know exactly where the plume comes from, and if it can influence the cloud field. If the cloud is generated up-wind and the plume is generated down-wind, any correlation between aerosol concentration and cloud properties might be just coincident and meaningless, and cannot be considered as evidence of aerosol indirect effects. However, for statistical studies, such cases are

allowed as long as they do not cause "systematic bias". For example, we assume that there are eight different wind directions, and aerosols can only interact with clouds in case 1 as shown in Fig. 3.1. Due to the assumption that there is no physical connection between the aerosol plumes and cloud fields in cases 2-8, any correlations between them may be just coincident and random. As a result, these random correlations between clouds and aerosols may cancel out and lead to no correlation at all. If we consider all these eight cases together, since case 1 has physical processes (aerosol indirect effects) involved, the overall correlation may show up and it has physical meaning. Therefore, the key is not to remove all non-physical correlations, which is almost impossible for statistical studies, but to: 1) minimize the "noise" caused by non-physical correlations so true physical correlations can show up; 2) eliminate "systematic bias", such as meteorological conditions driving both aerosols and clouds, e.g. the swelling effect of water vapor, cloud contamination, etc.

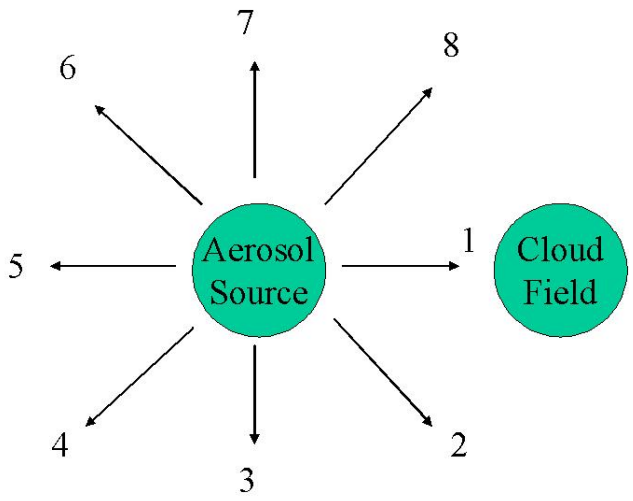

Fig. 3.1. Diagram showing aerosol and cloud interaction under eight different wind directions.

The above discussion leads to our methods to solve the challenges 2) and 3). To minimize the "noise", we restrict the study area over tropical regions where the cloud systems are mainly locally generated cumulus clouds. This minimizes the influence caused by aerosol effects on other kinds of clouds such as stratiform clouds. Such clouds, as implied by our ground-based study, are much less significant to the aerosol invigoration effects. In this study, we still use the method adopted by many other studies [*Koren et al.,* 2005, 2008; *Lin et al*., 2007], which is using AOT obtained simultaneously from pixels near clouds to represent aerosols entering clouds. This method has been proven valid in regions where locally generated convective clouds are dominant such as the Amazon basin [*Koren et al*., 2008]. AOT is also proven to be a good proxy of CCN [*Andreae*, 2009].

To minimize to the "systemic bias", several steps are conducted. First, AOT<0.6 is used to minimize the influence of clouds contamination, since contaminated pixels by clouds are usually has higher retrieved AOT. Second, since precipitation washes out aerosols, we may get false "rain suppression effect" due to cleaner atmosphere under higher rainfall frequency. However, the effect can not explain any positive correlation between aerosol loading and rainfall frequency. Therefore, any increases of rainfall frequency or rain rate with aerosols are not caused by this false effect. Third, correlations between AOT and the atmospheric stability and column water vapor are examined to minimize possibilities of false relations between AOT and clouds.

All data from CloudSat/CALIPSO products in 2007 are averaged in $1^o \times 1^o$ grids in order to match with the MODIS Level 3 aerosol product that has a $1^o \times 1^o$ resolution. Only data within 20^oS-20^oN are used to make sure the dominant cloud type is the

convective cloud. Grids with AOT > 0.6 are excluded in our study to reduce possible cloud contamination. Cloud top and base heights are converted to temperature using temperature profiles in the ECMWF-AUX product in order to define different cloud types: warm base mixed-phase clouds with base temperature (CBT) > 15^{o}C and CTT < -4^{o}C, relatively cold base mixed-phase clouds with CBT in the range of 0-15^{o}C and CTT <-4^{o}C, and liquid clouds with CBT>0^{o}C and CTT > 0^{o}C (Table 3.2). Only single layer clouds are considered here. The aerosol index (AI), which is a product of AOT and aerosol angstrom exponent, is binned and the dependences of averaged cloud properties in each bin on the aerosol index are examined over ocean. How the rain rate and its distribution change with aerosol index is also examined. Over land, AOT is used instead of the aerosol index as the angstrom exponent retrieved from MODIS over land is not quantitative [*Levy et al.*, 2010]. Tests on dependences of LTSS and column water vapor on the aerosol index or AOT are also done over both land and ocean.

Table 3.2. Definition of warm and cold base mixed-phase clouds and liquid clouds in this study.

	Warm base mixed-phase clouds	Cold base mixed-phase clouds	Liquid clouds
Cloud base temperature	>15^{o}C	0-15^{o}C	>0^{o}C
Cloud top temperature	<-4^{o}C	<-4^{o}C	>0^{o}C

3.4 Results

Fig. 3.2 shows the cloud top temperature and ice water path as functions of AI and AOT for different cloud types defined in Table 3.2. As discussed before, the aerosol

invigoration effect is more significant for warm base mixed-phase clouds than for cold base clouds, because of a longer distance for cloud particles to grow before freezing for warm base clouds. Moreover, there should be no invigoration effect for liquid clouds due to the absence of ice processes. This hypothesis is confirmed by the changes in the cloud top temperature and ice water path with AI and AOT for different cloud types. As shown In Fig. 3.2, the cloud top temperature for warm base mixed-phase clouds over ocean decreases dramatically with AI, while the cloud top temperature for liquid clouds does not decrease at all. The decreasing rate for cold base mixed-phase clouds lies in between. Correspondingly, the ice water path also increases for both warm and cold base mixed-phase clouds but with a higher increasing rate for the former. The increased ice water path indicates enhanced ice processes, in which more latent heat is released to invigorate the convection when liquid cloud particles are freezing. The similar results are also observed over land. The deeper clouds and enhanced ice processes in polluted conditions could lead to enhanced rainfall as suggested by previous studies [*Khain et al*., 2005; *Lin et al*., 2006]. Therefore, the relationship between AI and the precipitation rate from the CloudSat precipitation radar was also examined.

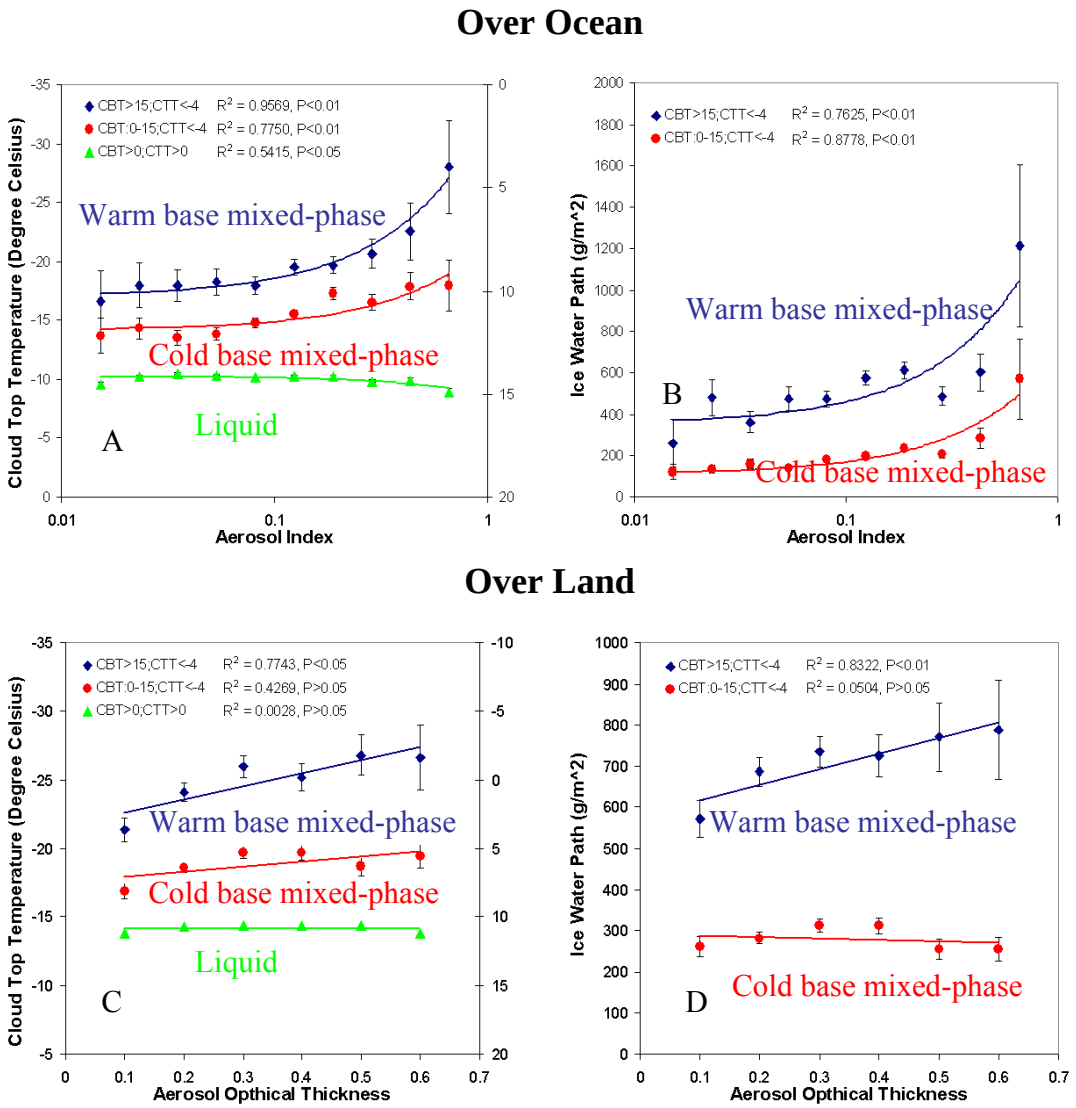

Fig. 3.2. Cloud top temperature (A and C) and ice water path (B and D) as functions of AI or AOT for warm (blue dots) and cold (red dots) base mixed-phase clouds and liquid clouds (green dots) over ocean (upper) and land (lower). The ice water path for liquid clouds is not shown. The right axes of A and C are for liquid clouds. The aerosol index is in a logarithmical scale.

Strikingly, the precipitation rate shows very different responses to the increase of AI for mixed-phase and liquid clouds (Fig. 3.3). The precipitation rate increases with AI for mixed-phase clouds but decreases with AI for liquid clouds. Please note that only

clouds with rain rate > 1mm/h were examined, as the invigoration effect is only significant for deep clouds [*Rosenfeld et al*., 2008], which favor the production of heavy rain. To increase sample sizes, mixed-phase clouds were no longer divided into warm and cold base clouds. As a result, only two types of clouds were considered here: mixed-phase and liquid clouds. The sample sizes before and after combining warm and cold base mixed-phase clouds are shown in Table 3.3. Results show very distinctive responses of the precipitation rate to the increase of AI for these two types of clouds. For mixed-phase clouds, the precipitation rate increases and cloud top temperature decreases with AI. This result provides strong evidence that aerosols enhance precipitation by inducing stronger convection in mixed-phase convective clouds. However, for liquid clouds, the precipitation rate decreases and cloud top temperature has no significant change. One thing to note is that precipitation may also influence aerosols by washing them out, leading to a false aerosol effect on the rain rate. We would argue that if this were the case, we should obtain similar trends for both mixed-phase and liquid clouds, because the washing-out effect works the same way for both types of clouds. However, the rain rates for these two types of clouds respond very distinctively to the increase of AI, which cannot be explained by the washing-out effect of rain. Besides, AOD and cloud/rain data were not obtained at the same locations, but nearby.

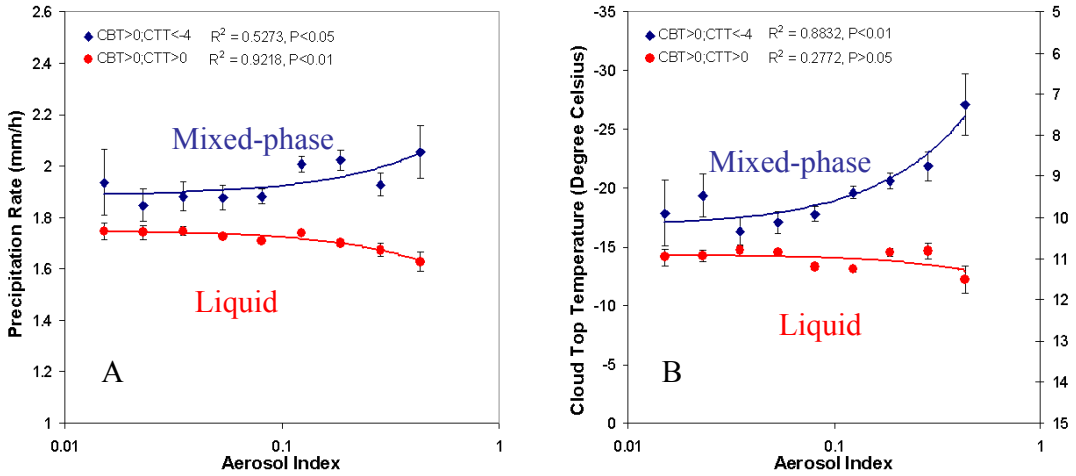

Fig. 3.3. Precipitation rate (A) and corresponding cloud top temperature (B) as functions of AI for mixed-phase (blue dots) and liquid clouds (red dots) over ocean. Please note only clouds with the precipitation rate higher that 1 mm/h are included here. The right axis of B is for liquid clouds. The unit is ^{o}C.

Table 3.3. Total sample sizes of liquid and mixed-phase clouds before and after combining warm and cold base clouds. Cloud types are defined in Table 3.2.

	Liquid clouds	Mixed-phase clouds	
		Warm base	Cold base
Sample size before combining two types of mixed-phase clouds	16356	1128	890
Sample size after combining two types of mixed-phase clouds	16356	2018	

To further ensure that our previous results are caused by aerosol effects instead of other factors, we test the dependence of several meteorological variables on AI or AOT. In another words, we try to check if AI or AOT are proxies of some meteorological variables. Two important atmospheric conditions affecting cloud formation are correlated with AI or AOT: column water vapor and the lower tropospheric static stability (LTSS). Results show that for mixed-phase clouds (blue dots in Fig. 3.4), neither column water vapor nor LTSS is dependent on AI or AOT or their dependence on AI or AOT can not explain the changes in cloud top temperature or precipitation rate. For

example, LTSS is found to be positively correlated with AOT over land (Fig. 3.4D), which means that the atmosphere is more stable instead of more unstable as AOT is high. Clouds tend to develop higher in unstable conditions, therefore, the positive correlation between LTSS and AOT cannot explain the decrease of cloud top temperature with AOT (blue dots in Fig. 3.2D). Admittedly, the increase of cloud top temperature with AI for liquid clouds (green dots in Fig. 3.2) could be caused by the positive correlation between LTSS and AOT (Fig. 3.4B). Tests for clouds with the precipitation rate >1mm/h also rule out the possible influences of column waver vapor and LTSS on the dependences of the precipitation rate on AI (Fig. 3.5).

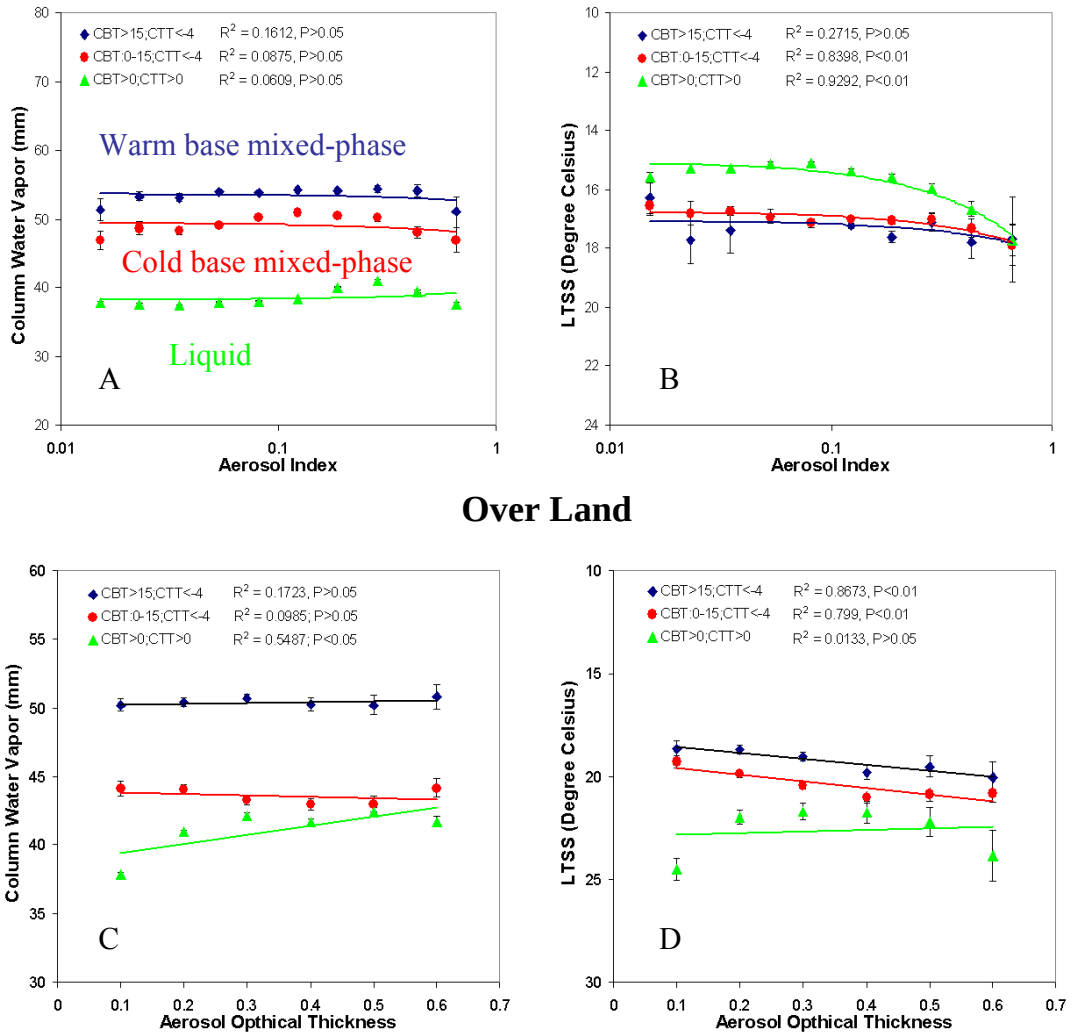

Fig. 3.4. Tests on the dependences of column water vapor (A and C) and LTSS (B and D) on AI over ocean (upper) and AOT over land (lower) for warm (blue dots) and cold (red dots) base mixed-phase clouds and liquid clouds (green dots). Please note LTSS is in a reverse order. Smaller LTSS means more unstable atmosphere.

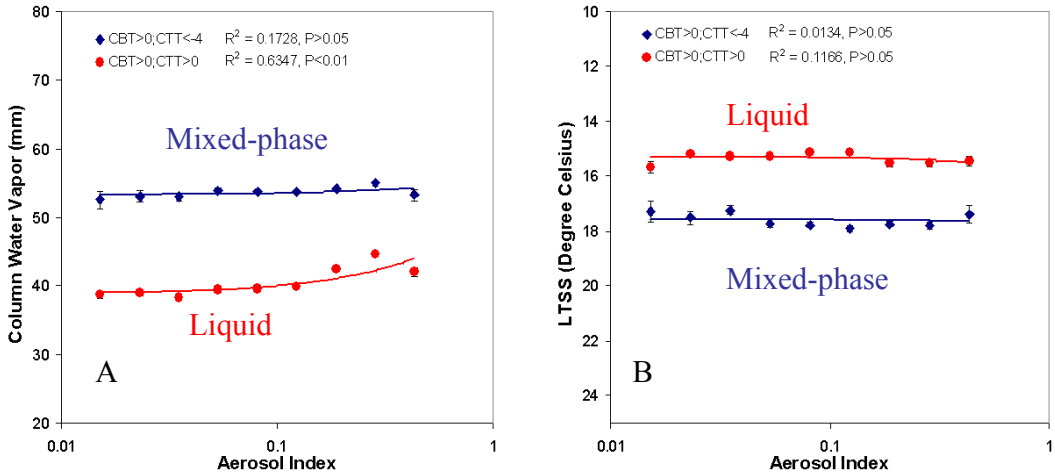

Fig. 3.5. Tests on the dependences of column water vapor (A) and LTSS (B) on AI over ocean for mixed-phase (blue dots) and liquid clouds (red dots). Please note only clouds with the precipitation rate higher that 1 mm/h are included here.

The increase of the precipitation rate with AI for mixed-phase clouds and the decrease of the precipitation rate for liquid clouds should greatly change the overall precipitation rate distribution. Fig. 3.6 shows the frequency of occurrence of different precipitation rates in relatively clean and polluted conditions. In relatively polluted conditions, the frequency of occurrence of higher precipitation rates is higher than that in clean conditions. Conversely, the frequency of occurrence of lower precipitation rates is lower than that in clean conditions. This result indicates that aerosols could change the hydrological cycle by changing the frequency of heavy or light rain, even though the mean rain rates remain unchanged. Tests on column water vapor and LTSS under clean and polluted conditions were also conducted as shown in Fig. 3.7. No systematic difference was found between clean and polluted conditions. These tests do not support the contention that the change in the rain rate distribution is caused by systematic differences in meteorological conditions.

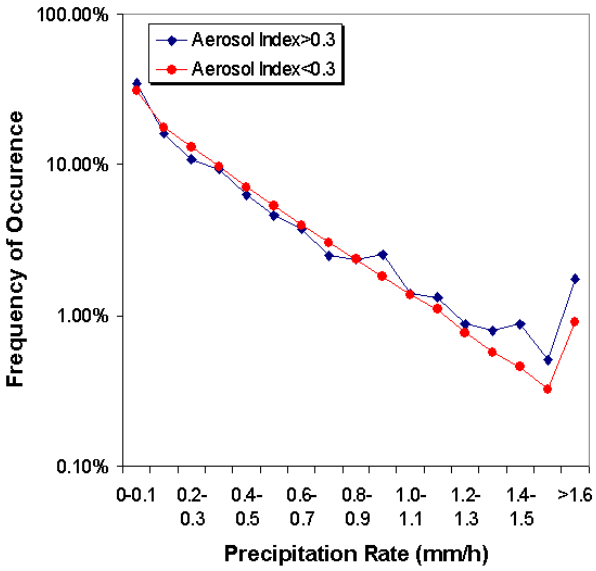

Fig. 3.6. Frequency of occurrence of different precipitation rates in relatively clean and polluted conditions.

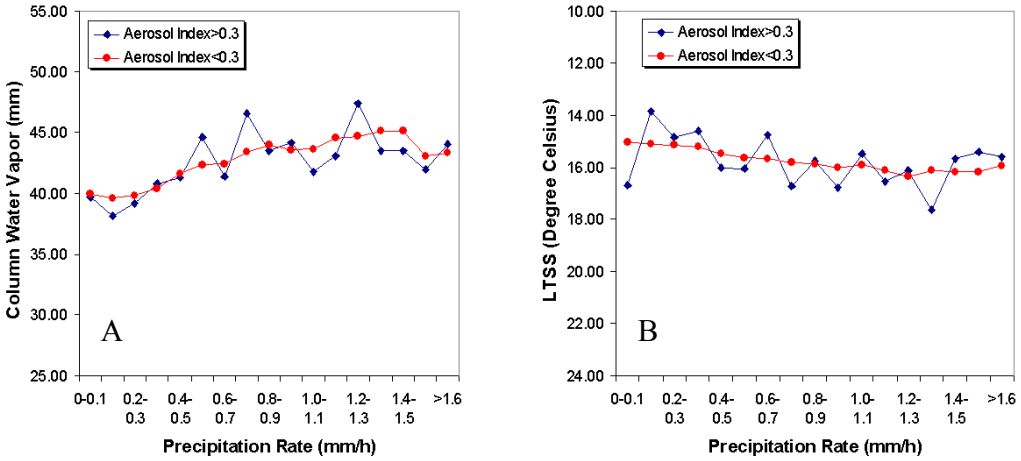

Fig. 3.7. Column water vapor (A) and LTSS (B) for clouds with different precipitation rates in clean and polluted conditions. Please note LTSS is in a reverse order.

3.5 Conclusions

Satellite data from CloudSat over tropics are demonstrated to be useful for understanding some basic processes involved in the invigoration effect, despite some inherent shortcomings, whose impact is lessened, if not eliminated in this study. More evidence of the invigoration effect of aerosols is revealed by analyzing satellite observations over a large spatial domain, consistent with the findings from long-term ground-based observations over the South Great Plains as shown in Chapter 2.

By dividing clouds in the tropical region into three categories based on their top and base temperature, we find that the invigoration effect only exists in mixed-phase clouds, and its strength is determined by the cloud base temperature. Warm base clouds have a stronger invigoration effect than cold base clouds. The direct evidence is the decreasing trend of cloud top temperature with AI for both warm and cold base mixed-phase clouds, with a higher increasing rate for the former. Cloud ice water paths also increase with AI or AOT for mixed-phase clouds. However, for liquid clouds, there is no decrease in cloud top temperature with increasing aerosol loading, indicating the absence of the invigoration effect. Tests on the dependences of column water vapor and LTSS on AI or AOT show that the above results are unlikely to be caused by the changes in them.

The different effects of aerosols on mixed-phase and liquid clouds induce very distinctive responses of precipitation rates to the increase of AI. The precipitation rate increases with AI for mixed-phase clouds, corresponding to the decrease in cloud top temperature with AI. However, the rain rate decreases for liquid clouds as AI increases. This result indicates that aerosols may not only suppress precipitation through microphysical and radiative processes, but also enhance precipitation through complex

thermodynamic processes. This phenomenon has a large impact on the overall distribution of precipitation rates. Our result shows that heavy rain becomes more frequent and light rain becomes less frequent in polluted conditions compared with that in clean conditions.

Chapter 4 : Validation and Understanding of MODIS Aerosol Products Using Ground-based Measurements from the Handheld Sunphotometer Network in China

4.1. Introduction

Besides aerosol indirect effects such as the albedo effect, aerosol radiative forcing is also widely recognized as one of the largest sources of uncertainty among all sources of forcing to the Earth's climate system [*IPCC 2007*]. Reduction of this uncertainty requires a substantially improved knowledge of basic aerosol optical properties on a global basis, such as AOT, single scattering albedo (SSA) and asymmetry factor, especially over aerosol-laden regions.

This task cannot be fulfilled without the use of remote sensing data which provides global coverage on a continuous basis. While numerous global aerosol products exist, the majority are only available over dark oceans, e.g., those retrieved from conventional meteorological sensors such as the AVHRR [*Nakajima and Higurashi*, 1998; *Mishchenko et al.*, 1999; 2003; *Stowe et al.*, 2002; *Ignatov et al.*, 2004], and the Sea-viewing Wide Field-of-view Sensor (SeaWiFS) [*Wang et al.*, 2005]. Due to the small number of spectral channels and thus highly limited information content, the datasets usually contain large uncertainties partially due to inherent assumptions made in the retrieval algorithms [*Jeong et al.,* 2005a, b; *Lee et al*., 2009; *Li et al*., 2009]. The major issues in these products include calibration, cloud screening, selection of aerosol models and the surface effect [*Li et al*., 2009]. AOT retrievals are available over land from MODIS [*Kaufman et al.*, 1997a; *Remer et al.*, 2005], the Multi-Angle Imaging Spectroradiometer (MISR) [*Diner et al.*, 2005; *Kahn et al.*, 2005], the Total Ozone

Mapping Spectrometer (TOMS) [*Torres et al.*, 2002] and the Sea-viewing Wide Field-of-view Sensor (SEAWIFS) [*Hsu et al.*, 2004]. Validation of the MODIS AOT retrievals against the global ground-based measurements from the Aerosol Robotic Network (AERONET) [*Holben et al.*, 1998] generally show inferior quality over land [*Chu et al.*, 2002; *Ichoku et al.*, 2002] than over the oceans [*Remer et al.*, 2005]. Two factors were identified as causes of the bulk of the errors in satellite measurements, namely, surface reflectance and aerosol type governing, in particular, aerosol absorption. Validation of the MODIS AOT retrievals against the global ground-based measurements from the Aerosol Robotic Network (AERONET) [*Holben et al.*, 1998] generally show the MODIS/AERONET regression of AOT over land [*Chu et al.*, 2002; *Ichoku et al.*, 2002] resulted in slope less than one and positive offsets. The former indicates that MODIS tends to underestimate the aerosol optical depth for large AOD, which means the aerosol models used in Collection 4 (C4) may not be able to truly represent the aerosol conditions. The latter means that even there are no aerosols in the atmosphere (AOD observed by AERONET is zero), MODIS still gets positive retrievals, probably due to the error of the surface reflectance.

The surface albedo problem is related to bright surfaces that induce erroneous estimation of surface albedo values. The current MODIS algorithm cannot perform aerosol retrievals over bright surfaces. Three approaches can be used to overcome this problem. One is the MISR approach which relies on the contrast due to variable pathlengths [*Kahn et al.*, 2005]. The second approach is to use reflectances at shorter wavelengths where the surface albedo is generally darker [*Hsu et al.*, 2004]. The third

approach involves using a combination of measurements made in the ultraviolet and visible regions [*Jeong and Li*, 2005a].

To remedy the identified problems, substantial modifications were introduced to the second-generation aerosol retrieval algorithm applied to MODIS data [*Levy et al*., 2007a,b]. In C4 (pervious version), the surface reflectance of blue and red bands is considered one-quarter and one-half of the surface reflectance of SWIR (short wave infrared) band. However, in Collection 5 (C5, the new version), the surface reflectance of blue and red band is considered as a function of surface reflectance of SWIR band and the function depends on the scattering angle and the Normalized Difference Vegetation Index (NDVI). The aerosol models used in C5 are also modified based on AERONET observation. Six aerosol models are derived to represent the whole AERONET dataset. They are the two models that represent very clean conditions, one coarse-dominated model and three fine mode models. Since only limited bands are used to retrieve aerosols over land, it is impossible to decide which fine mode should be used. So the fine mode model is assigned before retrieval based on the location and seasons. The coarse model used in C5 is non-spherical model instead of spherical model used in C4, and the atmosphere is no longer considered transparent to SWIR band in C5 algorithm. However, the modifications hinge on AERONET measurements that provide essential aerosol optical data for the correction of the atmospheric effects. Since the AERONET sites are mostly located in the US and Europe, improvements may thus have regional biases depending on the amount of data used in tuning the algorithm. Unfortunately, heavy aerosol loading usually occurs over under-sampled regions of the globe whose impact on the estimation of global aerosol radiative forcing is more significant than elsewhere.

China is among the heavy aerosol-laden regions of the world with few ground-truth measurements [*Li C.C et al*., 2003; *Li et al*., 2004; *Chaudhry et al*., 2007]. Prior to 2004, only sporadic aerosol data were available for short periods of time (a couple of months), together with one AERONET site in the center of Beijing [*Eck et al*., 2005; *Xia et al*., 2005, 2006]. Thanks to the East Asian Study of Tropospheric Aerosols: an International Regional Experiment (EAST-AIRE), established in 2004 as a joint research venture between US and China [*Li et al*., 2007b], continuous aerosol measurements have been made across China using both automated and hand-held sunphotometers. The automated Cimel-318 instruments are deployed at three sites as part of the AERONET. They have collected data continuously since 2004 in northern (Xianghe, near Beijing), southeastern (Taihu, near Shanghai) and western (Namco, near Lhasa) China. A preliminary analysis of AERONET data revealed some distinct aerosol features unique to the region [*Li et al*., 2007a]. This study will make use of hand-held sunphotometers, simply referred to as hazemeters [*Hao et al.*, 2005], data that have a greater spatial coverage but less optical information. The data were acquired at 25 stations across China as a part of the EAST-AIRE observation network [*Xin et al.*, 2007]. A detailed description of the data is given in the following section.

The main objectives of this study are to evaluate both versions of the MODIS aerosol product and to understand any discrepancies between satellite retrievals and ground observations. Given the meagerness of ground-based measurements, the evaluation and understanding of any problems are crucial to improve satellite retrievals in this region in order to fill a big gap existing in global aerosol-related studies. This chapter is structured as follows. The data sets employed are introduced in section 4.2.

Section 4.3 compares the two latest versions of the MODIS aerosol products. Section 4.4 presents comparisons between satellite retrievals and ground measurements. Also reported in this section are the investigations into the causes for the discrepancies with the main focus on surface reflectance and single scattering albedo (SSA). The study is concluded in section 4.5.

4.2. Data

4.2.1 MODIS Aerosol Products

MODIS instruments are on board two NASA Earth Observation System (EOS) platforms, the Terra and Aqua satellites. The Terra satellite is on a descending orbit flying southward across the equator around 10:30 local sun time, while the Aqua satellite is on an ascending orbit flying northward around 13:30 local sun time. MODIS data are coincident with CSHNET hazemeter data acquired from 10:00 to 14:00 on a half-hourly basis. While the MODIS has 36 channels ranging from 0.41 to 14 μm at different spatial resolutions (250 m, 500 m and 1 km), seven channels are used for aerosol retrievals, namely 0.47, 0.55, 0.66, 0.86, 1.24, 1.67 and 2.12 μm. Three of the channels (0.47, 0.66 and 2.12 μm) are used for retrieving aerosol parameters over land, while the remaining channels are used for retrieving aerosol parameters over ocean, cloud masking and other procedures.

It is worth noting that the cloud screening method used for aerosol retrievals [*Remer et al*., 2005; *Martin et al*., 2002] is not the same as that used for generating MODIS cloud products [*Ackerman et al*., 1998]. This is to avoid misclassification of heavy aerosols as clouds. After nominal cloud screening, the remaining potentially clear

pixels are subject to further screening by eliminating the brightest 50% and darkest 25% of the pixels over land in an attempt to eliminate cloud contamination and cloud shadowing effects. As a result, the resolution of the MODIS aerosol product is degraded to 10 km.

There are two MODIS aerosol retrieval algorithms developed for use over oceans [*Tanre et al*., 1997] and land [*Kaufman et al*., 1997a]. This study is concerned with the land algorithm that has been modified the most since the original version was proposed before launch [*Kaufman et al*., 1997a]. The algorithm has been improved over the years with two milestone versions described in *Remer et al.* [2005] and *Levy et al.* [2007a], leading to two distinct products C4 and C5. C4 provides the most complete global aerosol data retrieved from Terra and Aqua platforms since their launches, with an expected uncertainty of 0.05±0.15AOT at 0.55μm. While the expected accuracy is met in general, significantly larger errors are found in certain regions [*Chu et al*., 2002; *Remer et al*., 2005; *Levy et al*., 2005]. An outstanding common problem was a systematic overestimation of AOT under the condition of low aerosol loading, in comparison with the AERONET ground-based retrievals. On a global scale, the two types of AOT data are related by $AOT_{MODIS} = 0.1 + 0.9\ AOT_{AERONET}$. Over regions where there are no, or few, ground measurements that could otherwise be used to train the algorithm, errors remain largely unknown.

In general, AOT retrievals are mainly influenced by two factors: surface reflectance and aerosol type. Except in the presence of large coarse-mode aerosols, atmospheric transmittance due to aerosols is generally high, allowing the retrieval of surface reflectance at longer wavelength channels. In C4 retrievals, the MODIS algorithm

assumes constant ratios of surface reflectance at red and blue channels versus that at 2.12 μm. In C5 retrievals, the ratios are modified to be functions of the scattering angle and the normalized difference vegetation index derived from reflectances at 1.24 and 2.12 μm channels [*Levy et al*., 2007a]. Aerosol type selection was also refined by taking advantage of aerosol optical properties, especially the single scattering albedo, retrieved from the AERONET [*Levy et al*., 2007b]. Since the AERONET has a highly variable density around the world, the improvement varies considerably from region to region. For example, a fixed model with SSA=0.9 is still assumed over the vast territory of China except along a very narrow strip in the east coastal region.

4.2.2 Hazemeter Data

The hand-held sunphotometers have been deployed in other field campaigns such as the SAFARI in Africa [*Hao et al*., 2005]. A nation-wide aerosol observation network, the Chinese Sun Hazemeter Network (CSHNET), was established in 2004 and includes 25 stations distributed across China (Fig. 4.1) representing different ecological and geographic regions [*Xin et al*., 2007]. Daily continuous measurements of aerosol optical depths at 3 wavelengths (405 nm, 500 nm, 650 nm) have been made since August 2004. This is the first, large-scale attempt at collecting aerosol observations in China. Before this, only spotty measurements were made.

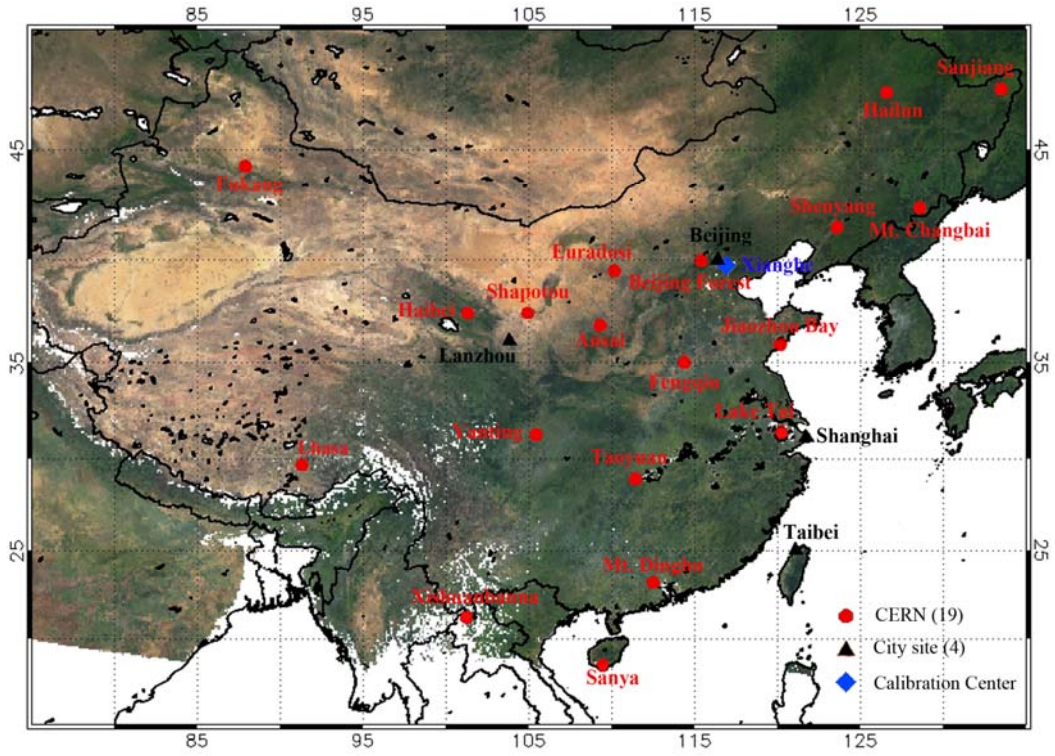

Fig. 4.1. Location of hazemeter sites in China

Many new features concerning the spatial and temporal variations of AOT and particle size were found through the analyses of data acquired so far [*Xin et al*., 2007]. Those relevant to this study are summarized as follows. Overall, AOT is larger in central and southeast China. There are many anthropogenic sources of aerosols in southeast China. In winter, the majority of observation sites in northern China are under the influence of biomass and fossil fuel burning which produce heavy loadings of fine-mode aerosols. From spring to summer, many eastern stations experienced rises in AOT and decreases in Angstrom exponent, α, due to the humidity-swelling effect [*Jeong et al*., 2007]. Desert or desert-like stations in western China are more affected by the coarse-mode mineral dust aerosols, with a maximal loading in spring. Many sites in eastern

China show aerosol properties characteristic of mixtures of pollutants, mineral aerosols, and smoke aerosols.

In addition to initial calibrations using the AERONET facilities at the NASA Goddard Space Flight Center, the hazemeters were further calibrated against the Cimel sunphotometer in China from time to time by means of both instrument inter-comparisons and the Langley method [*Xin et al*., 2007]. The results show the slope of the regression line between the two sets of AOD is close to 1.0 at 405 nm, 500 nm and 650 nm. The hazemeter results are generally consistent with the CIMEL results with disagreements on the order of 2% to 6%. But overall the Hazemeter tends to over predict AOD. The latest systematic calibration of all hazemeters deployed in China was carried out in August 2006 at Lhasa through side-by-side comparisons against a newly calibrated Cimel-318 sunphotometer. Overall, the hazemeters degraded by about 10% over two years, much less than the discrepancies found between satellite and ground retrievals as shown in this study.

The hazemeter data are matched with the satellite retrievals in time and space following the method of *Ichoku et al.* [2002]. Data from the ground-based hazemeters were averaged within 30 minutes of the satellite overpass times and are compared with the means of the MODIS retrievals within a 25-km radius around each ground station.

4.3. Comparisons between the two collections of MODIS aerosol product

The distributions of the yearly mean AOT from MODIS C4 and C5 during one whole year of 2005, and their differences are presented in Fig. 4.2. Overall, AOT shows rather dramatic changes across China. Large AOT (>0.7) occurs over east-central China

and the Sichuan basin. The lowest AOT (<0.2) is seen over the Qinghai-Tibet plateau. Intermediate values (0.3~0.6) are observed in southern China and northwest China. Detailed regional features will be discussed later based on hazemeter ground observations. The two versions of the MODIS products have substantial differences that are larger in the north than in the south. Over almost half of China in the north, their differences range from –20% to –50%. In general, the C5 retrievals are less than the C4 retrievals, as is seen more clearly in the scatterplot and histogram of Fig. 4.3a and 4.3b. Peaks in the histograms of AOT are similar (~0.28) for both product versions, but the C4 data have a greater number of AOT>0.3 than the C5 data. The majority of the differences fall within -0.2~0.0, as seen from the histogram of their differences in Fig. 4.3c.

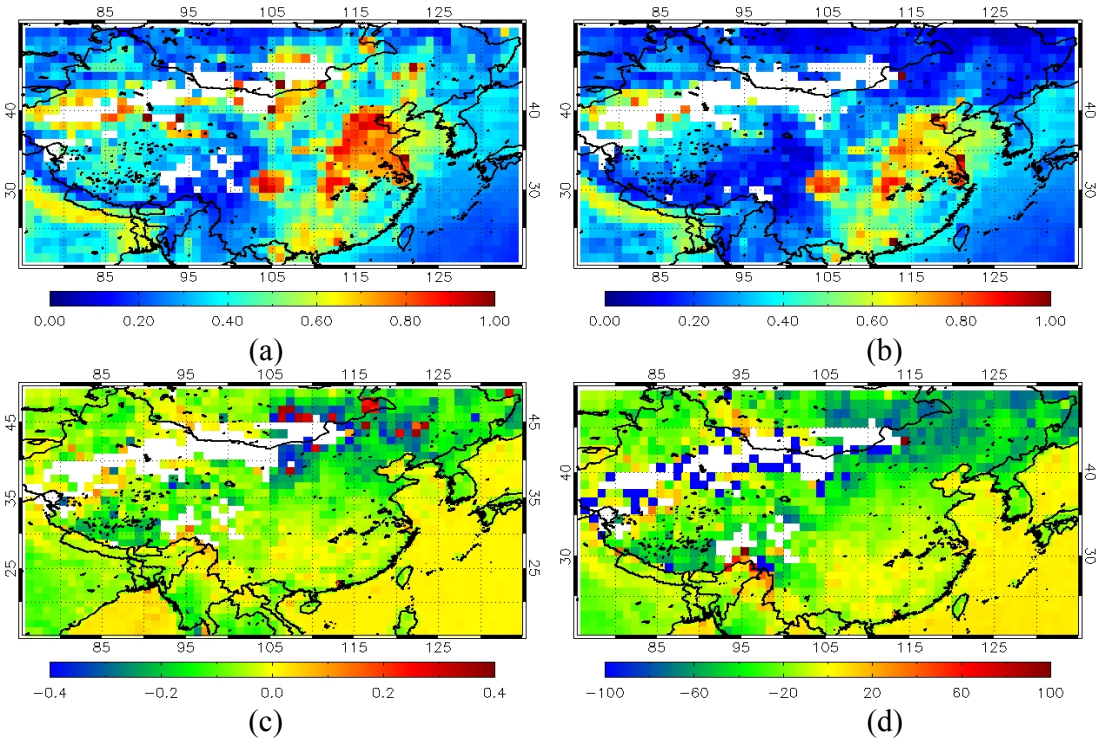

Fig. 4.2. Annual mean AOT from MODIS collection C4 (a), C5 (b), their absolute difference (C5-C4) (c), and relative difference (C5-C4)/C4×100 (%).

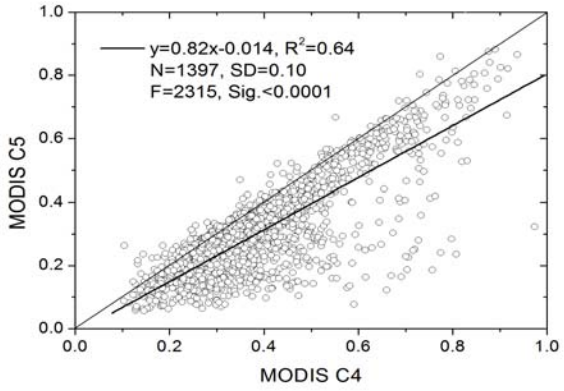

(a)

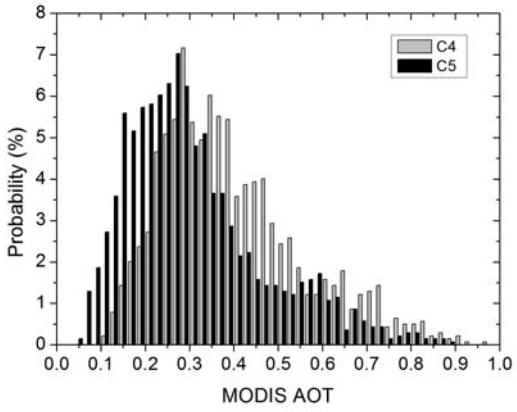

(b)

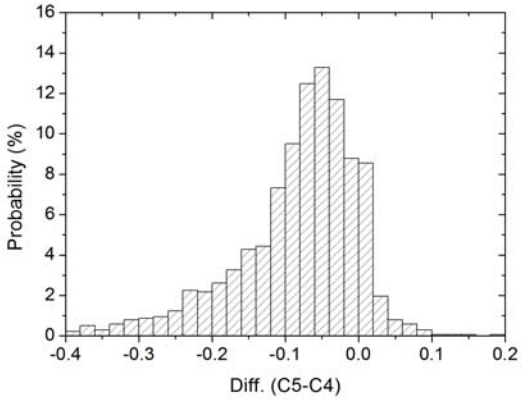

(c)

Fig. 4.3. (a) Scatterplot of AOT from MODIS collections C4 and C5; (b) Histogram of AOT from MODIS collections C4 and C5; (c) Histogram of AOT differences between MODIS collections C4 and C5.

Given that surface reflectance plays an important role in aerosol retrievals over land, surface reflectances across the region were estimated from MODIS Level 1 seasonal composites of minimum reflectances that used nominal atmospheric corrections employing surface topography, an assumed AOT=0.2 and an aerosol of the continental type. From the seasonal minimum reflectance data, annual minimum reflectance at the two visible channels (0.47 μm and 0.66 μm) and SWIR channel (2.12 μm) are shown in Fig. 4.4a, b, and c. While the values are not precise due to assumed aerosol properties, it is sufficient to view their gross spatial patterns. Evident is the very bright surface covering a large fraction of northern and northwest China, rendering the region unsuitable, or marginally suitable for aerosol retrievals, especially in the red channel.

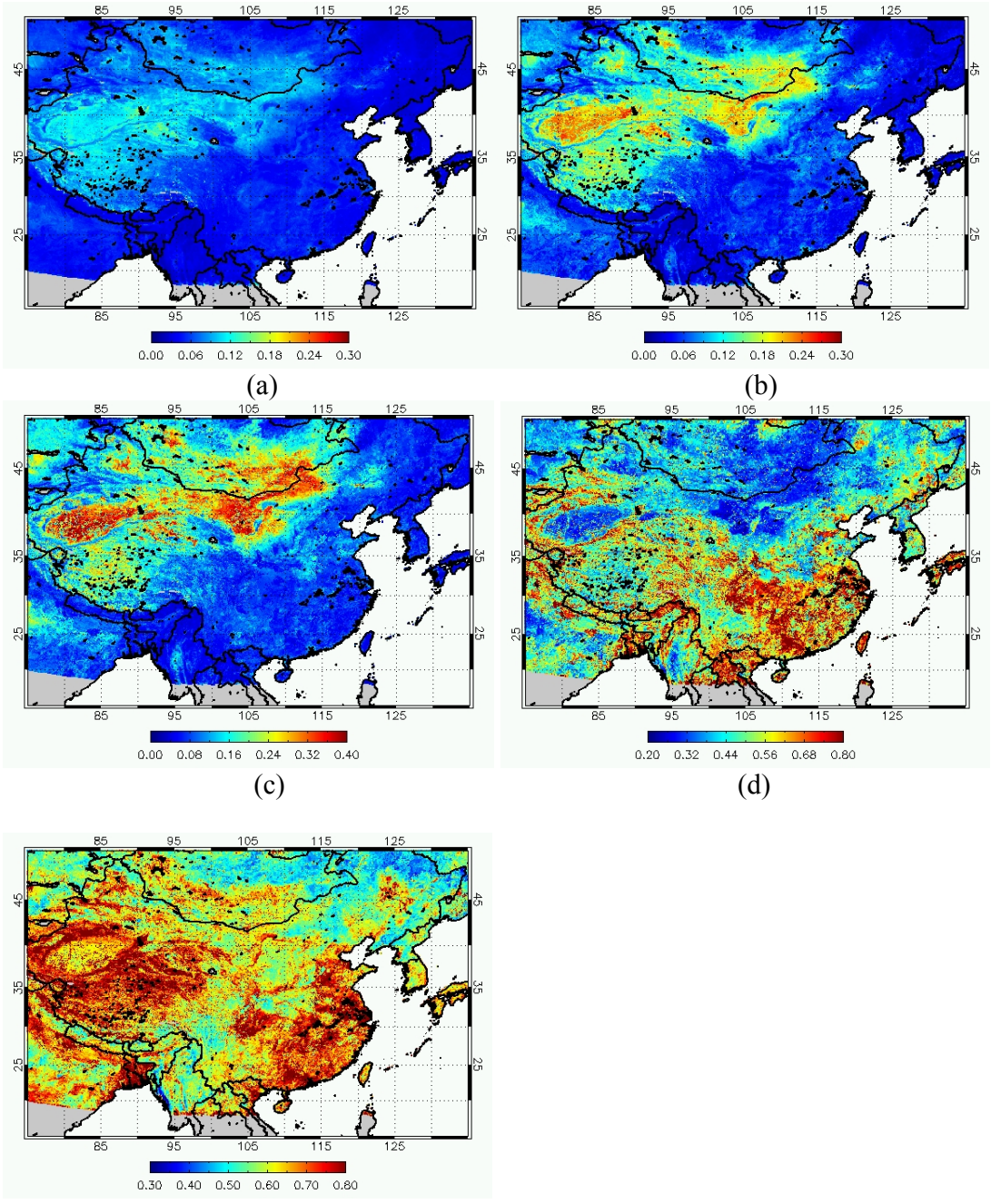

Fig. 4.4. Annual minimum reflectance at 0.47 μm (a), 0.66 μm (b), and 2.12 μm (c), and VIS/SWIR ratios of 0.47/2.12 (d), 0.66/2.12 (e).

As stated earlier, the MODIS algorithm retrieves surface reflectance at shorter wavelengths (0.47 μm and 0.66 μm) from the longer wavelength (2.12 μm). Fixed

empirical ratios ($\rho_{0.47}/\rho_{2.12}$=0.25 and $\rho_{0.66}/\rho_{2.12}$ =0.5) were used in the C4 algorithm [*Kaufman et al*., 1997b]. The ratios over the study area are plotted in Fig. 4.4c and 4d. These two figures show strong spatial variations with values differing significantly from the constants used in the C4 algorithm. In general, the ratios are lager than the assumed values, leading to underestimation of surface reflectances and overestimation of AOT. This is especially the case for the blue band ratio that is quite different from the assumed value over the study region. Even for dark pixels ($\rho_{2.12}$< 0.2) and dense green vegetated areas as seen in Fig. 4.4c and Fig. 4.1, the ratios deviate significantly from the assumed values.

To estimate more precisely the reflectances and their ratios, clear-sky MODIS data are matched with ground measurements for AOT<0.2. To do a precise atmospheric correction, we would need a complete set of aerosol optical properties, namely, AOT, single scattering albedo and asymmetry factor. Since the effect of assuming different aerosol models on atmospheric correction decreases with decreasing AOT, the correction was done only for AOT<0.2 and assuming the continental aerosol model. In a sensitivity test, correction was performed for AOT<0.1 but little difference in the results was found.

The resulting surface reflectances at the blue, red and SWIR bands are shown in Fig. 4.5 for all the sites and for each season. The reflectances have linear relationships and the correlation coefficient is much larger between the red and SWIR channels than between the blue and SWIR channels. The data scattering around the linear regression lines indicates retrieval uncertainties, which are substantial for the blue channel. The regression coefficients, slopes and the offsets are subject to change with season, with the

greatest correlation found during the summer and the worse correlation found during the winter.

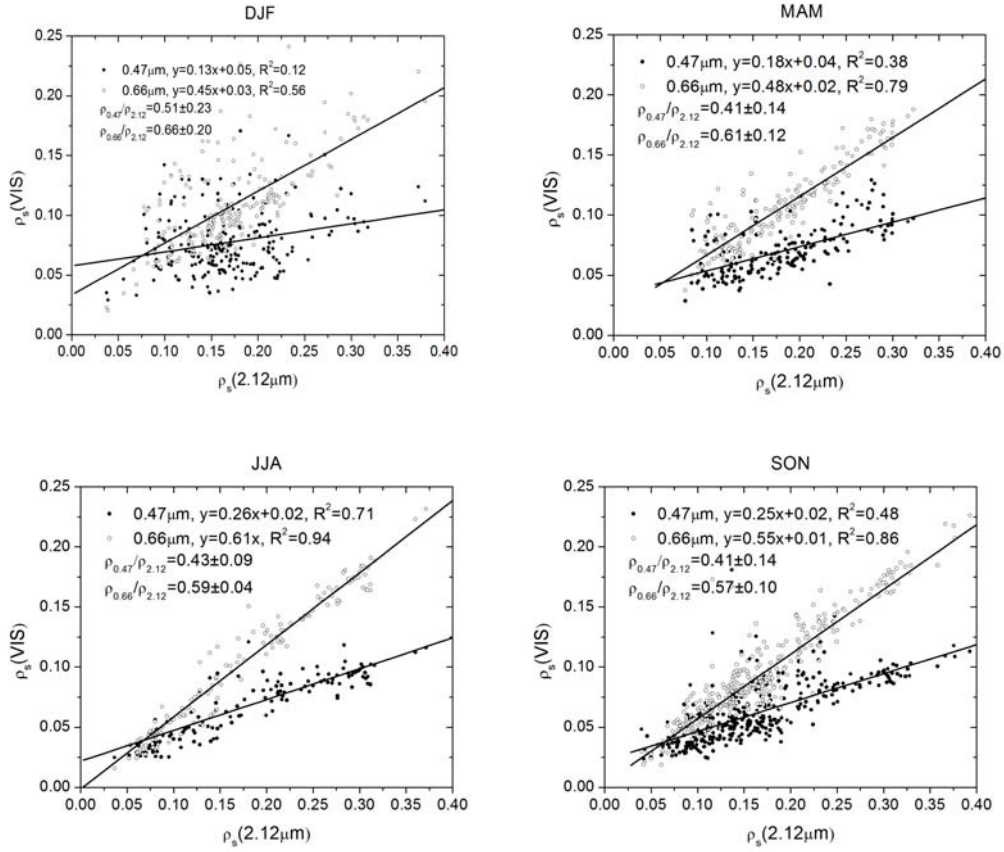

Fig. 4.5. Relationships between surface visible and SWIR reflectances derived from MODIS TOA radiances using atmospheric corrections when ground-based hazemeter AOT<0.2. Linear regression best-fit lines are plotted for four seasons.

As demonstrated in *Levy et al*. [2007a], the variation of the ratios is partially caused by their dependence on the vegetation condition and the viewing geometry. In order to validate the parameterizations used to account for these two factors, the ratios were compared with the vegetation index and the scattering angle as shown in Fig. 4.6. Also plotted are the linear regression fit between the ratio and the two variables, namely, $NDVI_{SWIR}$ and the scattering angle (Θ), defined as follows:

$$NDVI_{SWIR} = \frac{\rho_{1.24} - \rho_{2.12}}{\rho_{1.24} + \rho_{2.12}}$$

$$\Theta = \cos^{-1}(-\cos\theta_0 \cos\theta + \sin\theta_0 \sin\theta \cos\phi)$$

where θ_0, θ and ϕ are the solar zenith, viewing zenith and relative azimuth angles, respectively. The reflectance ratios have moderate correlations with the two variables, but the dependence is weak for the scattering angle.

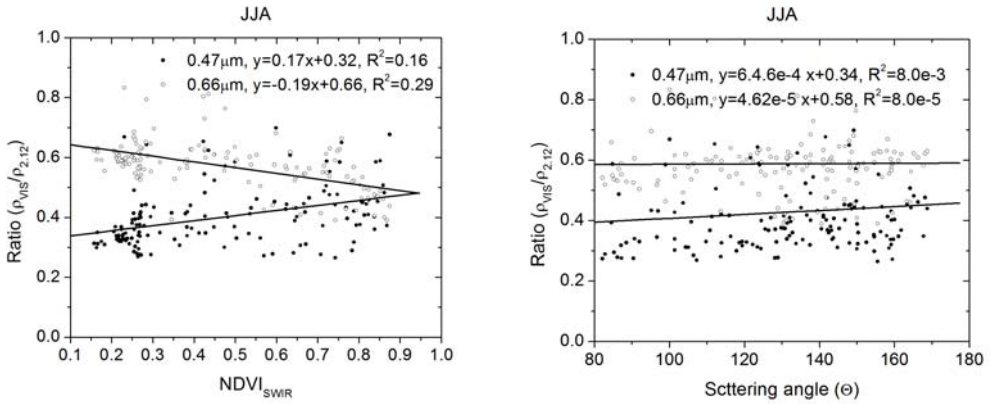

Fig. 4.6. Scatterplot of the reflectance ratios (VIS/SWIR) versus the NDVISWIR (left) and scattering angle (right).

4.4. Comparisons between AOT from the Hazemeters and MODIS

Fig. 4.7 is a scatterplot showing the comparisons of AOT from ground measurements at all sites in China (differentiated by different symbols) and the MODIS retrievals AOT from Collection 4 (left) and Collection 5 (right), respectively. Clearly, the Collection 5 aerosol product is superior to the Collection 4 aerosol product. In the comparison with Collection 4, there is a large positive offset (0.179) and small slope less than 1 (0.74), consistent with the results from previous studies. When the aerosol optical

depth is small, the satellite-retrieved AOT is overestimated. In comparison with Collection 5, the offset is much smaller (0.047), and slope is close to unity (0.98). The correlation coefficients are 0.66 (R^2=0.44) to 0.84 (R^2=0.72) for C4 and C5, respectively. Note that the expected error of the MODIS retrieval is given by 0.05±0.15*AOT. About 45.70% of the C4 retrievals fall within this range, which increases to 56.74% in the C5.

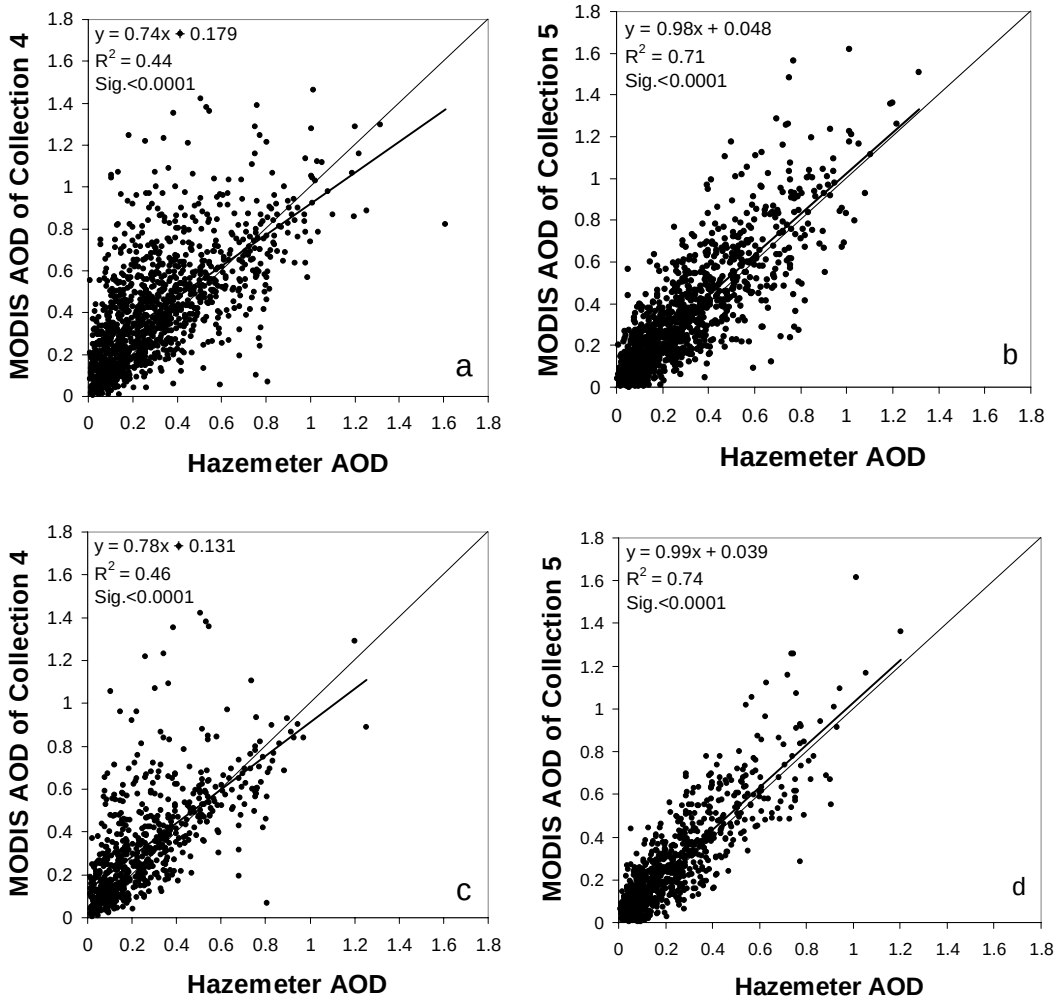

Fig. 4.7. Comparison of MODIS AOT from C4 (left) and C5 (right) with ground-based hazemeter measurements made at all hazemeter stations. The lower two panels show the same comparisons but for selected data based on standard deviation (see text for details).

Another useful measure of the data quality is the variability of AOT as denoted by the standard deviations (SD) computed from samples over space (MODIS/50km) and time (hazemeters/0.5 hour). In principle, AOT over a 50-km^2 domain does not vary much except over regions near major emission sources, which is not the case for the hazemeter sites located in remote areas. Were the variability driven by the natural variability, SDs from MODIS and hazemeters would have similar distributions and magnitudes, provided that the spatial and temporal scales are matched. Fig. 4.8 shows three histograms of the SD computed from C4 and C5 and the hazemeters. There are marked differences between the histograms in terms of both distribution and magnitude. The SDs from the two MODIS products are substantially larger than that from the hazemeters, while SDs from the C5 are significantly smaller than the C4. The long-tail of SD from MODIS results primarily from the artifacts of the retrievals that are addressed in subsequent sections. While the vast majority of the SD computed from hazemeter AOD data are very small (e.g. 80% with SD<0.03), a handful of data do have exceptionally large SD for which the data quality are questionable. If we limit our analyses to SD<0.05 for hazemeter data, and SD<0.1 for MODIS data, the agreements between satellite retrievals and ground observations is improved, as seen from the lower two panels of Fig. 4.7, e.g. the R^2 for C5 increasing from 0.72 to 0.75, *S* from 0.98 to 0.99, and *O* decreasing from 0.048 to 0.039.

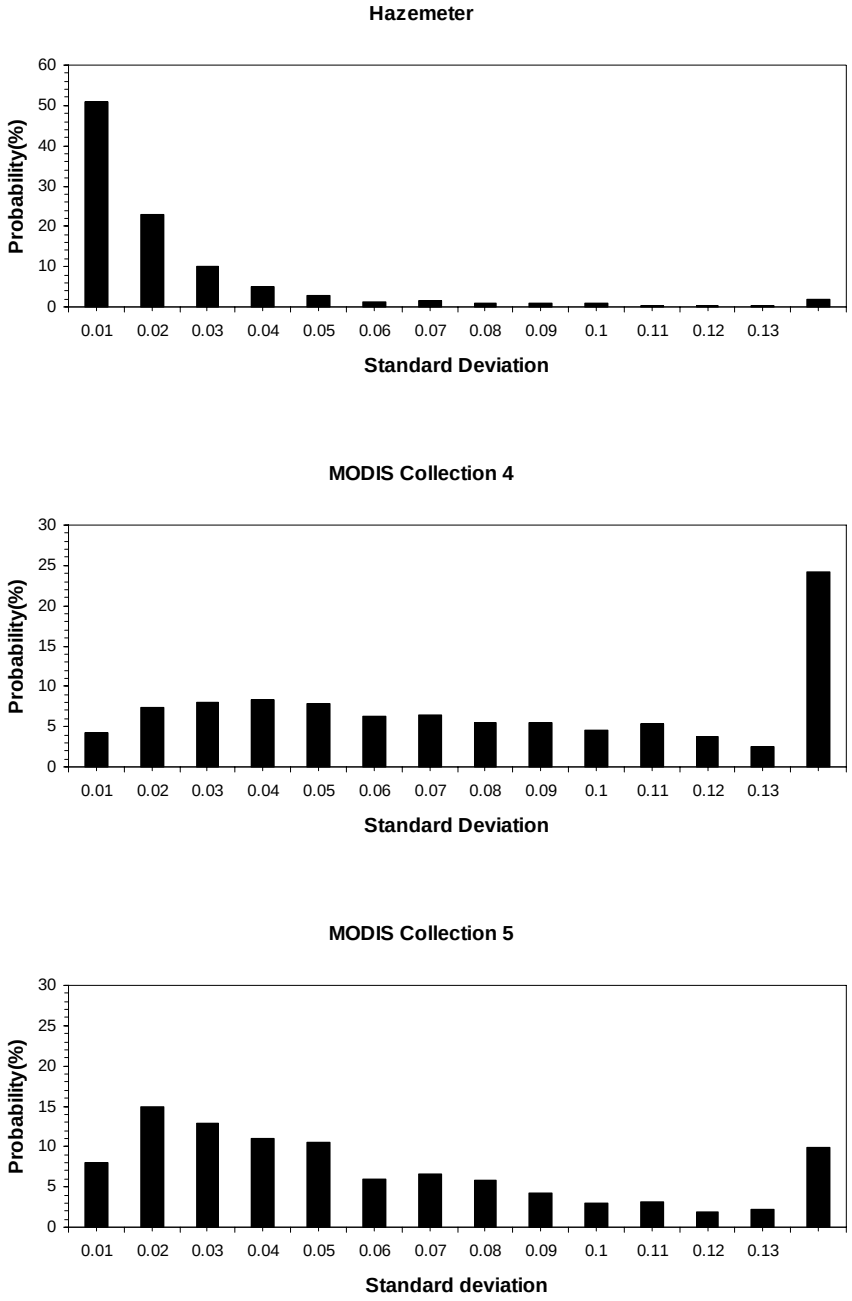

Fig. 4.8. Histograms of the probability of occurrence for the standard deviation of AOD from hazemeters in time, and MODIS collection 4 and 5 data in space.

As expected, the performance of the MODIS retrieval varies from station to station.

Fig. 4.9 presents the statistics of the comparisons with MODIS Collections 4 and 5 for individual sites. For almost all sites, the correlation is better for C5 than for C4, with the mean R^2 value increasing from 0.37 for C4 to 0.55 for C5. The values for some sites, for example, Beijing Forest and Xianghe, are close to 0.9. But for some sites, especially the desert sites and sites with complicated land surfaces, the correlation is poor. Significant improvement by the C5 is apparent in terms of the slope and offset as well. Some extremely large or small values for slope, for example Haibei (-0.33) and Eerduosi (2.13), have been improved to reasonable values close to unity. The mean of the slope increases from 0.74 to 0.95; the mean of the offset decreases from 0.176 to 0.055.

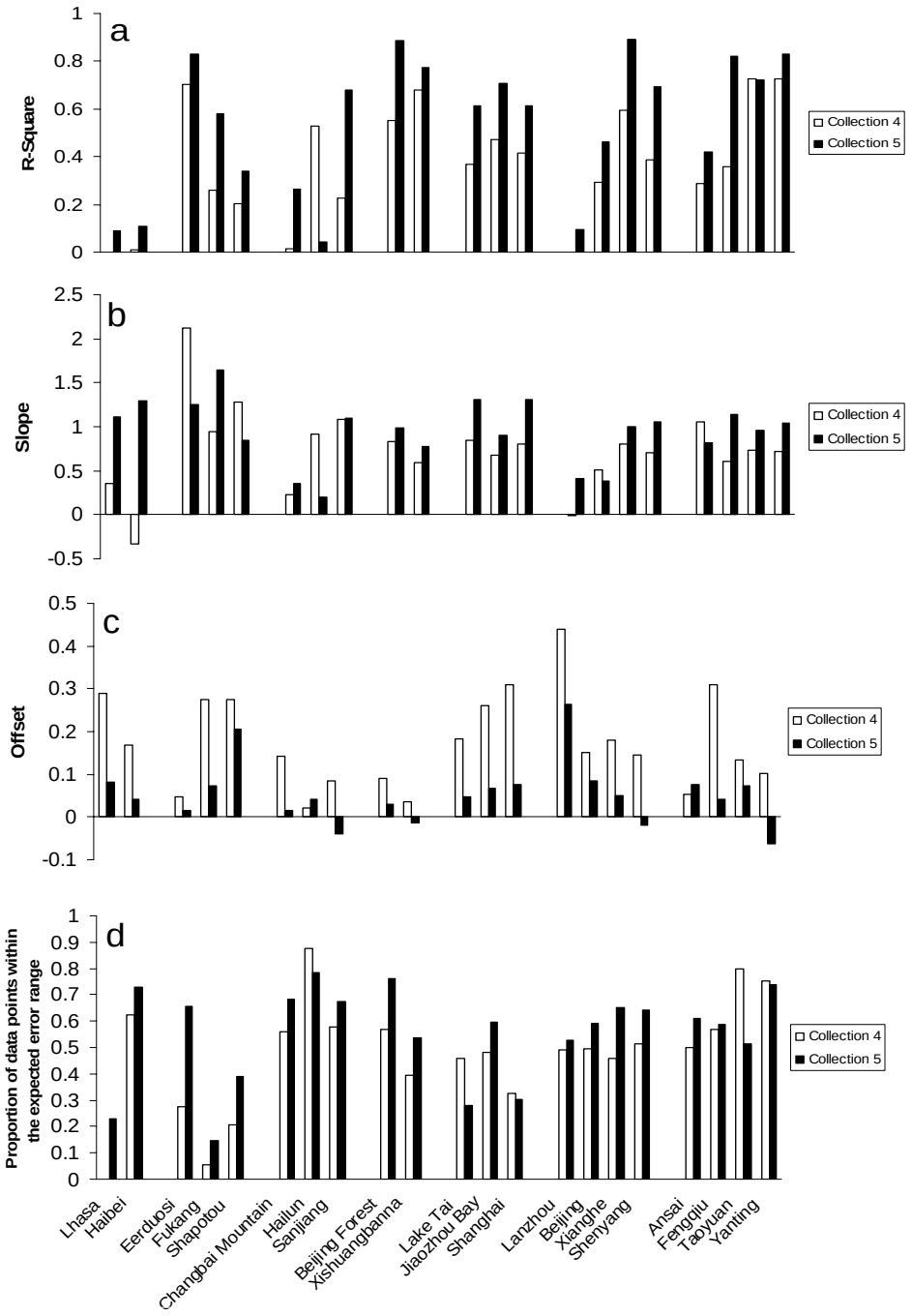

Fig. 4.9. The statistics of linear regressions between MODIS and hazemeter data at individual sites: the square of the correlation coefficients (a), slope (b), offset (c). (d) The probability of data falling within the expected error range.

We further classified the hazemeter sites into different groups based on ecosystem to see how different land surfaces affect the retrievals. Results for four distinct categories are presented here: desert, forest, urban, and suburban and agricultural. Other small miscellaneous categories such as lakes and the Tibetan plateau were also analyzed but not shown.

The most common land cover type is farmland located in either remote agricultural areas or near urban areas, referred to as suburban regions in this study. Results obtained from six farmland sites are shown in Fig. 4.10. The Xianghe and Shenyang sites are located near urban areas, while the remaining four sites are in remote areas of central China dominated by farmland. Overall, the comparisons are encouraging for these sites, as attested by the high correlation coefficients, small offsets and slopes close to unity. The best results are found over Xianghe, presumably due to the homogeneous surface reflectance and relatively stable aerosol properties.

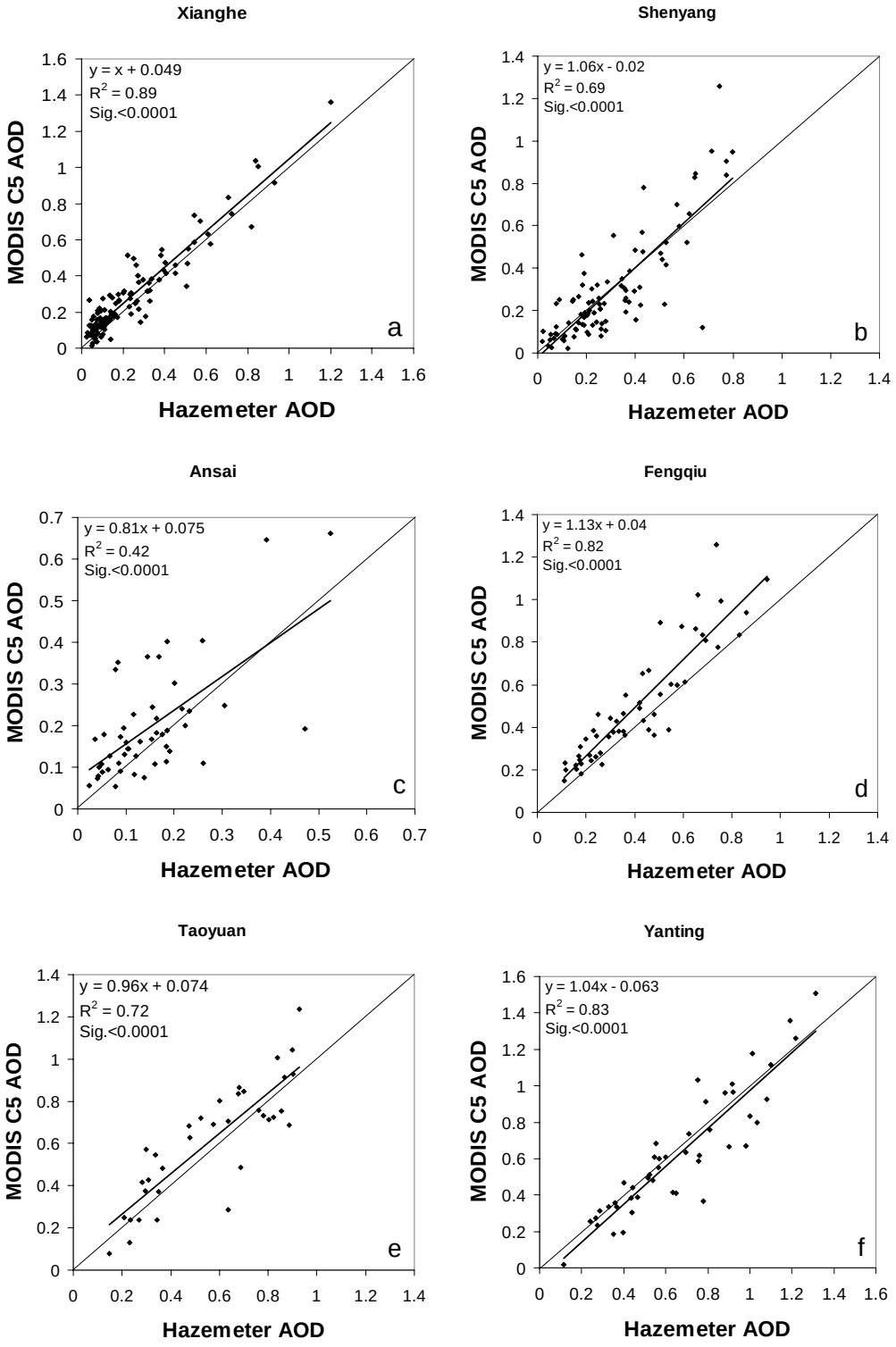

Fig. 4.10. Comparison between MODIS collection 5 and hazemeter AOTs for 6 agricultural and suburban sites.

Much worse results were obtained over two urban sites located near the centers of Beijing and Lanzhou cities, shown in Fig. 4.11. The Beijing urban site is only 70 km away from Xianghe, but over that distance, the surface conditions change from a rural farmland to a complex urban landscape. As a result, the comparison weakens considerably with S=0.38, O= 0.086, R^2=0.46, in comparison to S=0.99, O=0.049, and r^2=0.89 for Xianghe. At the Lanzhou site, the comparison is even worse than in Beijing, with O=0.26, S=0.41, and r^2=0.09. Lanzhou is located in a valley basin surrounded by barren mountains in the heartland of the Northwest Plateau. The city has a high concentration of dust particles mixed with heavy industrial pollutants. The complicated landscape and strong local emissions in most cities pose the greatest challenge in any satellite retrieval of aerosol properties.

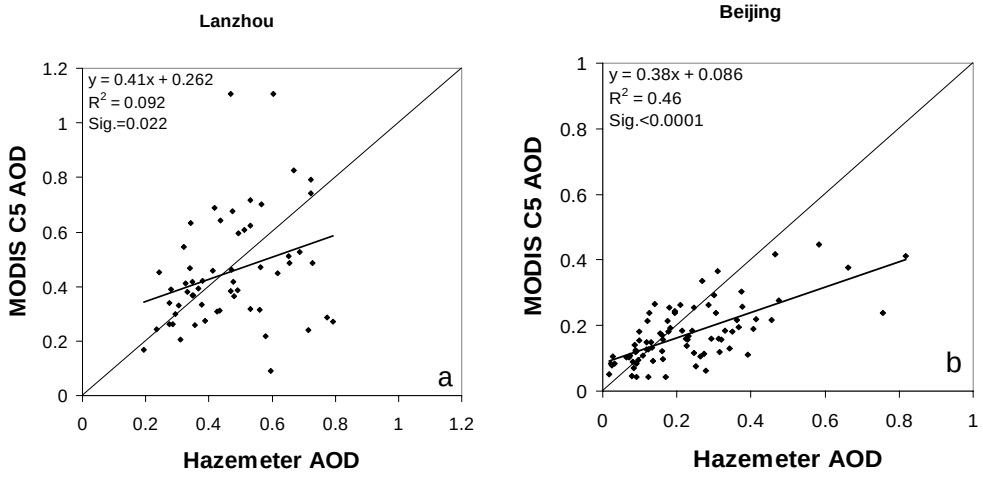

Fig. 4.11. Same as Fig. 4.10 but for two urban sites.

Fig. 4.12 shows the comparisons at three desert or semi-desert sites located in northern China. Although these sites are referred to as desert sites, AOT retrievals can still be performed because the surfaces are not as bright as typical desert surfaces in other parts of the world. The Shapotou site is situated in an arid part of the Tengger Desert. The

Fukang station is located in the transition zone from a glacial environment to a desert environment and the Eerdousi station is situated in a sandy grassland ecosystem. At all sites, AOT was overestimated by the MODIS C5 algorithm by varying degrees, depending on the specific surface condition and aerosol type. Agricultural and pastoral activities take place in the regions surrounding the latter two sites, leading to changes in dominant aerosol types during the year, as inferred from the Angstrom exponent computed from the spectral AOT measured by hazemeters (not shown). Aerosol particles are small during autumn and winter because of biomass burning by the local farmers. The systematic overestimation of AOT indicates biases due to the selection of an incorrect aerosol model in the retrieval. At the Shapotou station, dust aerosols are more persistent given the dominance of dust particles in this more desert-like region.

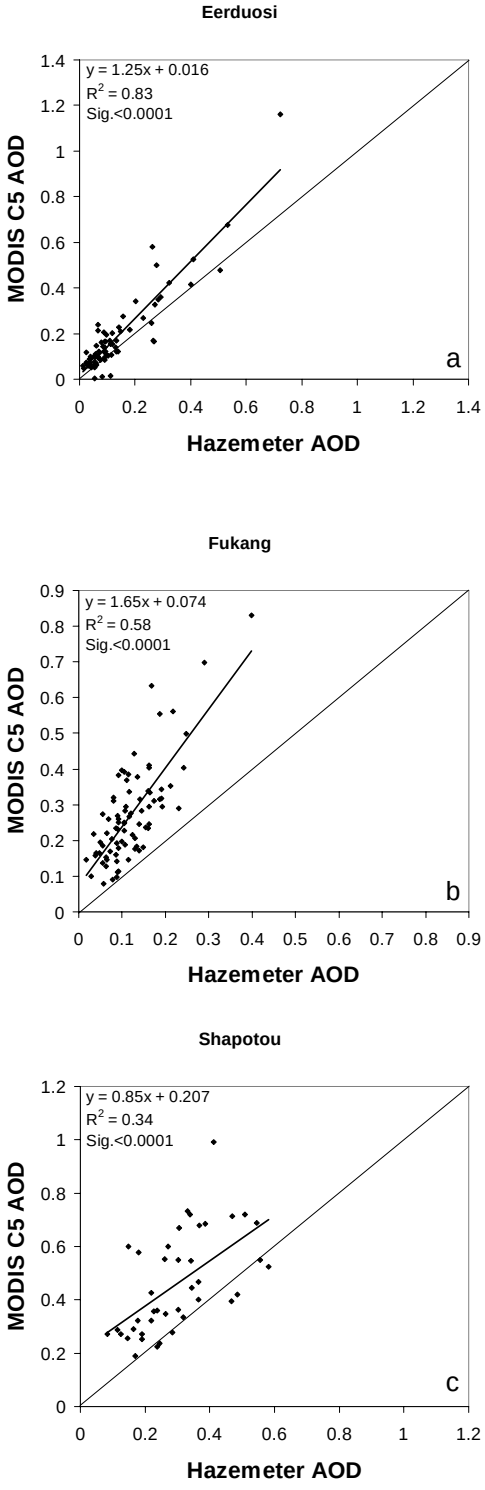

Fig. 4.12. Same as Fig. 4.10 but for 3 desert and semi-desert sites.

Fig. 4.13 shows the comparison results at three forest sites, which are located in different parts of China. One is at the southern tip of China (Xishuangbanna) and the other two are in northern China. The results are mixed due to distinct environments. At Xishuangbanna and Changbai Mountain sites, AOT was underestimated, whereas much better agreement was found over the forest in the westerly remote suburb of Beijing influenced by regional aerosol emission sources from Beijing and Hebei, and also dust transport from Inner Mongolia and Shanxi provinces. At this site, the three indices are R^2=0.89, S=0.98 and O=0.028. Substantially smaller values for the slope are found at the two mountain sites.

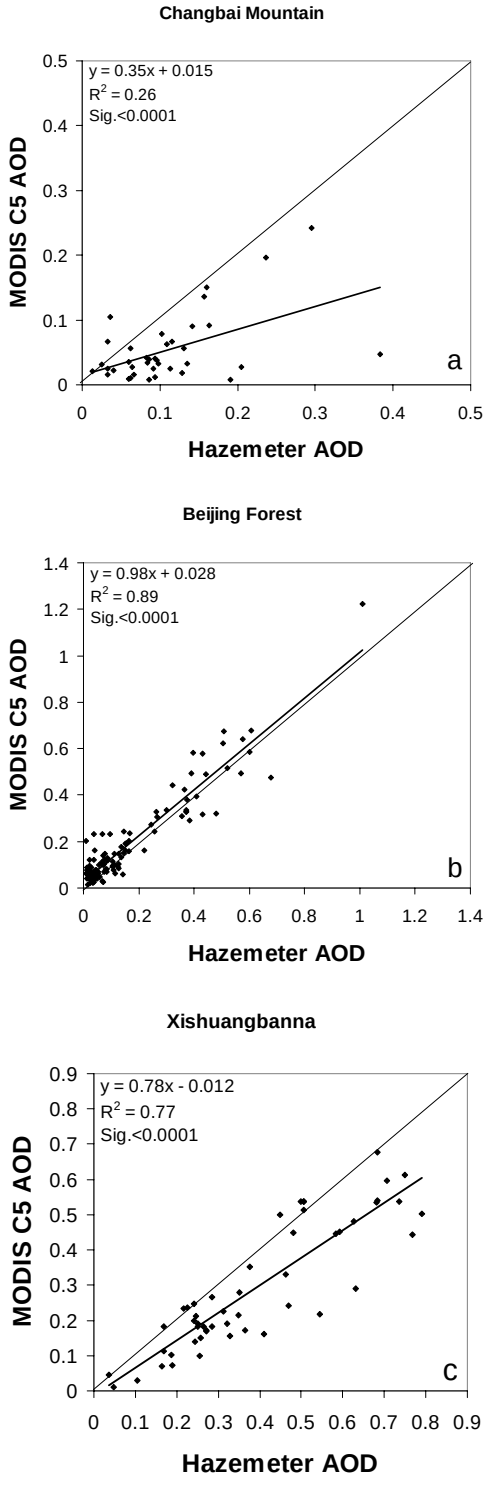

Fig. 4.13. Same as Fig. 4.10 but for 3 forest sites.

As pointed out earlier, the VIS-SWIR conversion is a major source of error. This is more clearly seen in Fig. 4.14 where comparisons for some representative sites are presented. It shows the AOT comparisons for C4 (left panel) and C5 (middle panel), and the corresponding relationships between VIS and SWIR surface reflectances (right panel) obtained after atmospheric corrections. Note that the representation is good in general, as the same/similar features are found for all or most of the sites in the same category. At all three desert and semi-desert sites, surface reflectances are underestimated, causing an overestimation of aerosol optical depth by both C4 and C5 algorithms, although the overestimation is much smaller for C5 than for C4. On the contrary, at the two forest sites (Xishuangbanna and Changbai Mountain), surface reflectances are overestimated and the AOT is underestimated. At the Beijing forest station, surface reflectance is only slightly overestimated (10%), roughly consistent with the good agreement in the AOT comparison. More overestimation (25%) of surface reflectance is found for the Xianghe site, which would lead to an underestimation of AOT. However, the site showed a very good agreement in AOT with O=0.05 and S=1. It is thus conjectured that other factors must come into play to cancel the error incurred by surface reflectance. This turns out to be the overestimation of the single scattering albedo. The site is fortunately equipped with a Cimel sunphotometer from which the single scattering albedo is retrieved for AOT > 0.4 [*Dubovik et al*., 2002]. The annual mean AOT and ω_o at the site are 0.82 and 0.92, respectively, at 500 nm [*Li et al*., 2007a; *Li et al.*, 2007].

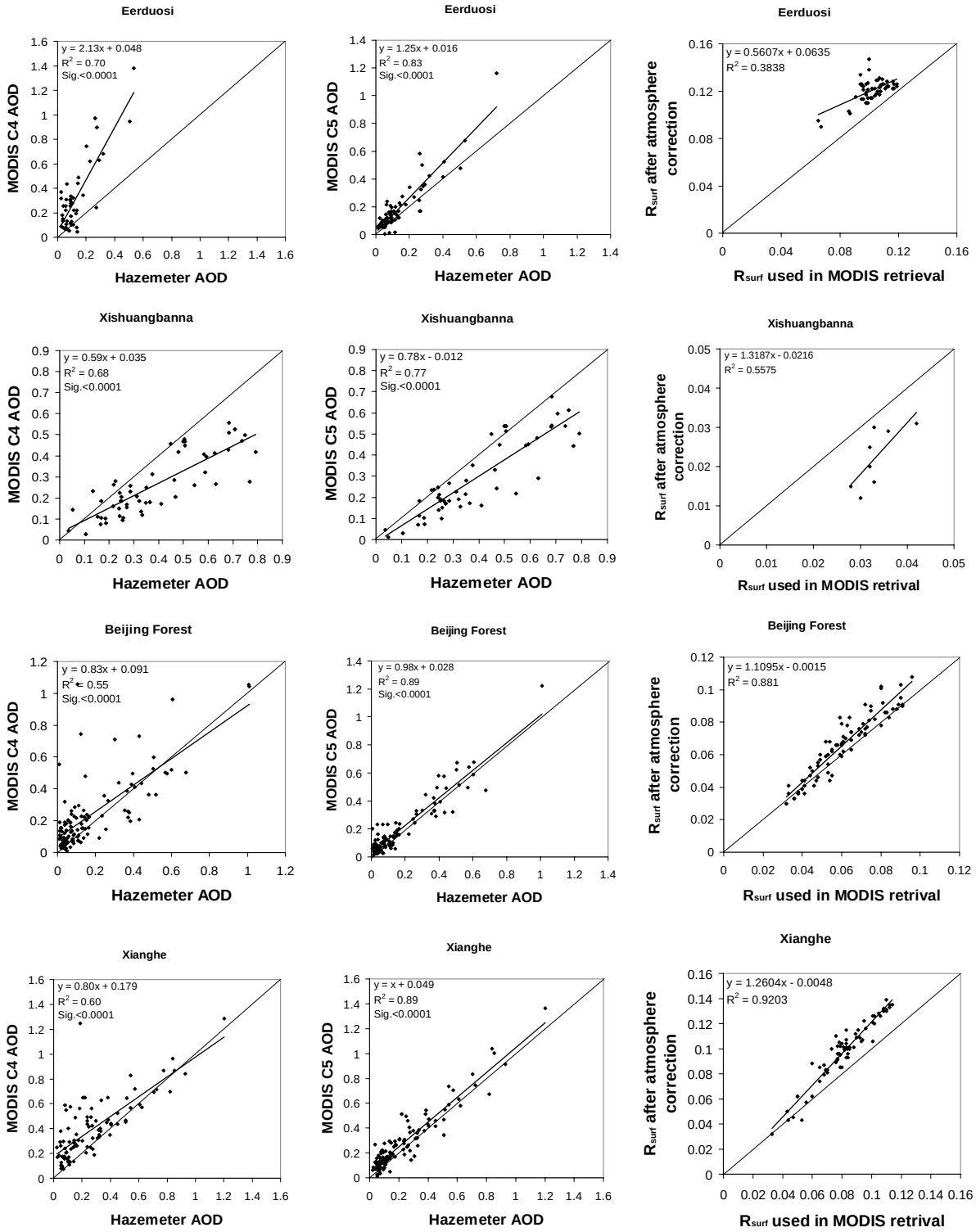

Fig. 4.14. Comparisons between AOT from MODIS C4 (left), C5 (middle) as a function of hazemeter AOT, with reference to the comparison of surface reflectances (right).

The aerosol model used in the C5 algorithm was obtained from a combination of three, fine-dominated (spherical) aerosol modes and one coarse-dominated (spheroid) aerosol mode. The coarse-mode phase function is substantially different from that of the C4 coarse-mode due to the assumption of spheroids instead of spheres [*Levy et al*., 2006b]. The fine-dominated aerosol modes were assigned a 'neutral' absorption (SSA~0.90) for all seasons across China, except for a narrow strip along the eastern China Sea. This simplification is necessary due to a lack of measurements of ω_o. In reality, ω_o varies rather dramatically as indicated by the time series of ω_o estimated from a Cimel sunphotometer deployed at Xianghe [*Li et al*., 2007b].

4.5. Summary

Aerosols have been recognized as the source of the largest uncertainty among all climate forcing agents due largely to a poor knowledge of their loading, optical, physical and chemical properties, and their inhomogeneous distribution. While remote sensing can provide global coverage, retrieval of aerosol variables requires more *a priori* knowledge than what is conveyed in satellite measurements. Unfortunately, there has been a dearth of ground aerosol measurements over the majority of major aerosol source regions around the world, including China.

Recently, the MODIS aerosol retrieval algorithm over land was modified dramatically, from which a new generation of products, denoted as Collection 5, is being generated to replace the widely-used Collection 4 product. In the development of the new algorithm, advantage was taken of ground-based aerosol retrievals from the AERONET to develop improved relationships between surface visible and near-IR reflectances and

aerosol models. Since AERONET data over China was scarce during the process of improving the retrieval algorithm, its performance is unknown over this vast region of complex surface and atmospheric properties.

Under the aegis of the EAST-AIRE project, a network of hand-held sunphotometers was established across China and has been in continuous operation since 2004. The data are used in this study to evaluate the aerosol products in the two most recent collections retrieved from the MODIS. The comparisons attest to the superior quality of the C5 collection over the C4 collection, in terms of all regression indices, i.e. smaller offsets, slopes closer to unity and higher correlation coefficients. Nevertheless, the performance of the C5 algorithm varies with surface and aerosol types. AOTs over bright surfaces (deserts, semi-deserts, urban areas) are generally overestimated, whereas underestimation of AOT is found over some forest sites.

To sort out the contribution of various factors, the surface reflectance was derived on clear and clean days with AOT<0.2. The resulting reflectances are compared with those estimated from the MODIS 2.12 μm channel. They are close to the true values for the majority of cases with good agreement in AOT, and differ for those with large discrepancies in AOT. The direction of the discrepancies in AOT is in accordance with those in reflectance. This attests that surface reflectance is still the major cause of inaccurate retrievals over land, despite the substantial improvement made by the C5 algorithm. In urban and suburban sites, the surface effects are often mixed with aerosol type effects, which may enlarge or suppress the AOT discrepancies depending on the amount of aerosol absorption assumed in the retrieval. Since both surface and aerosol types change with season, the discrepancies in AOT also show a strong seasonal pattern,

especially over northern China, with more overestimation during the winter than during the summer.

The generally more accurate retrievals of aerosol properties in the MODIS C5 aerosol product than in C4 provide more reliable data sets to study aerosol effects on climate. In the next chapter, we will incorporate the MODIS C5 product into a climate model to study the aerosols effect on regional climate in China.

Chapter 5 : Increase of Wintertime Fog in China: Potential Impacts of Increasing Aerosol Loading on the Eastern Asian Monsoon Circulation

5.1 Introduction

Aerosols may change regional climate by scattering or absorbing solar radiation [*Ramanathan et al*., 2001]. In China, aerosol loading has increased dramatically since the 1970s [*Luo et al.,* 2001]. This increase has the potential to affect regional climate via its direct and indirect effects [*Ramanathan et al.,* 2001; *Li,* 2004; *Qian and Giorgi,* 1999; *Qian et al.,* 2003; *Niu et al*., 2010]. Using coupled atmosphere-ocean general circulation models, *Ramanathan et al.* [2005] and *Lau et al.* [2008] demonstrated that aerosols have significantly changed the South Asian monsoon system during the summer although the mechanisms they proposed are somewhat different [*Lau and Kim,* 2006a; *Chung and Ramanathan*, 2006]. *Menon et al.* [2002] showed that absorbing aerosols may enhance the upward motion in southern China and increase precipitation during the summer monsoon season. Less attention has been paid to changes in the East Asian monsoon during the winter season and the impact of aerosols on winter fog events.

Heavy fog, which may extend over tens to hundreds of kilometers and last for several days, is a major weather hazard in winter in northern China. Not only does fog reduce visibility and cause accidents, it also affects human health, especially for people with respiratory problems. Fog is more likely to occur when wind speed is low, relative humidity is high and surface temperature is low [*Sachweh and Koepke*, 1995; *Niu et al.,* 2009]. Case studies [*Zhang et al.,* 2005*; Pu et al.*, 2008] also showed that in a stable boundary layer with temperature inversion, low-level warm air advection with sufficient

water vapor makes fog persist for a longer time. These studies suggest that the change in the frequency of wintertime fog events may be highly related to meteorological conditions, which are greatly influenced by wintertime cold front activities and ultimately by the variation in the East Asia winter monsoon. Attempts have been made to discover the dynamic and thermodynamic conditions favoring the formation, maintenance and dissipation of fog in China [*Niu et al.*, 2009].

The East Asian winter monsoon, characterized by strong winds from the northwest and outbreaks of cold air over northern China, has dramatically changed during the last several decades, which is the subject of a number of studies [*Guo,* 1994*; Xu et al.,* 1999*; Shi,* 1996]. Since the mid-1980s the East Asian winter monsoon has significantly weakened. In the meantime, winter surface temperatures in northern China have increased, resulting in 17 consecutive significantly warmer winters in China on record up to the year 2000 [*Wang,* 2006]. During the same period, both wind speed and the frequency of windy days decreased [*Xu et al.,* 2006]. These systematic changes are likely a response to the external forcings such as changes in tropical sea surface temperature (SST), global or regional scale warming, or aerosol forcing.

Global warming is most significant in the middle to high latitudes during the Eurasian winter season [*Flato and Boer,* 2001]. The reduced thermal contrast between middle and high latitudes may lead to weak winter monsoon as revealed by several studies [*Hori and Ueda,* 2006*; Hu et al.,* 2000, 2003*; Kimoto,* 2005]. Other factors such as tropical ocean warming, forcing of the Tibetan plateau, and internal variability may also greatly influence the East Asian monsoon system [*Lau et al.,* 2006b; *Wu et al.,* 2009; *Wang et al.,* 2008b; *Zhu and Wang,* 2002; *Jhun and Lee*, 2004]. Some observational

results can not be explained solely by aerosol effects [*Yu and Zhou,* 2007; *Yu et al.,* 2004]. Therefore, we do not rule out the influences of these factors on the change of the East Asian winter monsoon although we mainly focus the potential influences of aerosols and global scale warming in the study.

In this study, we analyze trends in the frequency of fog events, relative humidity, and the frequency of light winds, together with changes in the general circulation pattern, to examine how weakening of the East Asian winter monsoon and aerosols may influence winter fog over northern-central China. In the following section, data sets used are described. Section 5.3 presents results from the analysis of trends in fog occurrence and associated meteorological variables, as well as the pattern of regional general circulation. Based on these analyses, a hypothesis is made and tested by means of model simulations using the National Center for Atmospheric Research Community Climate Model (NCAR/CCM3) regarding the role of aerosols, which is given in Section 5.5. Section 5.6 summarizes the study.

5.2 Data Sets and Model Used

The meteorological data used in this study were obtained from the National Climatic Data Center (NCDC) of the National Oceanic and Atmospheric Administration (NOAA). This dataset provides hourly meteorological records, including surface temperature, dew point temperature, wind speed and "present weather", from the 1950s to 2007. "Present weather" describes weather events such as rain, snow, fog, clouds and other important types of weather phenomena. Daytime data from 1976 to the present are used in this study because many gaps exist in earlier records due to instrument

malfunctions [*Liu et al.*, 2004a]. Three hundred and ninety sites with more than 20 years' worth of data were used in this study.

Large-scale meteorological variables such as geopotential heights, sea level pressure, surface wind and water vapor were obtained from the National Centre for Environmental Prediction (NCEP) reanalysis which is a retroactive record of more than 50 years' worth of global analyses of atmospheric fields [*Kistler et al.*, 2001].

Various trend analyses were conducted. The annual frequency of fog events is calculated by dividing the number of fog observations by the total number of observations in each year. The change of it during recent 30 years is then calculated using linear regression analysis. Trends in other quantities such as wind speed and occurrence of light winds are also obtained using the same methodology. Changes in the atmospheric circulation pattern are examined in order to investigate possible causes for the changes in the frequency of fog events. Changes in 500hPa geopotential heights, sea level pressure, 850hPa wind, and low-level water vapor transport divergence between the first 13 years and the last 13 years from 1976 to 2001 were calculated on the basis of monthly mean values from NCEP reanalysis data.

5.3 Observational Evidences

5.3.1 Frequency of Fog, Wind Speed and Cold-air Surges

Fig. 5.1a shows the mean fog frequency in winter over China at 390 sites from 1976 to 2007. The fog frequency is calculated by dividing the number of fog events by the total number of observations for each station. Fog events occurred more frequently over eastern-central China, especially along the Yangtze River corridor, than over other

parts of China in the past three decades. Fig. 5.1b shows changes in the frequency of fog events (percent per year) during wintertime obtained from linear regression analysis. Of the 390 sites, the frequency of fog events significantly decreased at 128 sites, increased at 110 sites and showed no significant change at the remaining sites. The most significant increase in the frequency of fog events, with a maximum value of about 0.3 percent per year, is over eastern-central China, the most heavily populated region of the country. Data from the southeastern region and Sichuan basin area shows a decrease in the frequency of fog events over the same time period. There is no consistent pattern in other areas of the country.

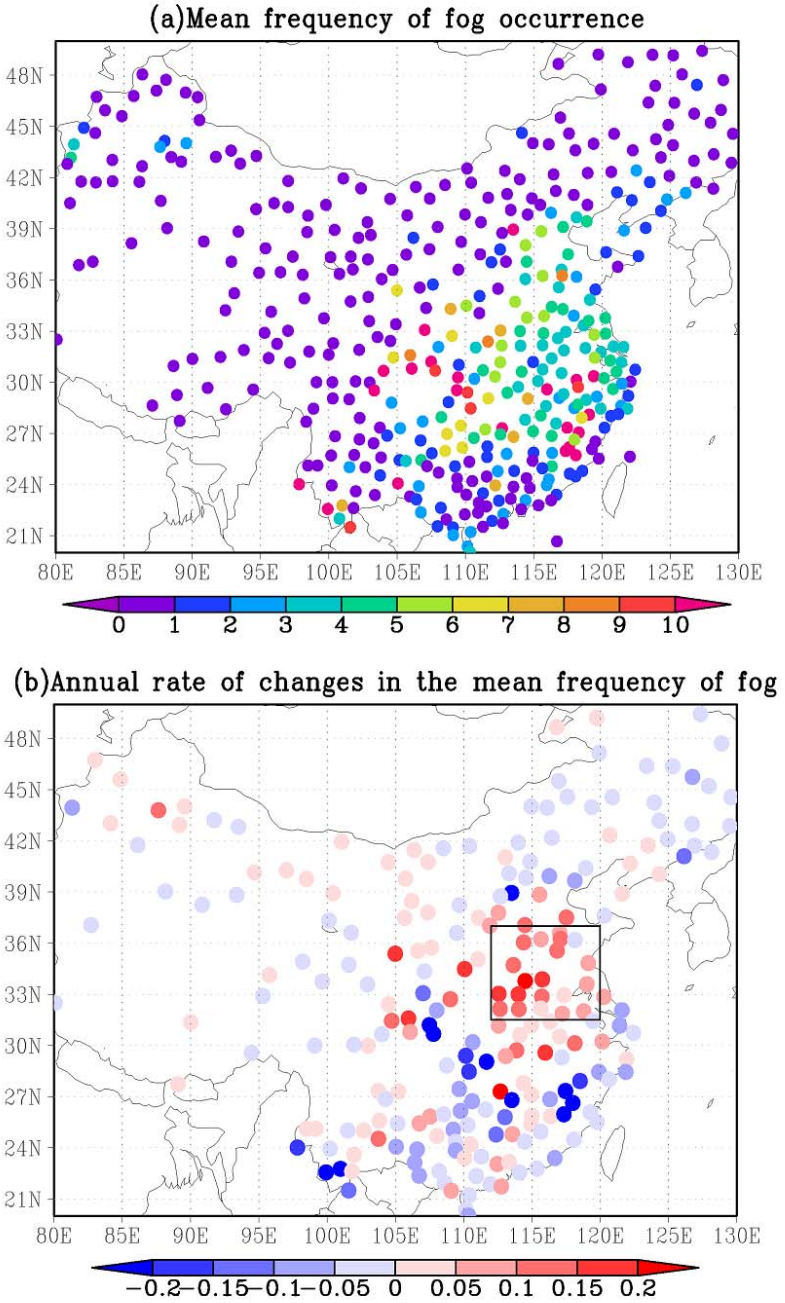

Fig. 5.1. (a) The mean frequency of fog occurrence in winter (%) and (b) the annual rate (percentage per year) of changes in the mean frequency of fog occurrence during wintertime over China at 390 sites from 1976 to 2007. Only stations with trends at the 5% significance level are shown in (b).

Fog usually forms over a plain under stable atmospheric conditions of light wind, sufficient moisture and low temperature [*Sachweh and Koepke*, 1995; *Zhang et al.,* 2005]. The common types of fog over eastern-central China are radiation and advection fog. Both types of fog need sufficient water vapor, stable atmosphere which is often accompanied by temperature inversion, and cold land surface [*Niu et al.,* 2009]. The change in the frequency of fog events is likely associated with changes in some, if not all, of these factors. Therefore, changes in relative humidity during this period are first examined. The geographical pattern of the change in relative humidity is very similar to that of Fig 5.1b, showing a significant increase over eastern-central China and a decrease over southern China (shown later in Fig. 5.4b).

During winter, the dry, cold air mass brought in by the prevailing northwesterly Siberian high pressure system is unfavorable for fog formation [*Zhang et al.,* 2005]. The time series of averaged frequency of fog events, averaged wind speed and the frequency of light winds are shown in Fig. 5.2. The area-averaged frequency of fog events significantly increased from around 2% in 1976 to around 5% in 2007, more than doubling during the last 30 years. During the same period, the area-averaged wind speed fell from about 3.7 m/s to about 3 m/s. Correspondingly, the frequency of light winds (wind speeds less than 1.6 m/s) increased from 9% in the 1970s to 14% in the beginning of the twenty-first century. The trends in Fig. 5.2 are significant at greater than 95% confidence levels.

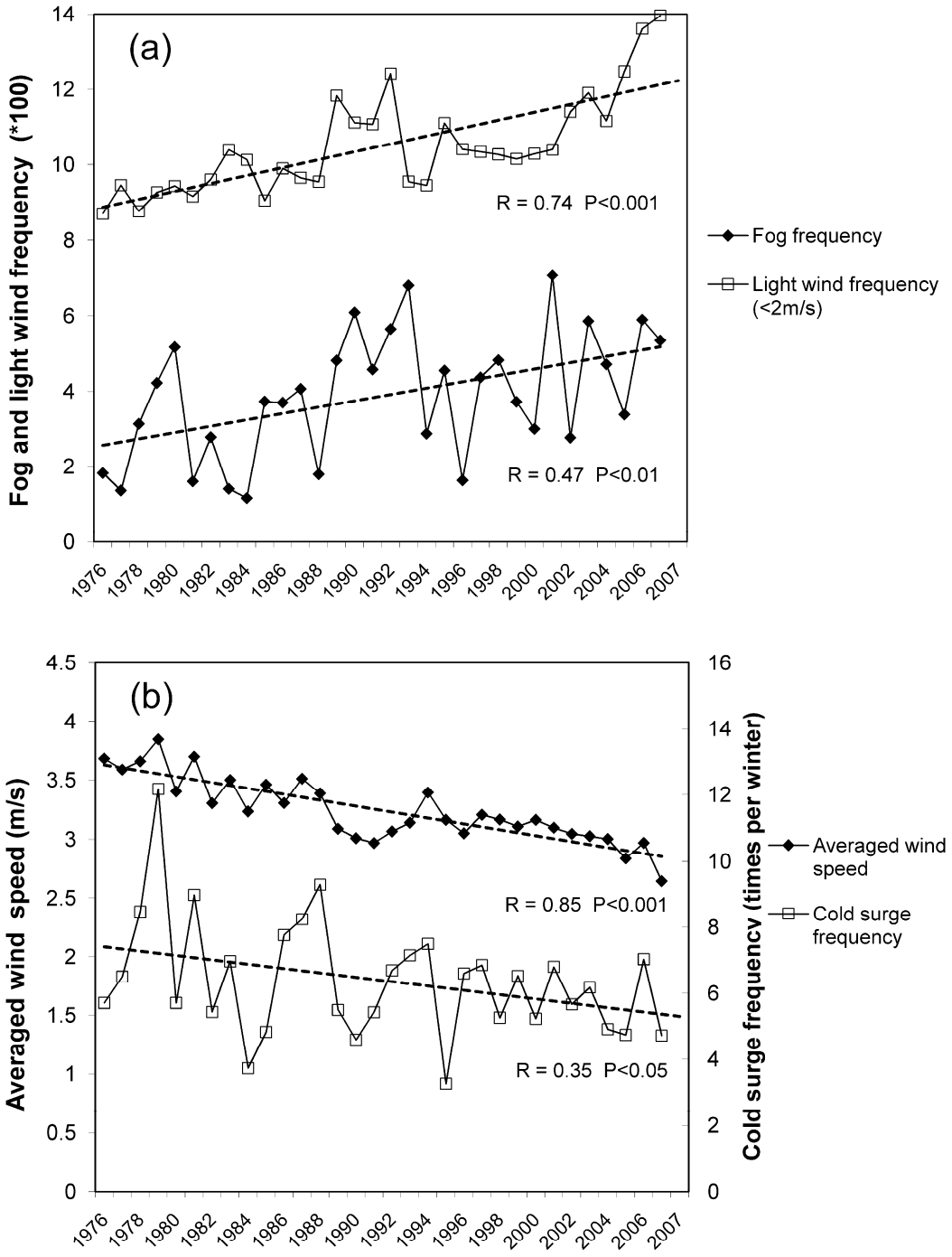

Fig. 5.2. Time series of (a) mean frequencies of fog occurrence and light wind and (b) the frequencies of cold-air surges and mean wind speed over the boxed area in Fig. 5.1b.

The decrease in wind speed and increase in the occurrence of calm atmospheric conditions may suggest a weakening of the East Asian winter monsoon. As the East Asian winter monsoon weakened, the frequency of cold surges from the north also dropped. A variety of definitions for cold surges, such as changes in surface temperature, surface pressure, and wind speed, have been used [*Wang,* 2006]. The frequency of cold surges here is defined as the number of times in each winter season that the daily averaged surface temperature drops by more than 4 degrees Celsius from the previous day. Fig. 5.2b shows the time series of the frequency of cold surges and averaged wind speed. The area-averaged frequency of cold surges decreased from about 7 to about 5 times per winter during the recent past 30 years. This trend also has a confidence level of over 95%.

5.3.2 Change in the General Circulation Pattern

The decrease in wind speed over East Asia is corroborated by a similar decrease in various East Asian winter monsoon indices [*Gao,* 2007]. These indices include land and sea pressure differences [*Shi,* 1996], regionally-averaged meridional winds in the lower troposphere [*Ji et al.,* 1997; *Chen et al.,* 2001], zonal winds in the higher troposphere [*Jhun and Lee,* 2004], and the strength of the East Asian trough [*Sun and Sun,* 1995]. These findings suggest that weakening of the East Asian winter monsoon may be associated with climate changes on a broader scale. General circulation pattern changes are examined by using NCEP reanalysis data from 1976 to 2001 in order to determine any relation between the frequency of fog events and the strength of the East Asian winter monsoon indices.

As one of the most important atmospheric systems active in Eurasia during the winter months, the Siberian High has a direct and significant impact on the East Asian winter monsoon circulation, particularly on sea level pressure and northerly winds along the East Asian coast [*Wu and Wang,* 2002]. Fig. 5.3a shows the mean sea level pressure and 850hPa wind vectors during winter seasons from 1976 to 2001. The winter monsoon circulation advects cold air masses from Siberia to the East Asian continent and more southerly regions. The prevailing weather episodes in winter in East Asia are outbreaks of cold-air surges which are marked by the invasion of extremely cold and dry air from the northwest [*Wang,* 2006].

Fig. 5.3b shows the differences in mean sea level pressure and 850hPa wind (or anomalous flow) from 1976 to 2001 (the mean from 1989 to 2001 minus the mean from 1976 to 1988). The Siberian high appears to have weakened over the course of the past 26 years. In most areas, the anomaly wind vector is opposite to the prevailing wind which suppresses the prevailing wind; this is consistent with surface observations [*Xu et al.,* 2006]. Over the eastern-central China region, the change in sea level pressure is accompanied by a wind anomaly from the southeast direction along the eastern coastal area and a wind anomaly from the north in southern China. This results in the transport of less dry and cold air to eastern-central China but more to the southern parts of China. Such changes may explain the increase in relative humidity and fog frequencies over eastern-central China and the decrease of these quantities in the southeastern region.

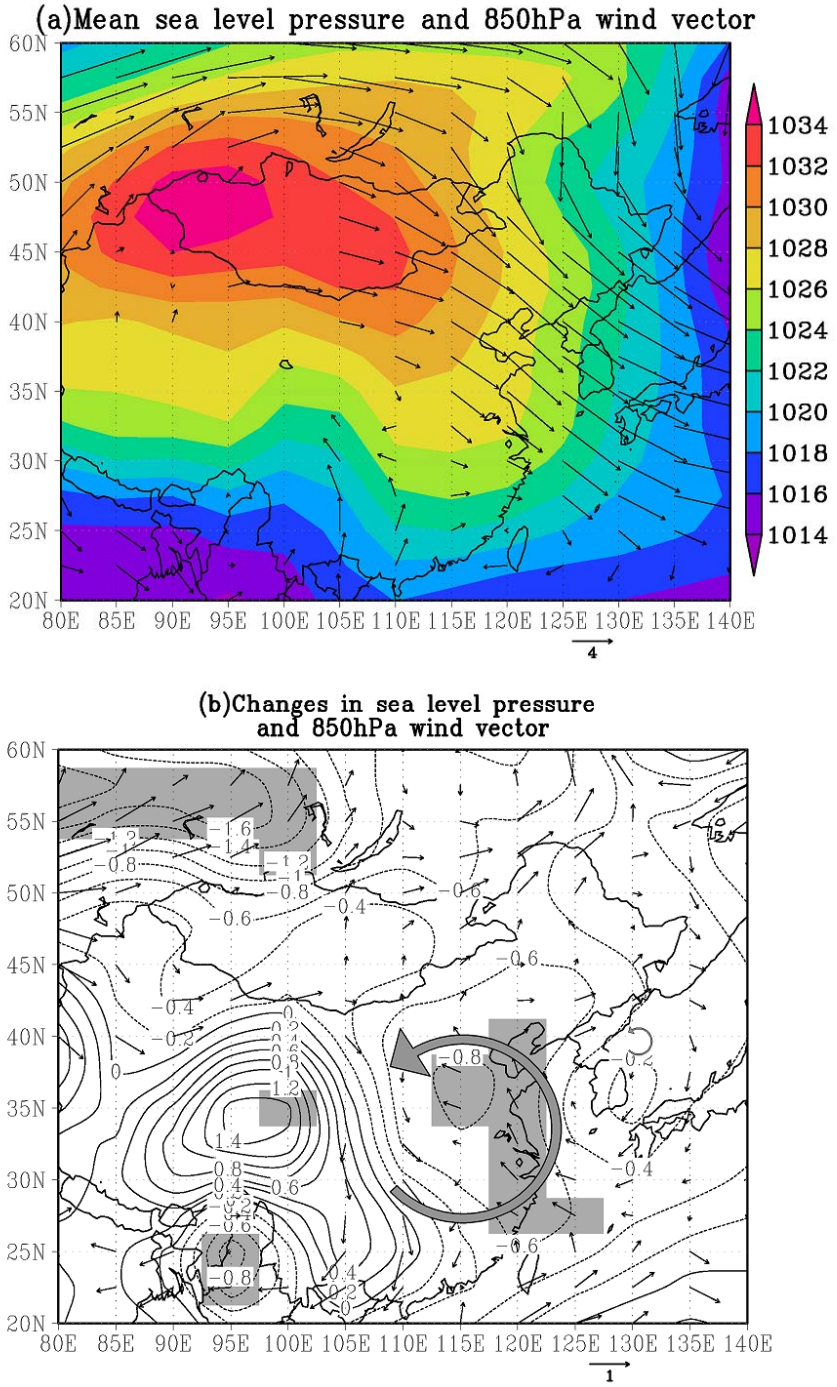

Fig. 5.3. Wintertime sea level pressures (hPa) and 850hPa wind vectors (m/s) from the NCEP reanalysis: (a) mean values from 1976 to 2000, and (b) the difference (1989-2000 minus 1976-1988). Wind vectors over topography higher than 850hPa are masked out. Shaded areas are at the 5% significance level.

The above explanation is also corroborated by the change in water vapor transport divergence. Water vapor transport divergence is defined as $\nabla \bullet qv$, where q is the water vapor mixing ratio and v is the horizontal velocity of the air [*Houghton*, 1985]. Since fog and relative humidity are observed near the surface, only the water vapor transport divergence in the lower atmosphere from the surface to 850hPa was calculated. The rate of its change during the past 26 years is shown in Fig. 5.4a (difference between 1989-2001 and 1976-1988). Note that a positive value means that water vapor has diverged and vice-versa. Water vapor convergence over eastern-central China and water vapor divergence over southern China correspond to an increase and decrease in the frequency of fog events and in relative humidity in the two regions (Fig. 5.4b), respectively. The above results suggest that the increase in the frequency of fog events in recent years is highly related to changes in wind speed and direction and water vapor fluxes due to the circulation change.

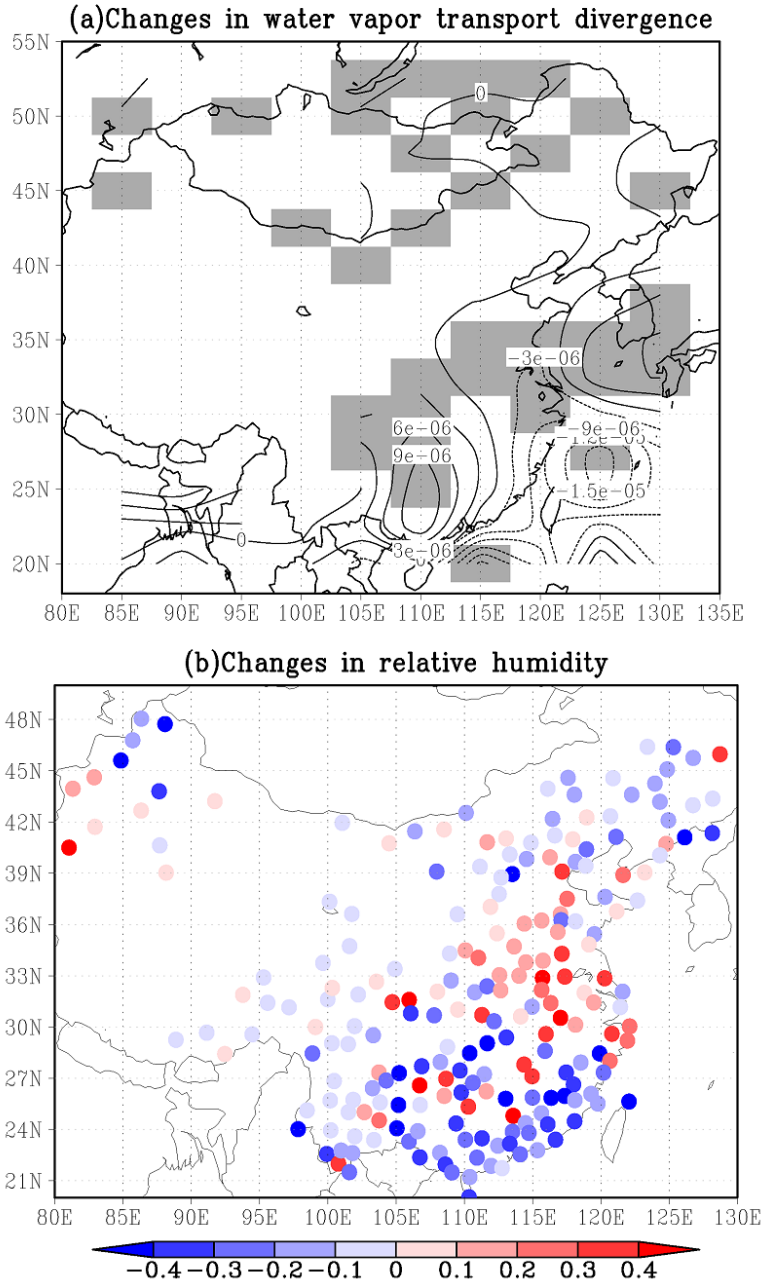

Fig. 5.4. Changes in (a) water vapor transport divergence (contours, unit: kg/kg/m^2/s) below 850hPa and (b) relative humidity (%). Shaded areas are at the 5% significance level. Only stations with trends at the 5% significance level are shown in (b).

5.4 Global Warming Effect and Other Factors

While changes in the aforementioned variables are linked to the increasing trend of fog occurrence, they are not the ultimate forces driving the trend, as their own changes are likely responses to certain external forcings such as greenhouse gases and aerosols. This argument is reached after an extensive survey of previous global warming studies based both on models and observations and our own modeling results concerning the effect of aerosols on the factors that influence fog occurrence. Admittedly, we cannot rule out the possibility that these changes result from natural variations, but it is safe to point to the possibility that the changes were affected to some degree by the steady and dramatic increase of the two primary external forces in this region.

Previous model simulations and ground-based measurements demonstrated that global warming is more pronounced at high latitudes than at low latitudes [*Delworth and Knutson,* 2000; *Min et al.,* 2004; *Flato and Boer,* 2001]. The reduced thermal contrast between south and north diminishes the transport of energy through baroclinic waves and diminishes the strength of troughs and ridges as seen in the change of 500hPa geopotential heights shown in Fig. 5.5. Geopotential heights in the trough region are increased. Behind the trough and near the surface, the associated high pressure system is weakened (Fig. 5.3b). As a consequence, the transport of cold air originating from the East Asian trough at high latitudes becomes less powerful, which is a key indicator of the weakening winter monsoon in East Asia. Such arguments have been supported by many observational and modeling studies [*Hori and Ueda,* 2006*; Xu et al.,* 2006*; Hu et al.,* 2000, 2003*; Kimoto,* 2005]. Meteorological records from the past three decades [*Xu et al.,* 2006] reveal that surface wind speed has decreased steadily. Yet, the change is negatively

correlated with near-surface air temperature, which suggests a possible relationship between wind speed reduction and regional and global warming. The observed changes in surface temperature, wind speed and relative humidity in eastern-central China are generally consistent with the projected change under the global warming scenario [*Hu et al.,* 2000, 2003]. *Kimoto* [2005] showed that under the global warming scenario, the weakened winter monsoon is associated with the shallower and northeastwardly shifted planetary wave trough over the east coast of the Eurasian Continent. *Hori and Ueda* [2006] and *Hu et al.* [2000] showed that the weakening of the East Asian winter monsoon is a result of global warming. However, other factors such as the forcing of the Tibetan Plateau, the snow cover over Euraisian continent, tropical SST, and the Arctic Oscillation were also shown to influence the East Asian winter monsoon [*Murakami,* 1987; *Watanabe and Nitta,* 1999; *Zhang et al.,* 1997; *Wang et al.,* 2000; *Gong et al.,* 2001]. These results indicate that planetary-scale features such as the tropical convective center near the western Pacific, the Siberian high, and the 500hPa trough and ridge over East Asia are inherently related to each other to influence the East Asian winter monsoon. Global warming together with these factors therefore appear to contribute to the change in the frequency of fog occurrence, although there is no consensus on which one is dominant.

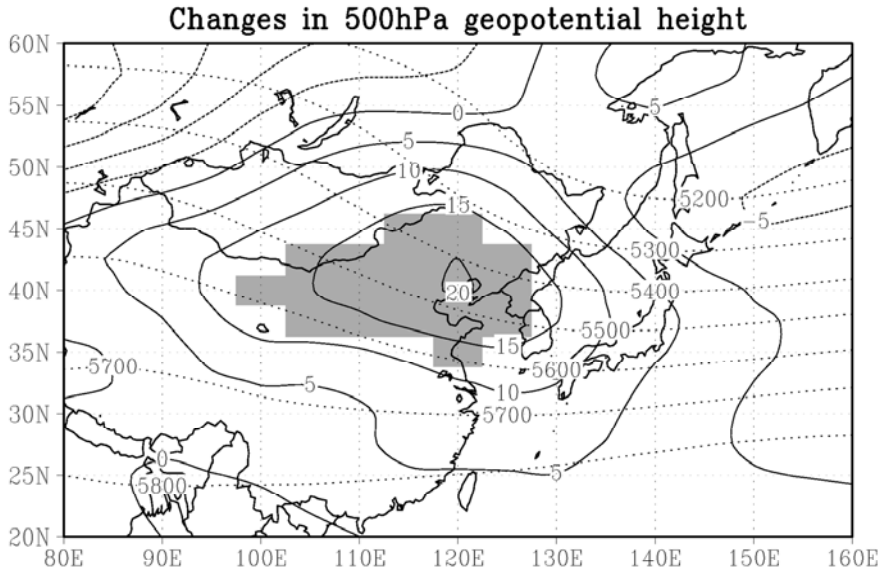

Fig. 5.5. Changes in 500hPa geopotential height (contours, unit: m) from NCEP reanalysis (1989-2001 means minus 1976-1988 means). The dotted lines are averaged 500hPa geopotential heights from 1976-2001. Shaded areas are at the 5% significance level.

5.5 The Impact of Increasing Aerosol Loading

Aerosol loading over China has increased since the 1960s, as inferred from ground-based radiation measurements [*Luo et al.,* 2001*; Kaiser and Qian,* 2002]. Fig. 5.6a shows mean MODIS aerosol optical depths (AOD) during wintertime periods from 2000 to 2008. The large grey area represents bright surfaces over which there are no satellite retrievals. Most strikingly, AOD is largest in eastern China where the population density is highest and where economic growth is fastest in the country. Meteorological records showed that the frequency of clean atmospheric conditions in eastern-central China has continuously declined over the past 30 years (Fig. 5.6b). Here, visibility is used

as a proxy of clean atmospheric conditions: higher than a threshold corresponding to 75% of the maximum visibility observed at a particular location. Fog events, which also reduce visibility, are excluded in calculating the frequency of clean atmospheric conditions. The average frequency of clean atmospheric conditions over eastern-central China in winter decreased from around 26% to around 14% from 1976 to 2007. Moreover, the aerosols over eastern-central China are highly absorbing based on several studies on aerosol single scattering albedo (SSA) using a variety of retrieval methods [*Zhao and Li*, 2007; *Lee et al.*, 2007; *Xia et al.*, 2006]. For example, *Xia et al.* [2006] reported that the mean SSA in Beijing is around 0.9 at 550nm wavelength in all seasons and is even lower in winter based on 33 month observations by a CIMEL radiometer. The nationwide value of SSA retrieved from a sun-photometer network is 0.89 ± 0.04 according to the study of *Lee et al.* [2007]. Such high absorbing aerosols may heat the atmosphere, also generate a cyclonic circulation anomaly as shown in the NCEP reanalysis data, and therefore affect the fog formation.

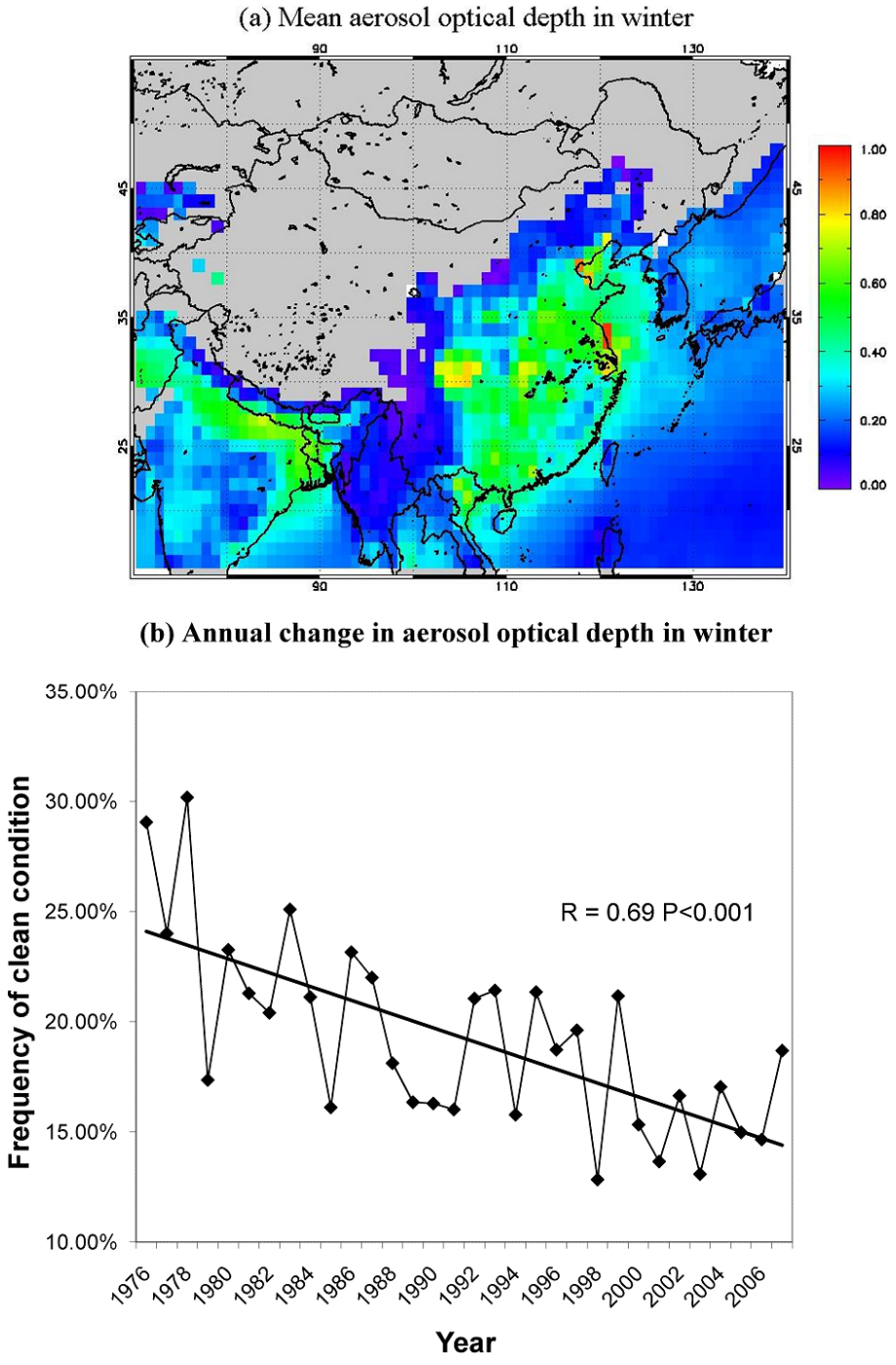

Fig. 5.6. (a) Mean MODIS AOD in winter and (b) the change in the frequency of clean atmospheric conditions in eastern-central China from 1976 to 2007.

5.5.1 Model Setup

To quantify such aerosol effect, we employed the National Center for Atmospheric Research's Community Climate Model (CCM3), which is easy to use and performs soundly. It was run at the T42-L26 resolution of 2.8^o by 2.8^o with 26 vertical layers. The model contains an annually-cyclic tropospheric aerosol climatology consisting of three-dimensional, monthly mean distributions of aerosol masses for sulfate, sea salt, black and organic carbon, and soil dust. It was generated using the Model for Atmospheric Chemistry and Transport (MATCH) which assimilates satellite-retrieved AOD from the NOAA Pathfinder II data set [*Stowe et al.,* 1997], integrated to present-day conditions [*Collins et al.,* 2001, 2002*; Rasch et al.,* 1997]. The mass concentrations of different aerosol species were modified by scaling the AOD climatology based on the MODIS Collection 5 AOD product whose quality has been validated in the region [*Li et al.,* 2007c*; Mi et al.,* 2007]. The original aerosol vertical distribution and aerosol components are retained. The climatological annual cycle of sea surface temperature was used in the model. Two types of model simulations were conducted: with and without anthropogenic aerosols over China as experimental and control runs, respectively. In the experiment without anthropogenic aerosols, the sulfate, black carbon and organic carbon aerosols were removed. In the experiment with anthropogenic aerosols, all types of aerosols were kept. In the model, the column mass concentration of BC accounts for about 4% of total column mass concentration of aerosols, while the column mass concentration of sulfate aerosols accounts for about 30% in all seasons. In winter, BC accounts for about 8% of the total column mass concentration and sulfate accounts for about 44%. The annual mean and wintertime aerosol single scattering albedo (SSA) over

eastern China (105°E-120°E, 20°N-45°N) from model outputs are around 0.92 and 0.90, respectively. In both experiments, the sea surface temperature, green house gases and other forcing were the same. Each of the experiments was run for 20 years and the model outputs for the last 10 years (in equilibrium) were averaged. The differences of the outputs from these two experiments were used to demonstrate the changes caused by anthropogenic aerosols. Note that the model does not include aerosol indirect effects so any differences can only illustrate the potential impact of aerosols on atmospheric dynamics through radiative transfer processes.

5.5.2 Results

All meteorological variables (temperature, pressure, precipitation, radiation, etc.) are output and analyzed, but only those variables of direct importance to fog occurrence and maintenance are presented and discussed here. Fig. 5.7a shows the annual mean of AOD from MODIS during 2000-2008. AOD is very high at several locations including eastern-central China, the Sichuan basin, and the southern coastal region. The blank areas without MODIS retrievals are substituted by data from the original dataset in the CAM model. Fig. 5.7b shows the mean sea level pressure and 850hPa winds from the model simulation. The pattern is very similar to Fig. 5.3a with the Siberian high located over the Mongolia region and the prevailing northwest wind over eastern-central China. This indicates the model captures the most important feature of the winter monsoon circulation. However, a discrepancy in wind direction over southern China is noted between the model simulation and the NCEP reanalysis data, implying some detailed features missing in the model. The comparison of the mean surface temperature between the model (in

which surface temperature means radiative surface temperature) and reanalysis is presented in Fig. 5.7c and 5.7d. The model simulated surface temperature very well with only slight overestimations over the Mongolia and the Tibetan regions. The magnitudes of the standard deviations of them are almost the same. However, the simulated specific humidity is not as good as the surface temperature. The model overestimates specific humidity in the south over ocean but underestimate it in the south over land (Fig. 5.7e and 5.7f).

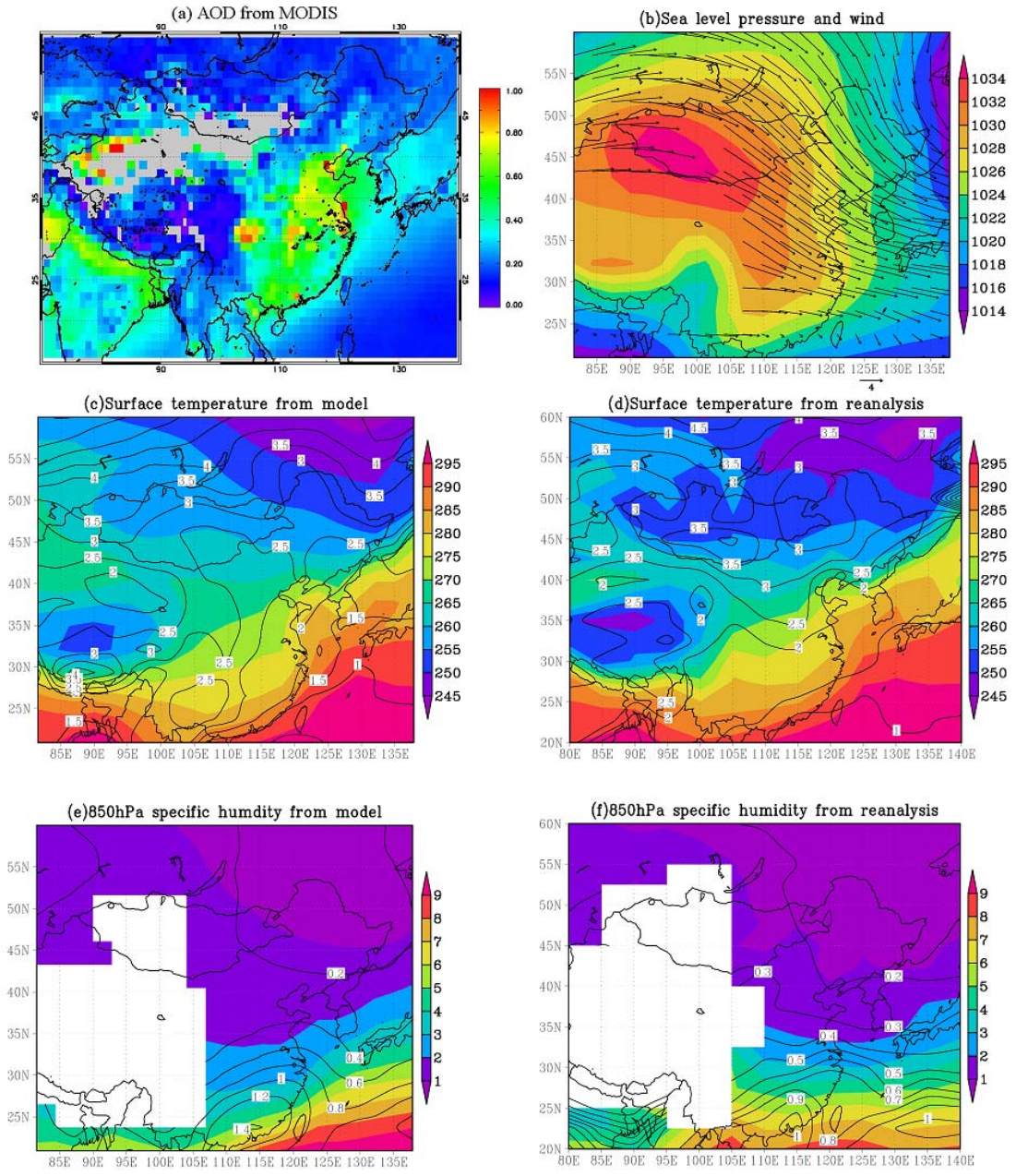

Fig. 5.7. Mean states of (a) AOD used in forcing the model from MODIS in all seasons during 2000-2008, (b) the sea level pressure (hPa) and 850hPa wind vectors (m/s) from the model simulation, surface temperature (K) from (c) the model simulation and (d) NCEP reanalysis data, and 850hPa specific humidity (kg/kg*1E3) from (e) the model simulation and (f) NCEP reanalysis data in winter. All the model results are from the simulation with anthropogenic aerosols. The contours are the standard deviations of the means. Values over topography higher than 850hPa were masked out in (e) and (f).

Fig. 5.8 presents the changes in surface short wave fluxes (8a), surface temperature (8b), sea level pressure, and 850hPa wind (8c). The differences between the two experiments with and without anthropogenic aerosols are used to show the changes caused by anthropogenic aerosols. As expected, aerosols greatly reduce the amount of shortwave radiation reaching the surface. The maximum reduction is greater than 30 W/m^2 over eastern-central China where the aerosol optical thicknesses are high (Fig. 5.6a). However, the change in surface temperature does not follow exactly the pattern of the change in shortwave flux reaching the ground. Surface temperature is lowered more in southern China than in northern China and is presumably caused by an aerosol-induced circulation change (discussed later), as well as the amount of solar radiation higher in the south than the north. As a result, the reduction in solar radiation by the same amount of aerosol loading is larger in the south than in the north. The maximum reduction is over 1.5^oC in the Sichuan basin region where AOD is always high (Fig. 5.6a and 4.7a). It is worth noting that China's industrialization and modernization dated back to the turn of the 1970s/1980s. Prior to this period, industrial activities were not as prevalent and thus less anthropogenic aerosols, especially secondary aerosols, would have been generated. Such a regional impact of anthropogenic aerosols on the East Asian monsoon circulation could be significant over the past several decades. A cyclonic anomaly flow is induced by aerosols over eastern-central China (Fig. 5.8c). The anomaly flow along the eastern coastal region from the southeast weakens the invasion of dry and cold air from the north. But the anomaly flow in central China from the northwest brings more cold air to the south. This is also one reason why the surface temperature decreases greatly over this region. Again, the distribution of the pressure anomaly (difference in sea surface pressure

between the control and experimental runs) grossly resembles the difference in NCEP pressure fields between the same two periods (1989-2001 minus 1976-1988) (Fig. 5.3b), although the Siberian high does not change as much as that from the NCEP reanalysis data.

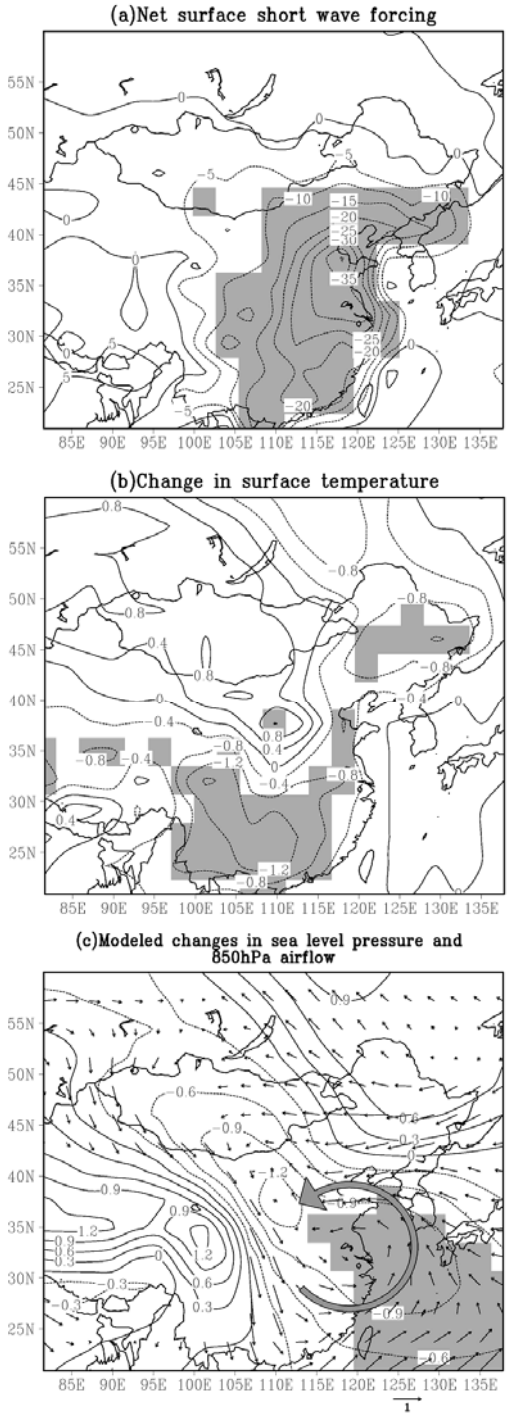

Fig. 5.8. (a) Net surface shortwave forcing (W/m^2) and changes in (b) surface temperature (^oC) and (c) sea level pressure (contours, unit: hPa) and 850hPa wind (arrows, unit: m/s) in winter caused by anthropogenic aerosols. Shaded areas are at the 10% significance level.

To further explore the causes for such changes, the mean latitude-height distributions of the temperature change, the meridional circulation anomaly and the zonal wind change over 110^{o}E-120^{o}E longitude regions are shown in Fig. 5.9. It is seen that aerosols greatly heat the atmosphere in the lower troposphere centered around 35^{o}N but cool the surface (Fig. 5.9a). Significant heating takes place between 900hPa and 800hPa with the maximum increase of air temperature over 0.8^{o}C. This leads to the upward motion in the north of 34^{o}N and a cyclonic circulation anomaly as shown in Fig. 5.8c. The cyclonic circulation anomaly weakens the prevailing northwesterly wind over eastern-central China but enhance the northerly wind over southern China. The large temperature drop over southern China is caused by such enhanced northerly wind. Correspondingly, the zonal wind speed also decreases in the north but increases in the south (Fig. 5.9b). Such a circulation change favors the formation of fog in the north but not in the south. The change in 850hPa specific humidity is also shown in Fig. 5.10. As expected, the specific humidity increase over eastern-central China but decreases over southern China. However, the changes over these regions are not very significant (at ~10% significance level) since the mean state of the specific humidity simulated by the model has relatively large standard deviations compared with the NCEP reanalysis data as shown before.

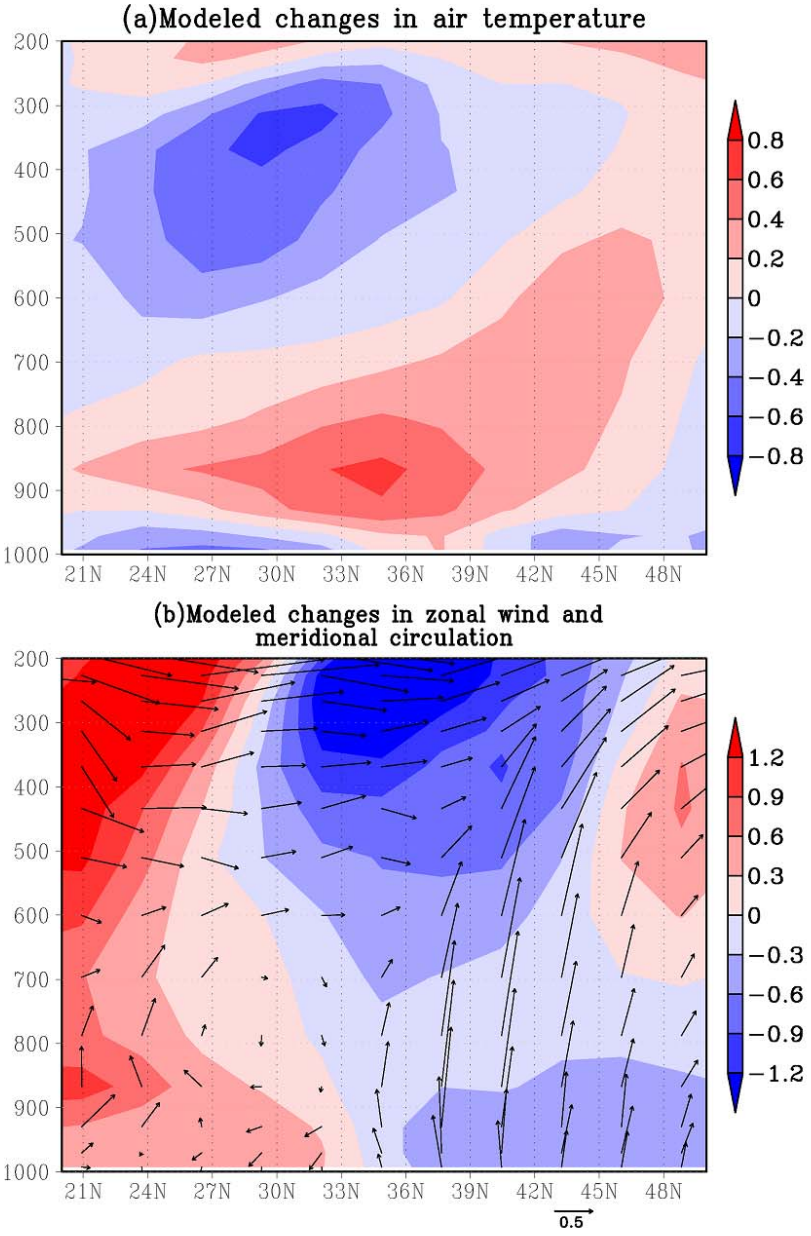

Fig. 5.9. (a) Changes in air temperature (^{o}C) and (b) zonal wind (shaded areas, unit: m/s) and meridional circulation (arrows, unit: 10^{-4} hPa/s for pressure velocity and m/s for meridional wind speed) averaged from 110^{o}E to 120^{o}E in winter from model simulations.

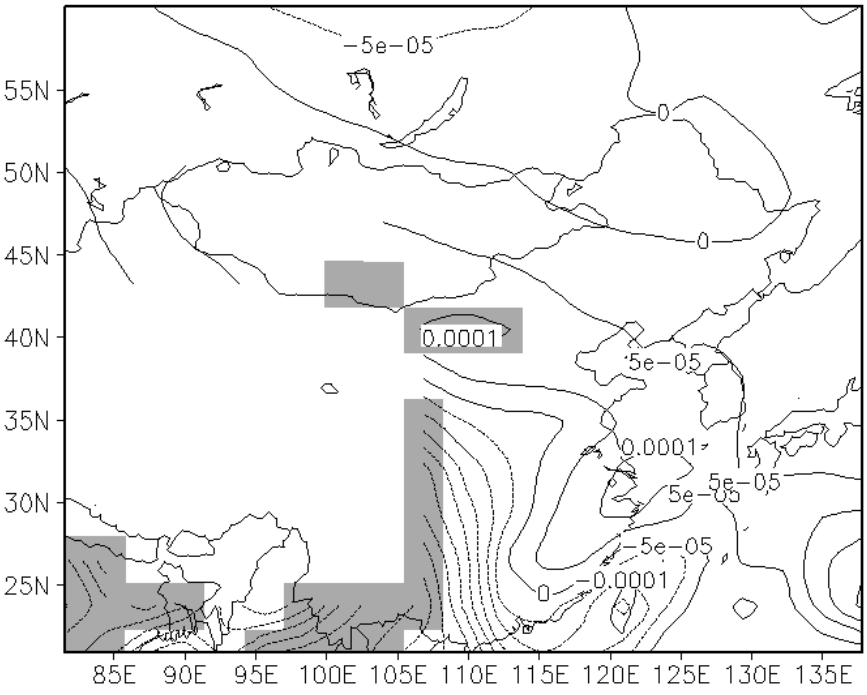

Fig. 5.10. Changes in 850hPa specific humidity (kg/kg) in winter caused by anthropogenic aerosols. Shaded areas are at the 10% significance level.

5.6 Conclusions

The frequency of fog events during winter over eastern-central China has significantly increased during the past 30 years. Meanwhile, wind speed and the frequency of cold-air surges dropped but the frequency of light wind events increased. The surface relative humidity also increased over the region with a similar pattern to the change in fog frequency. These changes attest to the weakening of the East Asian winter monsoon which may be induced by several important factors such as global warming, the tropical SST anomaly, and the change of snow cover over the Eurasian region. Global-scale warming may reduce the thermal contrast between high and mid-latitudes, weaken troughs and ridges of mid-latitude waves, and diminish the strength of the Siberian high and the East Asian winter monsoon. This leads to less invasion of dry and cold air from the northwest (cold fronts) and lower wind speed, creating a favorable background for fog. Other factors influencing the East Asian winter monsoon were mentioned but not discussed in detail here. The increase in atmospheric aerosols was shown to change the regional circulation as well in the same direction. High loadings of absorbing aerosols over China reduce the radiation at the surface, but heat the atmosphere, generating a cyclonic circulation anomaly over eastern-central China, a similar pattern to that revealed from the NCEP reanalysis data. The anomaly circulation weakens the northwesterly wind over eastern-central China, but enhances the northerly wind over southern China. As such, fog is easier to form over eastern-central China than over southern China. A major difference between the observed trend from the NCEP reanalysis data and model results is the change of the Siberian high. The increased AOD over the East Asian region does not lead to the weakening of the Siberian high as observed in the reanalysis data. This

result indicates that the increase of aerosols over this region may only have regional influences rather than global scale influences such as those induced by global warming. However, the effects of global warming and aerosols may still work in harmony to explain the changes in fog frequency over eastern-central and southern China in recent three decades, although the two effects are often thought to offset each other in the context of global warming in general.

Chapter 6 : Summary and Future Work

6.1 Summary

Using ten years of ground-based observations at the ARM SGP site and satellite observations over the tropical region, we provided solid evidence of the hypothesis of the aerosol invigoration effect. Both ground-based and satellite observations show that cloud top temperature decreases and ice water path increases with aerosol loading. In contrast, no decrease of cloud top temperature with aerosol loading for liquid clouds is observed, which confirms the importance of ice processes in the invigoration effect. The precipitation rate increases with aerosol loading for deep convective clouds due to the invigorated convection and enhanced ice processes, while it decreases for liquid clouds, in which warm rain processes are highly suppressed. The consequences of the above effects include changes in both cloud geometries and the precipitation distribution induced by aerosols. The aerosol invigoration effect could have a dramatic impact on the Earth's radiation budget, global or regional circulation patterns, and the hydrological cycle.

Aerosols can also change regional circulation patterns by scattering or absorbing solar radiation. A model simulation using the NCAR CAM model shows that absorbing aerosols may heat the atmosphere and change the regional circulation over the eastern-central China region. The change in the regional circulation, together with the weakening East Asian winter monsoon, may create favorite conditions for fog formation and lead to the increase in fog frequency in the region as observed in recent thirty years.

A comprehensive evaluation of Collection 4 and 5 MODIS aerosol products using ground measurements was also conducted. The Collection 5 product uses a new method to determine the surface reflectance and a new aerosol model to retrieve AOT. Substantial improvement was found in the Collection 5 AOT product over the Collection 4 AOT product. For individual sites, the improvement varies with surface and atmospheric conditions.

6.2 Significance and Implication of the Findings

Due to the decreased solar radiation and suppressed evaporation at the surface under polluted conditions, the overall hydrological cycle should be slowed down. However, redistributions of latent heat within a convective cloud system overpower such effects and result in more vigorous convection and enhanced precipitation. Much stronger upward motions above the freezing level in mixed-phase convective clouds are observed in polluted conditions relative to those in clean conditions in our study. The upward motions stay strong up to an average height of 10km. This effect changes regional circulation patterns [*Bell et al*., 2008]. It also has the potential to change larger scale circulations that affect global climate [*Grimm et al*., 1995].

The strong updraft and delayed onset of precipitation could result in more aerosol particles, water, and trace gases transported into the upper troposphere. This happens through invigorated convection and thunderstorms. Studies showed that convective clouds can transport pollutants from the boundary layer into the upper troposphere [*Pickering et al*., 1989; *Ryan et al*., 1992; *Luke et al*., 1992] and enhance the stratosphere-troposphere exchange of trace gases [*Poulida et al., 1996*; *Stenchikov et al., 1996*], although in certain conditions, clouds can form above the boundary layer, which prevents

the entry of air from the boundary layer to higher altitudes [*Pickering et al., 1988*]. Stronger convection due to aerosols can enhance the process of transport. Summertime deep convective clouds forming in polluted conditions (CN:5000-6000cm^{-3}) reach approximately 10km (-40^{o}C) on average as shown in Fig. 2.3, about 2km higher than those forming in clean conditions (CN:0-1000cm^{-3}). They carry cloud particles into the upper troposphere and have higher chance for overshooting into the stratosphere. The delayed onset of precipitation suppresses the wet scavenging of aerosols, creating a positive feedback to maintain the condition of high aerosol loading. More aerosols and other pollutants can be transported to higher altitudes. The invigorated convection also leads to more lightning activities in relatively polluted conditions as observed by *Bell et al*., [2009].

Smaller cloud particles caused by higher aerosol loading reflect more solar radiation and result in negative forcing at the top of the atmosphere (the Twomey effect). However, this effect can be compensated for by changes of the overall distribution of cloud geometries and cloud water content. Clouds with higher tops, which occur more frequently in polluted conditions, emit less long wave radiation than clouds with lower tops, leading to a warming instead of a cooling effect caused by the Twomey effect. The magnitude of such forcing has not been estimated yet.

The invigoration effect may have significant implications for the global hydrological cycle. One implication is that pollution can have very different influences on precipitation under different meteorological and environmental conditions over different parts of the world. Clouds over arid regions are usually shallow so in the presence of pollutants, precipitation is more likely to be suppressed due to the rain

suppression effect, exacerbating aridity. Conversely, aerosols in moist areas are likely to deepen convective clouds to worsen flooding due to the invigoration effect. The strong signal of humanity's impact on nature emerged from the long-term observations, and thus has tremendous social and economic consequences.

The invigoration effect may be superimposed on other aerosol effects, such as the aerosol radiative effect, leading to much more complex responses of clouds and precipitation to perturbations of aerosols. A boomerang shape of cloud fraction (Fig. 6.1) with increasing AOT is found by *Koren et al*. [2008], which is explained as the dominate effect of aerosol invigoration for the lower AOT range but much stronger heating in clouds for the higher AOT range, leading to evaporation of cloud particles. The same kind of shape of CAPE in response to an increased $CCN_{0.4}$ has also been proposed in a conceptual model by *Rosenfeld et al*. [2008]. However, the proposed underlying process is somewhat different. The decrease of CAPE is due to both surface cooling caused by the aerosol radiative effect and the suppression of convection by extremely high aerosol loading.

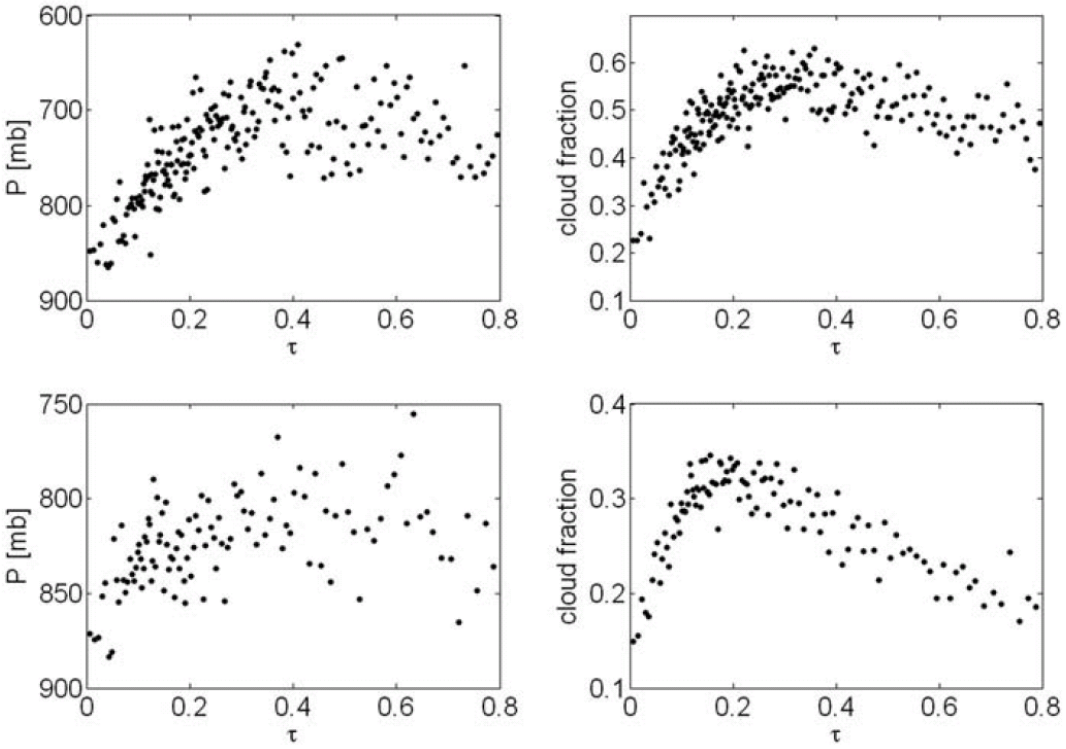

Fig. 6.1. Relationships between cloud properties and aerosol loading (estimated by τ). (Left panels) P versus τ. Lower P may indicate taller convective clouds that reach to higher levels of the atmosphere. (Right panels) Cloud fraction versus τ. The upper row shows all data and the lower row shows data restricted to a cloud fraction <0.5. The figure is from [*Koren et al*., 2008].

The observational evidence of aerosol effects on convective clouds and precipitation is a testimony to the hypotheses that human activities can redistribute clouds, and alter precipitation and latent heating profiles to a much greater extent than have thus far been accepted. Incorporation of these effects into climate models may reveal that aerosols have a much bigger anthropogenic forcing on the climate system that has not yet been accounted for in the vast majority of GCMs.

6.3 Areas of Interest in the Future

6.3.1 Global Impacts of the Aerosol Invigoration Effect

Aerosols invigorate clouds, leading to higher cloud tops and more frequent heavy rain. These effects could have significant impacts on the climate system. However, the magnitude of the warming effect due to higher cloud tops has not ever been estimated. Fortunately, the Clouds and Earth's Radiant Energy System (CERES) aboard the TERRA satellite provides the measurement of radiation fluxes at the top of the atmosphere (TOA). Using satellite data from MODIS, CloudSat/CALIPSO, and CERES, we will estimate the warming effect induced by the aerosol invigoration effect.

It is well known that GCMs tend to overestimate the formation of drizzle but underestimate the frequency of heavy rainfall. Though this is directly related to the parameterization of stratiform and convective clouds, it is also likely related to our poor understanding of the aerosol effects on these two kinds of clouds. Is it possible that we can improve simulations of precipitation in GCMs, if the different effects of aerosols on these two kinds of clouds are well represented in those models? To answer this question, we first need to estimate how aerosol indirect effects on clouds and precipitation are represented in GCMs by comparing them with results from observations, such as ground-based or satellite observations used in this study. The result may be used to generate more realistic parameterizations to improve model simulations.

6.3.2 Clouds in Extremely Polluted Conditions

In extremely polluted conditions, aerosols may have totally different influences on clouds and precipitation from those in moderately polluted conditions. Besides the

suppressed convection due to less solar radiation reaching the surface, ice rain processes could also be suppressed by aerosols if the aerosol concentration is too high, leading to a shift of the aerosol effect from the invigoration to the suppression of the convection and precipitation [*Rosenfeld et al*., 2008]. This is probably due to delayed freezing of smaller liquid cloud particles, causing super-cooled water to extend to lower temperature in highly polluted conditions [*Rosenfeld and Woodley*, 2000; *Lohmann and Feichter*, 2005]. In this case, no latent heat is released to invigorate the convection and the super-cooled water acts as a burden in rising air parcels. In the study of *Rosenfeld et al.* [2008], a conceptual model has shown that the CAPE increases with $CCN_{0.4}$ at first, but begins to decrease when $CCN_{0.4}$ is higher than 1200 cm^{-3}. However, no solid observational evidence has been provided to prove this hypothesis yet. There is another mechanism that can suppress cloud formation in extremely polluted conditions. In the cases with highly absorbing aerosols, clouds can also be invigorated in the low range of the aerosol concentration, but a high concentration of aerosols may eventually evaporate cloud particles, reduce cloud fractions, and suppress cloud development [*Koren et al*., 2008].

To test if clouds can be suppressed as aerosol loading is very high due to either of the above reasons, we extend the upper limit of the CN in Fig. 2.3B to 9000 cm^{-3} as shown in Fig. 6.2. We find that the cloud top temperature for warm base mixed-phase clouds decreases first with the CN and then increases gradually after the CN reaches above 6000 cm^{-3}. Unfortunately, the sample sizes are not very big, leading to large standard errors. Therefore, we do not draw any conclusion here. But this result could indicate that in highly polluted conditions, aerosols do begin to suppress convection and precipitation again, making aerosol effects on cloud and precipitation even more

complicated. This kind of study can greatly advance our understanding of the complexity of aerosol effects on clouds and precipitation.

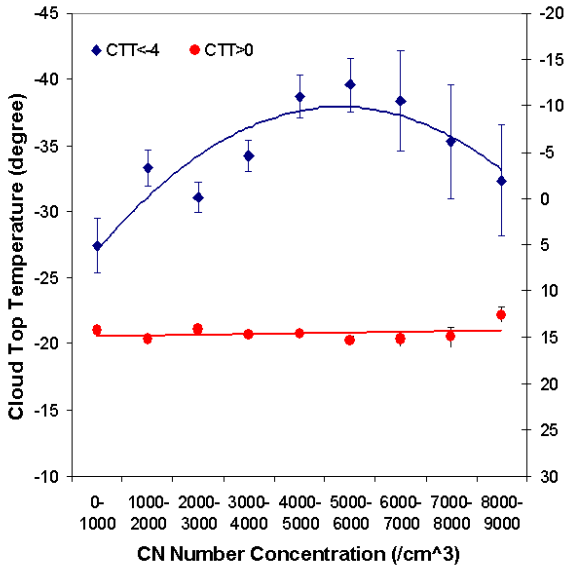

Fig. 6.2. Cloud top temperature as a function of CN number concentration for warm base mixed-phase (blue dots) and liquid clouds (red dots). Cloud top temperature is in reverse order. For warm base mixed-phase clouds, there are only 72 samples of clouds with CN in the range of 6000-9000cm^{-3}.

The above result indicates that different aerosol effects could co-exist and affect clouds and precipitation simultaneously. They may influence clouds and precipitation through three different pathways: radiative, microphysical and thermodynamic processes as discussed in Chapter 1. How aerosols influence climate through the combination of these pathways is of great interest in recent years [*Rosenfeld et al*., 2008; *Koren et al*., 2008]. Examination of these combined effects could help us to understand some contradictory results observed [*Khain et al*., 2008].

6.3.3 Aerosol Effects on Regional Climate over China

In China, aerosol loading has increased dramatically since the 1970s due to increased industrial emissions [*Luo et al.*, 2001]. As shown in Chapter 1, the high aerosol loading greatly cools the surface and heats the atmosphere [*Li et al.*, 2007a; *Xia et al.*, 2007]. The heating due to absorbing aerosols is shown to cause a cyclonic circulation pattern, which reduces invasions of cold air from the north, and increases fog frequency over eastern central China in winter from our model simulations in Chapter 5. These results indicate that the strong radiative effect of aerosols may change the winter monsoon and therefore the regional climate in China. Whether the strong aerosol radiative forcing also contributes the change in the summer monsoon, leading to changes in rainfall and other meteorological variables is also of great interest, as the summertime rainfall was shown to increase in the south but decreases in the north in recent several decades [*Xu*, 2001]. Meanwhile, the surface wind speed over the majority of areas in China also decreases [*Xu et al.*, 2006]. Model simulations using a climate model may be conducted to examine the influence of aerosols on the summer monsoon over China.

The high concentration of aerosols may also have dramatic impacts on clouds and precipitation through indirect effects. A hypothesis was proposed that the presence of high sulfate aerosol concentrations in eastern China is responsible for the discrepancy of the rain detection (Fig. 6.3) between TRMM TMI (TRMM Microwave Imager) and PR (Precipitation Radar), which are sensitive to cloud liquid water and cloud particle sizes, respectively [*Berg et al.*, 2006]. Clouds with high water contents but smaller particle sizes due to high aerosol loading may be only detected as raining clouds by TMI but not by PR. Using the technique proposed by *Rosenfeld and Lensky* [1998] and MODIS cloud

products, we found that over regions where TMI detects rain while PR does not, cloud particle sizes are generally smaller and barely increase with heights compared with those in regions without discrepancy (not shown here). This result provides preliminary evidence of the hypothesis. Further evidence may need more accurate observations of aerosols, clouds and meteorological conditions. Thanks to the projects of the East Asian Study of Troposheric Aerosols: An International Regional Experiment (EAST-AIRE) [*Li et al.*, 2007b] and the ARM Mobile Facility deployment in China (AMF-China), we will have unprecedented data sets to pursue studies concerning indirect effects of aerosols. How to use the data collected during these two projects to test the hypothesis, and further study the aerosol indirect effect on cloud systems and precipitation patterns in a broad scope in this region will be a main topic in our future work.

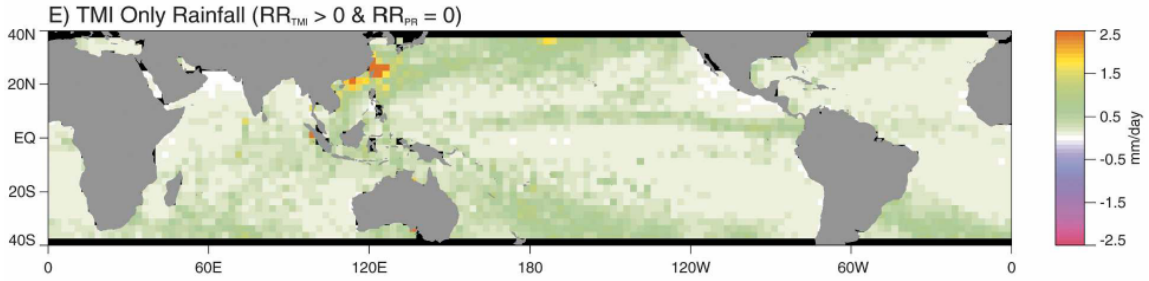

Fig. 6.3. Seasonal mean rainfall estimates from December 1999 through February 2000 based on matched pixels indicating rainfall by TMI only. [*Berg et al.*, 2006]

Bibliography

Albrecht, B. (1989), Aerosols, cloud microphysics, and fractional cloudiness, *Science*, 245, 1227–1230.

Andreae, M. O. et al. (2004), Smoking Rain Clouds over the Amazon, *Science* 303, 1337–1341.

Andreae, M. O. (2009), Correlation between cloud condensation nuclei concentration and aerosol optical thickness in remote and polluted regions, *Atmos. Chem. Phys*., 9, 543-556, doi:10.5194/acp-9-543-2009.

Ackerman, A.S., et al. (2000), Reduction of tropical cloudiness by soot. *Science*, 288, 1042–1047.

Ackerman, S.A., K.I. Strabala, W.P. Menzel, R.A. Frey, C.C. Moeller, and L.E. Gumley (1998), Discriminating clear-sky from clouds with MODIS, *J. Geophys. Res*., 103, 32141-32158.

Ackerman, T., G. Stokes, (2003), The atmospheric radiation measurement program. *Physics Today*, 56, 38-45.

Bell, T. L., D. Rosenfeld, K.-M. Kim, J.-M. Yoo, M.-I. Lee, and M. Hahnenberger (2008) Midweek increase in U.S. summer rain and storm heights suggests air pollution invigorates rainstorms. *J. Geophys. Res*., 113, D02209, doi:10.1029/2007JD008623.

Bell, T. L., D. Rosenfeld, and K.-M. Kim (2009), Weekly cycle of lightning: Evidence of storm invigoration by pollution, *Geophys. Res. Lett.*, 36, L23805, doi:10.1029/2009GL040915.

Berg, W, T L'Ecuyer, and C Kummerow (2006), Rainfall climate regimes: The relationship of regional TRMM rainfall biases to the environment, *Journal of Applied Meteorology* 45(3), 434-454.

Bollasina, M., and S. Nigam (2008), Indian Ocean SST, evaporation, and precipitation during the South Asian summer monsoon in IPCC-AR4 coupled simulations, *Clim. Dyn*., doi:10.1007/s00382-008-0477-4.

Bollasina, M., and S. Nigam (2009), Absorbing aerosols and pre-summer monsoon hydroclimate variability over the Indian subcontinent: The challenge in investigating links, *Atmos. Res*., 94, 338–344.

Brenguier, J.L., et al. (2000a), Radiative properties of boundary layer clouds: droplet effective radius versus number concentration, *J. Atmos. Sci*., 57, 803–821.

Brenguier, J.L., et al. (2000b), An overview of the ACE-2 CLOUDYCOLUMN closure experiment, *Tellus*, 52B, 815–827.

Brenguier, J.L., H. Pawlowska, and L. Schuller (2003), Cloud microphysical and radiative properties for parametrization and satellite monitoring of the indirect effect of aerosol on climate. *J. Geophys. Res.*, 108(D15), 8632, doi:10.1029/2002JD002682.

Bréon F-M., et al. (2002), Aerosol Effect on Cloud Droplet Size Monitored from Satellite, *Science,* 295, 834; DOI: 10.1126/science.1066434.

Chaudhry, Z., J. V. Martins, Z. Li, S.-C. Tsay, H. Chen, P. Wang, T. Wen, C. Li, and R. R. Dickerson (2007), In-situ measurements of aerosol mass concentration and radiative properties in Xianghe, southeast of Beijing, J. Geophys. Res., 112, D23S90, doi:10.1029/2007JD009055.

Chen, W., H. F. Graf and R. Huang (2001), The interannual variability of East Asian winter monsoon and its relation to the summer monsoon, *Adv. Atmos. Sci.*, 17(1), 48–60.

Chu, D.A., Y.K. Kaufman, C. Ichoku, L.A. Remer, D. Tanré, and B.N. Holben (2002), Validation of MODIS aerosol optical depth retrieval over land, *Geophys. Res. Lett.*, 29(12), doi:10.1029/2001GL013205.

Chung, C. E., and V. Ramanathan (2006), Weakening of North Indian SST Gradients and the Monsoon Rainfall in India and the Sahel, *J. Climate*, 19, 2036-2045.

Clothiaux E. E. et al. (2000), Objective determination of cloud heights and radar reflectivities using a combination of active remote sensors at the ARM CART sites, J. Appl., Meteorol. 39, 645– 665.

Collins, W. D., P. J. Rasch, B. E. Eaton, B. V. Khattatov, J.-F. Lamarque, and C. S. Zender (2001), Simulating aerosols using a chemical transport model with assimilation of satellite aerosol retrievals: Methodology for INDOEX, *J. Geophys. Res.*, 106(D7), 7313–7336.

Collins, W. D., P. J. Rasch, B. E. Eaton, D. W. Fillmore, J. T. Kiehl, C. T. Beck, and C. S. Zender (2002), Simulation of aerosol distributions and radiative forcing for INDOEX: Regional climate impacts, *J. Geophys. Res.*, 107(D19), 8028, doi:10.1029/2000JD000032.

Delworth, T. L., and T. R. Knutson (2000), Simulation of early 20th century global warming, *Science*, 287, 2246– 2250.

Diner, D. J., J. V. Martonchik, R. A. Kahn, B. Pinty, N. Gobron, D. L. Nelson, B. N. Holben, 2005 Using angular and spectral shape similarity constraints to improve

MISR aerosol and surface retrievals over land. *Remote Sensing of Environment.* 94 (2), 155-171.

Eck, T. F., B. N. Holben, O. Dubovik, A. Smirnov, P. Goloub, H. B. Chen, B. Chatenet, L. Gomes, X.-Y. Zhang, S.-C. Tsay, Q. Ji, D. Giles, I. Slutsker (2005), Columnar aerosol optical properties at AERONET sites in central eastern Asia and aerosol transport to the tropical mid-Pacific, *J. Geophys. Res.*, 110, D06202, doi:10.1029/2004JD005274.

Ellis, T. D., T. L'Ecuyer, J. M. Haynes, and G. L. Stephens (2009), How often does it rain over the global oceans? The perspective from CloudSat, *Geophys. Res. Lett.*, 36, L03815, doi:10.1029/2008GL036728.

Fan, J., R. Zhang, G. Li, W.-K. Tao and X. Li (2007), Simulations of cumulus clouds using a spectral microphysics cloud-resolving model, *J. Geophys. Res.*, 112, D04201, doi:10.1029/2006JD007688.

Feingold, G., H. Jiang, and J. Y. Harrington (2005), On smoke suppression of clouds in Amazonia, *Geophys. Res. Lett.*, 32, L02804, doi:10.1029/2004GL021369.

Feingold, G., S.M. Kreidenweis, and Y.P. Zhang (1998), Stratocumulus processing of gases and cloud condensation nuclei: Trajectory ensemble model, *J. Geophys. Res.,* 103(D16), 19527–19542.

Feingold, G., W.L. Eberhard, D.E. Veron, and M. Previdi (2003), First measurements of the Twomey indirect effect using ground-based remote sensors, *Geophys. Res. Lett.*, 30(6), 1287, doi:10.1029/2002GL016633.

Feingold, G., W.R. Cotton, S.M. Kreidenweis, and J.T. Davis (1999), The impact of giant cloud condensation nuclei on drizzle formation in stratocumulus: Implications for cloud radiative properties, *J. Atmos. Sci.*, 56, 4100–4117.

Ferek, R.J., et al. (1998), Measurements of ship-induced tracks in clouds off the Washington coast, *J. Geophys. Res.*, 103, 23199–23206.

Flato, G., and G.J. Boer (2001), Warming asymmetry in climate change simulations, *Geophy. Res. Lett.*, 28, 195-198.

Freud, E., Rosenfeld, D., Andreae, M. O., Costa, A. A., and Artaxo, P. (2008), Robust relations between CCN and the vertical evolution of cloud drop size distribution in deep convective clouds, *Atmos. Chem. Phys.*, 8, 1661-1675, doi:10.5194/acp-8-1661-2008.

Gao, H. (2007), Comparison of East Asian winter monsoon indices, *Adv. Geosci.*, 10, 31–37.

Giorgi, F., X. Bi, and Y. Qian (2002), Direct radiative forcing and regional climatic effects of anthropogenic aerosols over East Asia: A regional coupled climate-chemistry/aerosol model study, *J. Geophys. Res.*, 107(D20), 4439, doi:10.1029/2001JD001066.

Gong, D., S. Wang, and J. Zhu (2001), East Asian winter monsoon and Arctic oscillation. Geophys, *Res. Lett.*, *28*, 2073–2076.

Gong, S.L., and L.A. Barrie (2003), Simulating the impact of sea salt on global nss sulphate aerosols, *J. Geophys. Res.*, 108(D16), 4516, doi:10.1029/2002JD003181.

Graßl, H.: Possible changes of planetary albedo due to aerosolparticles, in Man's Impact on Climate, edited by: W. Bach,J. Pankrath, and W. Kellogg, Elsevier, New York, 1979.

Grimm, A. M., and P. L. Silva Dias (1995), Analysis of tropical–extratropical interactions with influence functions of a barotropic model, J. Atmos. Sci., 52, 3538–3555.

Guo, Q. Y. (1994), Relationship between the variability of East Asia winter monsoon and temperature anomalies in China, *Q. J. Appl. Meteorology.,* 5, 218–225.

Han Q., W.B. Rossow and A.A. Lacis (1994), Near-global survey of effective droplet radii in liquid water clouds using ISCCP data, *J. Climate*, 7, 465–497.

Hansen, J., M. Sato, and R. Ruedy (1997), Radiative forcing and climateresponse. *J. Geophys. Res.*, 102, 6831–6864.

Hao, W.M., D.E. Ward, R.A. Susott, R.E. Babbitt, B.L. Nordgren, Y.J. Kaufman, B.N. Holben, and D.M. Giles (2005), Comparison of aerosol optical thickness measurements by MODIS, AERONET sun photometers, and Forest Service handheld sun photometers in southern Africa during the SAFARI 2000 campaign, *Int. J. Remote Sensing*, 26, 4169-4183.

Haynes, J. M., T. S. L'Ecuyer, G. L. Stephens, S. D. Miller, C. Mitrescu, N. B. Wood, and S. Tanelli (2009), Rainfall retrieval over the ocean with spaceborne W-band radar, *J. Geophys. Res*., 114, D00A22, doi:10.1029/2008JD009973.

Held, I.M., et al. (2005), Simulation of Sahel drought in the 20th and 21st centuries, *Proc. Natl. Acad. Sci. U.S.A.*, 102(50), 17891–17896

Holben, B.N., T.F. Eck, I. Slutsker, D. Tanré, J.B. Buis, A. Setzer, E. Vermote, J.A. Reagan, Y.J. Kaufman, T. Nakajima, F. Lavenu, I. Jankowiak, and A. Smirnov (1998), AERONET – a federated instrument network and data archive for aerosol characterization, *Remote Sens. Environ.*, 66, 1-16.

Hori, M. E., and H. Ueda (2006), Impact of global warming on the East Asian winter monsoon as revealed by nine coupled atmosphere-ocean GCMs, *Geophys. Res. Lett.*, 33, L03713, doi:10.1029/2005GL024961.

Houghton, J. T. (1985), The global climate, *Cambridge University Press*, 81.

Hsu, N.C., S.-C. Tsay, M.D. King, and J.R. Herman (2004), Aerosol properties over bright-reflecting source regions, *IEEE Trans. Geosci. Remote Sens.*, 42(3), 557-569.

Hu, Z.-Z., L. Bengtsson, and K. Arpe (2000), Impact of global warming on the Asian winter monsoon in a coupled GCM, *J. Geophys. Res.*, 105, 4607– 4624.

Hu, Z.-Z., S. Yang, and R. Wu (2003), Long-term climate variations in China and global warming signals, *J. Geophys. Res.*, 108(D19), 4614, doi:10.1029/2003JD003651.

Jhun, J. and E. Lee (2004), A new East Asian winter monsoon index and associated characteristics of the winter monsoon, *J. Climate*, 17(4), 711–726.

Ichoku, C, D.A. Chu, S. Mattoo, Y.J. Kaufman, L.A. Remer, D. Tanré, I. Slutsker, and B.N. Holben (2002), A spatio-temporal approach for global validation and analysis of MODIS aerosol products, *Geophys. Res. Lett.*, 29(12), doi:10.1029/2001GL013206.

Ignatov, A. J. Sapper, S. Cox, I. Laszlo, N.R. Nalli, and K.B. Kidwell (2004), Operational aerosol observations (AEROBS) from AVHRR/3 on board NOAA-KLM satellites, *J. Atmos. Oceanic Technol.*, 21, 3-25.

IPCC, 2007: Climate Change 2007: The Physical Science Basis. Contribution of Working Group I to the Fourth Assessment Report of the Intergovernmental Panel on Climate Change [Solomon, S., D. Qin, M. Manning, Z. Chen, M. Marquis, K.B. Averyt, M.Tignor and H.L. Miller (eds.)]. *Cambridge University Press*, Cambridge, United Kingdom and New York, NY, USA.

Jeong, M.-J., Z. Li (2005a), Quality, Compatibility and Synergy Analyses of Global Aerosol Products derived from the Advanced Very High Resolution Radiometers and Total Ozone Mapping Spectrometers, *J. Geophy. Res.*, 110, D10S08, doi:10.1029/2004JD00464.

Jeong, M.J , Z. Li, D.A. Chu, and S-T. Tsay (2005b), Quality and Compatibility Analyses of Global Aerosol Products Derived from the Advanced Very High Resolution Radiometers and the Moderate Imaging Spectroradiometer, *J. Geophy. Res.*, 110, D10S09, doi:10.1029/2004JD004648.

Jeong, M.-J., Z. Li, E. Andrews, and S.-C. Tsay (2007), Effect of aerosol humidification on the column aerosol optical thickness over the Atmospheric Radiation Measurement Southern Great Plains site, *J. Geophys. Res.*, 112, D10202,doi:10.1029/2006JD007176.

Ji, L, S. Sun, K. Arpe and L. Bengtsson (1997), Model Study on the interannual variability of Asian winter monsoon and its influence, *Adv. Atmos. Sci.*, 14(1), 1–22.

Jiang, H., G. Feingold, and W.R. Cotton (2002), Simulations of aerosol cloud-dynamical feedbacks resulting from of entrainment of aerosols into the marine boundary layer during the Atlantic Stratocumulus Transition Experiment, *J. Geophys. Res*., 107(D24), 4813, doi:10.1029/2001JD001502.

Jiang, H., et al. (2006), Aerosol effects on the lifetime of shallow cumulus, *Geophys. Res. Lett*., 33, doi:10.1029/2006GL026024.

Jiang, J.H., H. Su, M. Schoeberl, S.T. Massie, P. Colarco, S. Platnick, and N. Livesey (2008), Clean and polluted clouds: relationships among pollution, ice cloud and precipitation in South America, *Geophys. Res. Lett.* 35, L14804, doi:10.1029/2008GL034631.

Jiang, J.H., H. Su, S.T. Massie, P.R. Colarco, M.R. Schoeberl, and S. Platnick (2009), Aerosol-CO relationship and aerosol effect on Ice cloud particle size: Analyses from Aura MLSand Aqua MODIS observations, *J. Geophys. Res.* 114, D20207, doi:10.1029/2009JD012421.

Kahn, R., B. Gaitley, J. Martonchik, D. J. Diner, C. A. Crean, and B. Holben (2005), Multiangle Imaging Spectroradiometer (MISR) global aerosol optical depth validation based on 2 years of coincident Aerosol Robotic Network (AERONET) observation, *J. Geophys. Res.*, 110, doi:10.1029/2004JD004706.

Kaiser, D. P., and Y. Qian (2002), Decreasing trends in sunshine duration over China for 1954-1998: indication of increased haze pollution?, *Geophys. Res. Lett., 29*(21), 2042, doi:10.1029/2002GL016057.

Kaufman, Y.J., and I. Koren (2006), Smoke and pollution aerosol effect on cloud cover, *Science*, 313, 655–658, doi:10.1126/science.1126232.

Kaufman, Y.J. and R.S. Fraser (1997), The effect of smoke particles on clouds and climate forcing, *Science*, 277, 1636–1639.

Kaufman, Y.J. and T. Nakajima (1993), Effect of Amazon smoke on cloud microphysics and albedo - Analysis from satellite imagery, *J. Appl. Meteor.* 32, 729–744.

Kaufman, Y.J., et al. (2005), The effect of smoke, dust, and pollution aerosolon shallow cloud development over the Atlantic Ocean. *Proc. Natl.Acad. Sci. U.S.A.*, 102(32), 11207–11212.

Kaufman, Y. J., D. Tanre´, L. A. Remer, E. F. Vermote, A. Chu, and B. N. Holben (1997a), Operational remote sensing of tropospheric aerosol over land from EOS moderate resolution imaging spectroradiometer, *J. Geophys. Res.*, 102(D14), 17,051– 17,067.

Kaufman, Y.J., Wand, A.E., Remer, L.A., Gao, B.C., Li, R.R., and Flynn, L. (1997b), The MODIS 2.1-㎛ channel correlation with visible reflectance for use in remote sensing of aerosol. *IEEE Transactions on Geoscience and Remote Sensing*, 35, 1286-1298.

Khain, A., D. Rosenfeld, and A. Pokrovsky (2005), Aerosol impact on the dynamics and microphysics of deep convective clouds, *Q. J. R. Meteorol. Soc.*, 131, 1-25.

Khain, A., N. BenMoshe, and A. Pokrovsky (2008), Factors Determining the Impact of Aerosols on Surface Precipitation from Clouds: An Attempt at Classification, *J. Atmos. Sci.*, 65, 1721–1748.

Kimoto, M. (2005), Simulated change of the East Asian circulation under global warming scenario, *Geophys. Res. Lett.*, 32, L16701, doi:10.1029/2005GL023383.

Kistler, R. et al. (2001), The NCEP-NCAR 50-year reanalysis: Monthly means CD-ROM and documentation, *Bull. Am. Meteorol. Soc*., 82, 247– 267.

Klein, S. A., and D. L. Hartmann (1993), The seasonal cycle of low stratiform clouds, *J. Clim.*, 6, 1587– 1606.

Koren, I., Y.J. Kaufman, L.A. Remer, and J.V. Martins (2004), Measurements of the effect of smoke aerosol on inhibition of cloud formation, *Science*, 303, 1342–1345.

Koren, I., Y. J. Kaufman, D. Rosenfeld, L. A. Remer, and Y. Rudich (2005), Aerosol invigoration and restructuring of Atlantic convective clouds, *Geophys. Res. Lett*., 32, L14828, doi:10.1029/2005GL023187.

Koren, J. V. Martins, L. A. Remer, H. Afargan (2008), Smoke invigoration versus inhibition of clouds over the Amazon, *Science*, 321, 946– 949.

Hudak, D., H. Barker, P. Rodriguez, and D. Donovan (2006a), The Canadian CloudSat Validation Project. 4th European Conf. on Radar in Hydrology and Meteorology, Barcelona, Spain, 18-22 Sept., 2006, 609-612.

Hudak, D., H. Barker, K. Strawbridge, M. Wolde, A. Kankiewicz, and W. Strapp (2007), The Canadian CloudSat CALIPSO Validation Project: Evaluation ofsensitivity and sub-pixel variability of CloudSat data products. 33rd Conference on Radar Meteorology, AMS, Cairns, Australia, 6-10 August, 2007.

Hudak, D., P. Rodriguez1, H. Barker (2009), Results from the Canadian CloudSat CALIPSO Validation Project (C3VP), CloudSat/CALIPSO Science Team Meeting, Madison, Wisconsin, U.S., July 28-31, 2009.

Lau, K. -M, V. Ramanathan, G-X. Wu, Z. Li, S. C. Tsay, C. Hsu, R.Sikka, B. Holben, D. Lu, G. Tartari, M. Chin, P .Koudelova, H. Chen, Y. Ma, J. Huang, K. Taniguchi, and R. Zhang. (2008), The Joint Aerosol-Monsoon Experiment: A New Challenge in Monsoon Climate Research, *Bull. Am. Meteor. Soc*., 89, 369-383, DOI:10.1175/BAMS-89-3-369.

Lau, K.-M., and K.-M. Kim (2006a), Observational relationships between aerosol and Asian monsoon rainfall, and circulation, *Geophys. Res. Lett., 33*, L21810, doi:10.1029/2006 GL027546.

Lau, K. M., M. K. Kim, and K. M. Kim (2006b), Asian monsoon anomalies induced by aerosol direct effects, *Clim. Dyn*., 26, 855–864, doi:10.1007/s00382-006-0114-z.

Lebsock, M. D., G. L. Stephens, and C. Kummerow (2008), Multisensor satellite observations of aerosol effects on warm clouds, *J. Geophys. Res*., 113, D15205, doi:10.1029/2008JD009876.

Lee, K., Z. Li, Y.J. Kim, A. Kokhanovsky (2009), Atmospheric Aerosol Monitoring from Satellite Observations: A History of Three Decades, in Atmospheric and Biological Environmental Monitoring, *Springer Pub*.

Lee, K. H., Z. Li, M. S. Wong, J. Xin, Y. Wang, W.-M. Hao, and F. Zhao (2007), Aerosol single scattering albedo estimated across China from a combination of ground and satellite measurements, *J. Geophys. Res.*, *112*, D22S15, doi:10.1029/2007JD009077.

Lee, S. S., Donner, L. J., and Penner, J. E. (2010), Thunderstorm and stratocumulus: how does their contrasting morphology affect their interactions with aerosols?, *Atmos. Chem. Phys.,* 10, 6819-6837, doi:10.5194/acp-10-6819-2010.

Lelieveld, J., et al. (2002), Global air pollution crossroads over the Mediterranean. *Science*, 298, 794–799.

Levy, R.C., L.A. Remer, D. Tanré, Y.J. Kaufman, C. Ichoku, B.N. Holben, J.M. Livingston, P.B. Russell and H. Maring (2003), Evaluation of the MODIS retrievals of dust aerosol over the ocean during PRIDE. *J. Geophys. Res.*, 108 (D14), 10.1029/2002JD002460.

Levy, R. C., L. A. Remer, S. Mattoo, E. F. Vermote, and Y. J. Kaufman (2007a), Second-generation operational algorithm: Retrieval of aerosol properties over land from inversion of Moderate Resolution Imaging Spectroradiometer spectral reflectance, *J. Geophys. Res.*, 112, D13211, doi:10.1029/2006JD007811.

Levy, R. C., L. A. Remer, and O. Dubovik (2007b), Global aerosol optical properties and application to Moderate Resolution Imaging Spectroradiometer aerosol retrieval over land, *J. Geophys. Res.*, 112, D13210, doi:10.1029/2006JD007815.

Levy, R. C., Remer, L. A., Kleidman, R. G., Mattoo, S., Ichoku, C., Kahn, R., and Eck, T. F. (2010), Global evaluation of the Collection 5 MODIS dark-target aerosol products over land, Atmos. *Chem. Phys. Discuss.*, 10, 14815-14873, doi:10.5194/acpd-10-14815-2010.

Li, C., L. T. Marufu, R. R. Dickerson, Z. Li, T. Wen, Y. Wang, P. Wang, H. Chen, and J. W. Stehr (2007), In situ measurements of trace gases and aerosol optical properties at a rural site in northern China during East Asian Study of Tropospheric Aerosols: An International Regional Experiment 2005, J. *Geophys. Res.*, 112, D22S04, doi:10.1029/2006JD007592.

Li C.C., J.T. Mao, K-H.A. Lau, J.C. Chung, Z. Yuan, X. Liu, A. Zhu, G. Liu (2003), Characteristics of distribution and seasonal variation of aerosol optical depth in eastern China with MODIS products, *Chinese Sci. Bull.*, 48, 2488-2495.

Li, Z. (1998), Influence of absorbing aerosols on the inference of solar surface radiation budget and cloud absorption, *J. Climate*, 11, 5-17.

Li, Z. (2004), Aerosol and climate: A perspective from East Asia, *Observation, Theory and Modeling of Atmospheric Variability* (ed. Zhu), World Scientific Pub. Co., 501-525.

Li, Z., et al. (2007a), Aerosol optical properties and their radiative effects in northern China, *J. Geophys. Res.*, 112, D22S01, doi:10.1029/2006JD007382.

Li, Z., et al. (2007b), Preface to special section: Overview of the East Asain Study of Tropospheric Aerosols: an International Regional Experiment (EAST-AIRE), *J. Geophy. Res.* D22S00, doi:10.1029/2007JD008853.

Li, Z., F. Niu, K.-H. Lee, J. Xin, W.-M. Hao, B. Nordgren, Y. Wang, and P. Wang (2007c), Validation and understanding of Moderate Resolution Imaging Spectroradiometer aerosol products (C5) using ground-based measurements from the handheld Sunphotometer network in China, *J. Geophys. Res*., *112*, D22S07, doi:10.1029/2007JD008479.

Li, Z., X. Zhao, R. Kahn, M. Mishchenko, L. Remer, K.-H. Lee, M.Wang, I. Laszlo, T. Nakajima, and H. Maring (2009), Uncertainties in satellite remote sensing of aerosols and impact on monitoring its long-term trend: a review and perspective, *Ann. Geophys*., 27, 1–16.

Li, Z., K.-H. Lee, J. Xin, Y. Wang, W.-M. Hao (2010), First observation-based estimates of aerosol radiative forcing at the top, bottom and inside of the atmosphere, *J. Geophys. Res*., 115, D00K18, doi:10.1029/2009JD013306.

Liljegren, J. C., Two-channel microwave radiometer for observations of total column precipitable water vapor and cloud liquid water path, paper presented at Fifth Symposium on Global Climate Change Studies, Nashville, TN, 25–28 Jan 1994.

Lin, J. C., T. Matsui, R. A. Pielke Sr., and C. Kummerow (2006), Effects of biomass-burning-derived aerosols on precipitation and clouds in the Amazon Basin: a satellite-based empirical study, *J. Geophys. Res*., 111, D19204, doi:10.1029/2005JD006884.

Liu, B., M. Xu, M. Henderson, Y. Qi, and Y. Li (2004a), Taking China's temperature: Daily range, warming trends, and regional variations, 1955–2000, *J. Clim*ate, *17*, 4453– 4462.

Liu, G., H. Shao, J. A. Coakley Jr., J. A. Curry, J. A. Haggerty, and M. A. Tschudi (2003), Retrieval of cloud droplet size from visible and microwave radiometric measurements during INDOEX: Implication to aerosols' indirect radioactive effect, *J. Geophys. Res*., 108(D1), 4006, doi:10.1029/2001JD001395.

Loeb, N. G., and G. L. Schuster (2008), An observational study of the relationship between cloud, aerosol and meteorology in broken low-level cloud conditions, *J. Geophys. Res*., 113, D14214, doi:10.1029/2007JD009763.

Lohmann, U., J. Feichter (2005), Global indirect aerosol effects: a review. *Atmos. Chem. Phys*. 5, 715−737.

Luke, W. T., R. R. Dickerson, W. F. Ryan, K. E. Pickering, and L. J. Nunnermacker (1992), Tropospheric Chemistry Over the Lower Great Plains of the United States 2. Trace Gas Profiles and Distributions, *J. Geophys. Res.*, 97(D18), 20,647–20,670, doi:10.1029/92JD02127.

Luo, Y., D. Lu, X. Zhou, W. Li, and Q. He (2001), Characteristics of the spatial distribution and yearly variation of aerosol optical depth over China in last 30 years, *J. Geophys. Res.*, *106*(D13), 14,501–14,513.

Martins, J.V., L. Remer, Y.J. Kaufman, S. Mattoo, and R. Levy (2002), MODIS cloud screening for remote sensing of aerosols over oceans using spatial variability, *Geophys. Res. Lett.*, 29(12), doi:10.1029/2001GL013252.

Matheson, M. A., J. A. Coakley Jr., and W. R. Tahnk (2005), Aerosol and cloud property relationships for summertime stratiform clouds in the northeastern Atlantic from Advanced Very High Resolution Radiometer observations, *J. Geophys. Res*., 110, D24204, doi:10.1029/2005JD006165.

Menon, S., J. Hansen, L. Nazarenko, and Y. Luo (2002), Climate effects of black carbon aerosols in China and India, *Science*, *297*, 2250–2253.

Mi, W., Z. Li, X. Xia, B. Holben, R. Levy, F. Zhao, H. Chen, and M. Cribb (2007), Evaluation of the Moderate Resolution Imaging Spectroradiometer aerosol products at two Aerosol Robotic Network stations in China, *J. Geophys. Res*., *112*, D22S08, doi:10.1029/2007JD008474.

Miller, R.L., I. Tegen, and J. Perlwitz, 2004b: Surface radiative forcingby soil dust aerosols and the hydrologic cycle. *J. Geophys. Res*., 109, D04203, doi:10.1029/2003JD004085.

Min, S. K., E. H. Park, and W. T. Kwon (2004), Future projections of East Asian climate change from multi-AOGCM ensembles of IPCC SRES scenario simulations, *J. Meteor. Soc. Jpn*, *82*, 1187– 1211.

Mishchenko, M.I., I.V. Geogdzhayev, B. Cairns, W.B. Rossow, and A.A. Lacis (1999), Aerosol retrievals over the ocean by use of channels 1 and 2 AVHRR data: sensitivity analysis and preliminary results. *Appl. Optics*, 38, 7325-7341.

Mishchenko, M.I., I.V. Geogdzhayev, L. Liu, J.A. Ogren, A.A. Lacis, W.B. Rossow, J.W. Hovenier, H. Volten, O. Munoz (2003), Aerosol retrievals from AVHRR radiances: effects of particle nonsphericity and absorption and an updated long-term global climatology of aerosol properties, *J. Quantitative Spectroscopy and Radiative Transfer*, 79-80, 953-972.

Murakami, T. (1987), Effects of the Tibetan Plateau, *Monsoon Meteorology*, C. Chang, and T. Krishnamurti, Eds., Oxford University Press, 235–270.

Nakajima, T. and A. Higurashi (1998), A use of two-channel radiances for an aerosol characterization from space, *Geophys. Res. Lett.*, 25(20), 3815-3818.

Nakajima, T., A. Higurashi, K. Kawamoto, and J. Penner, 2001: A possible correlation between satellite-derived cloud and aerosol microphysical parameters. *Geophys. Res. Lett.*, 28, 1171–1174.

Niu, F., Z. Li, C. Li, K.-H. Lee, and M. Wang (2010), Increase of wintertime fog in China: Potential impacts of weakening of the Eastern Asian monsoon circulation and increasing aerosol loading, *J. Geophys. Res.*, 115, D00K20, doi:10.1029/2009JD013484.

Niu, S., C. Lu, H. Yu, L. Zhao, J. Lu (2009), Fog research in China: an overview, *Adv. Atmos. Sci.*, doi: 10.1007/s00376-009-8174-8.

Paeth, H., and J. Feichter, 2006: Greenhouse-gas versus aerosol forcingand African climate response. *Clim Dyn*., 26(1), 35–54.

Penner, J.E., X. Dong, and Y. Chen (2004), Observational evidence of a change in radiative forcing due to the indirect aerosol effect, *Nature*, 427, 231-234.

Pickering, K. E., R. R. Dickerson, G. J. Huffman, J. F. Boatman, and A. Schanot (1988), Trace Gas Transport in the Vicinity of Frontal Convective Clouds, *J. Geophys. Res.*, 93(D1), 759–773.

Pickering, K. E., R. R. Dickerson, W. T. Luke, and L. J. Nunnermacker (1989), Clear-sky vertical profiles of trace gases as influenced by upstream convective activity, *J. Geophys. Res.*, 94(D12), 14,879–14,892.

Poulida, O., R. R. Dickerson, and A. Heymsfield (1996), Stratosphere-troposphere exchange in a midlatitude mesoscale convective complex 1. Observations, *J. Geophys. Res.*, 101(D3), 6823–6836, doi:10.1029/95JD03523.

Pu, M. J., G. Z. Zhang, W. L. Yan, Z. H. Li (2008), Features of a rare advection-radiation fog event, *SCIENCE IN CHINA SERIES D: EARTH SCIENCES*, *51*(7), 1044-1052.

Qian, Y., and F. Giorgi (1999), Interactive coupling of regional climate and sulfate aerosol models over eastern Asia, *J. Geophys. Res., 104(D6),* 6477-6499.

Qian, Y., L. R. Leung, S. J. Ghan, and F. Giorgi (2003), Regional Climate Effects of Aerosols Over China: Modeling and Observation, *Tellus Series B, Chemical and Physical Meteorology, 55(4),* 914-934.

Ramanathan, V., P. J. Crutzen, J. T. Kiehl, and D. Rosenfeld (2001), Aerosols, climate and the hydrological cycle, *Science*, *294*, 2119–2124.

Ramanathan, V., and Coauthors (2005), Atmospheric brown clouds: Impact on South Asian climate and hydrologic cycle, *Proc. Natl. Acad. Sci. USA, 102*, 5326–5333.

Rasch, P. J., N. M. Mahowald, and B.E. Eaton (1997), Representations of transport, convection, and the hydrologic cycle in chemical transport models: Implications for the modeling of short-lived and soluble species, *J. Geophys. Res*., *102*, 28,127-28,138.

Remer, L. A., Y. J. Kaufman, D. Tanre, S. Mattoo, D. A. Chu, J. V. Martins, R-R. Li, C. Ichoku, R. C. Levy, R. G. Kleidman, T. F. Eck, E. Vermote, B. N. Holben (2005), The MODIS Aerosol Algorithm, Products and Validation, *J. Atmos. Sci.*, 62, 947-973.

Roberts, G. C., M. O. Andreae, J. Zhou, and P. Artaxo (2001), Cloud condensation nuclei in the Amazon Basin: "marine" conditions over a continent?, Geophys. Res. Lett., 28(14), 2807–2810, doi:10.1029/2000GL012585.

Rosenfeld, D. (2000), Suppression of rain and snow by urban and industrial air pollution, *Science*, 287, 1793–1796.

Rosenfeld, D., G. Gutman (1994), Retrieving microphysical properties near the tops of potential rain clouds by multispectral analysis of AVHRR data, *Atmospheric Research* 34, 259-283.

Rosenfeld, D. et al. (2008), Flood or drought: How do aerosols affect precipitation? *Science*, 321, 309.

Rosenfeld, D., and I. Lensky (1998), Satellite-based insights into precipitation formation processes in continental and maritime convective clouds, *Bull. Am. Meteorol. Soc*., 79, 2457–2476.

Rosenfeld, D., R. Lahav, A. Khain, and M. Pinsky (2002), The role of sea spray in cleansing air pollution over the ocean via cloud processes. *Science*, 297, 1667–1670.

Rosenfeld, D., and W. L. Woodley (2000), Deep convective clouds with sustained super-cooled liquid water down to −37.5°C, *Nature*, 405, 440–442.

Rotstayn, L.D., and U. Lohmann (2002), Tropical rainfall trends and theindirect aerosol effect. *J. Clim.*, 15, 2103–2116.

Ryan, W. F., R. R. Dickerson, G. J. Huffman, and W. T. Luke (1992), Tropospheric Chemistry Over the Lower Great Plains of the United States. 1. Meteorology, *J. Geophys. Res.*, 97(D16), 17,963–17,984, doi:10.1029/92JD01375.

Sachweh, M., and P. Koepke (1995), Radiation fog and urban climate, *Geophys. Res. Lett.*, 22(9), 1073–1076.

Shao, H., G. Liu, Why is the satellite observed aerosol's indirect effect so variable? *Geophys. Res. Lett.* 32, L15802 (2005).

Shi, N. (1996), Features of the East Asian winter monsoon intensity on multiple timescale in recent 40 years and their relation to climate, *J. Appl. Meteorol. Sci*., *7*(2), 175–182.

Sekiguchi, M., et al. (2003), A study of the direct and indirect effects of aerosols using global satellite data sets of aerosol and cloud parameters, *J. Geophys. Res.*, 108, 4699, doi:10.1029/2002JD003359.

Stenchikov, G., R. Dickerson, K. Pickering, W. Ellis Jr., B. Doddridge, S. Kondragunta, O. Poulida, J. Scala, and W.-K. Tao (1996), Stratosphere-troposphere exchange in a midlatitude mesoscale convective complex 2. Numerical simulations, *J. Geophys. Res.*, 101(D3), 6837–6851, doi:10.1029/95JD02468.

Stephens, G. L., and the CloudSat Science Team (2002), The CloudSat mission and the A-train. A new dimension of space observations of clouds and precipitation, Bull. Am. Meteorol. Soc., 83, 1771–1790, doi:10.1175/BAMS-83-12-1771.

Stevens, B., and G. Feingold (2009), Untangling aerosol effects on clouds and precipitation in a buffered system, *Nature*, 461, 607–613, doi:10.1038/nature08281.

Stokes, G. M., S. E. Schwartz (1994), The Atmospheric Radiation Measurement (ARM) program: Programmatic background and design of the cloud and radiation testbed. *Bull. Amer. Meteor. Soc*. 75, 1201-1221.

Stowe L. L., A. M. Ignatov, and R. R. Singh (1997), Development, validation and potential enhancements to the second generation operational aerosol product at NOAA/NESDIS, *J. Geophys. Res.*, *102*(D14), 16923–16934.

Stowe, L.L., H. Jacobowitz, G. Ohring, K.R. Knapp, and N.R. Nalli (2002), The Advanced Very High Resolution Radiometer (AVHRR) Pathfinder Atmosphere (PATMOS) climate dataset: Initial analyses and evaluations, *J. Clim.*, *15*, 1243-1260.

Sun, S. and B. Sun (1995), The relationship between the anomalous winter monsoon circulation over East Asia and summer drought/flooding in the Yangtze and Huaihe River valley, *Acta Meteorological Sinica*, *57*(4), 513–522.

Tanre´, D., Y. J. Kaufman, M. Herman, and S. Mattoo (1997), Remote sensing of aerosol properties over oceans using the MODIS/EOS spectral radiances, *J. Geophys. Res*., 102(D14), 16,971– 16,988.

Tao, W.-K., X. Li, A. Khain, T. Matsui, S. Lang, and J. Simpson (2007), Role of atmospheric aerosol concentration on deep convective precipitation: Cloud-resolving model simulations, *J. Geophys. Res*., 112, D24S18, doi:10.1029/2007JD008728.

Torres, O., P.K. Bhartia, J.R. Herman, A. Sinyuk, Paul Ginoux, and B. Holben (2002), A long-term record of aerosol optical depth from TOMS observations and comparison to AERONET measurements, *J. Atmos. Sci.*, 59, 398-413.

Twohy, C.H., et al. (2005), Evaluation of the aerosol indirect effect in marine stratocumulus clouds: droplet number, size, liquid water path, and radiative impact. *J. Geophys.Res*., 110, D08203, doi:10.1029/2004JD005116.

Twomey, S. A. (1959), The Nuclei of Natural Cloud Formation. Part II: The Supersaturation in Natural Clouds and the Variation of Cloud Droplet Concentrations, *Geofis. Pure Appl*., 43, 227–242.

Van den Heever, S. C., and W. R. Cotton (2007), Urban aerosol impacts on downwind convective storms, *J. Appl. Meteorol. Clim*., 46, 828-850.

Wang, B. (2006), The Asian Monsoon, *Springer/Praxis Publishing Co*., New York, 189.

Wang, B., Q. Bao, B. Hoskins, G. Wu, and Y. Liu (2008b), Tibetan Plateau warming and precipitation changes in East Asia, *Geophys. Res. Lett.*, *35*, L14702, DOI:10.1029/2008GL034330.

Wang, B., R. Wu, and X. Fu (2000), Pacific-East Asian teleconnection: How does ENSO affect East Asian climate?, *J. Climate*, *13*, 1517–1536.

Wang, C. (2005), A modeling study of the response of tropical deep convection to the increase of cloud condensation nuclei concentration: 1. Dynamics and microphysics, *J. Geophys. Res*., 110, D21211, doi:10.1029/2004JD005720.

Wang, M., K. D. Knobelspiesse, and C. R. McClain (2005), Study of the Sea-Viewing Wide Field-of-View Sensor (SeaWiFS) aerosol optical property data over ocean in combination with the ocean color products, *J. Geophys. Res.*, *110*, D10S06, doi:10.1029/2004JD004950.

Watanabe, M., and T. Nitta (1999), Decadal change in the atmospheric circulation and associated surface climate variations in the Northern Hemispheric winter, *J. Climate*, *12*, 494–510.

Winker, D. M., Pelon, J. R., and McCormick, M. P. (2003), The CALIPSO mission: spaceborne lidar for observation of aerosols and clouds, *Proc. SPIE*, 4893, 1–11.

Wu, B., and J. Wang (2002), Winter Arctic Oscillation, Siberian High and East Asian Winter Monsoon, *Geophys. Res. Lett.*, *29*(19), 1897, doi:10.1029/2002GL015373.

Wu, B., T. Zhou, and T. Li (2009), Seasonally evolving dominant interannual variability modes of East Asian Climate, *J. Climate*, *22*, 2992–3005.

Wurzler, S., T.G. Reisin, and Z. Levin (2000), Modifi cation of mineral dust particles by cloud processing and subsequent effects on drop size distributions. *J. Geophys. Res.*, 105(D4), 4501–4512.

Xia, X. A., H. B. Chen, P. C. Wang, X. M. Zong, and P. Gouloub (2005), Aerosol properties and their spatial and temporal variations over north China in spring 2001, *Tellus, Ser. B*, 57, 28–39.

Xia, X. A., H. B. Chen, P. C. Wang, W. X. Zhang, P. Goloub, B. Chatenet, T. F. Eck, and B. N. Holben (2006), Variation of column-integrated aerosol properties in a Chinese urban region, *J. Geophys. Res.*, *111*, D05204, doi:10.1029/2005JD006203.

Xia X., H. Chen, Z. Li, P. Wang, J. Wang (2007), Significant reduction of surface solar irradiance induced by aerosols in a suburban region in northeastern China, *J. Geophys. Res*., 112, D22S02, doi:10.1029/2006JD007562.

Xin, J., Y. Wang, Z. Li, P. Wang, W.-M. Hao, B.L. Nordgren, S. Wang, G. Liu, L. Wang, T. Wen, Y. Sun, Hubo (2007), Aerosol optical depth (AOD) and Ångström exponent of aerosols observed by the Chinese Sun Hazemeter Network from August 2004 to September 2005, *J. Geophys. Res*., 112, D05203, doi:10.1029/2006JD007075.

Xu, J.J., Q.G. Zhu, and T.H. Zhou (1999), Sudden and periodic changes of East Asia winter monsoon in the past century, *Q. J. Appl. Meteor*., *10*, 1–8.

Xu, M., C.-P. Chang, C. Fu, Y. Qi, A. Robock, D. Robinson, and H. Zhang (2006), Steady decline of east Asian monsoon winds, 1969–2000: Evidence from direct ground measurements of wind speed, *J. Geophys. Res.*, *111*, D24111, doi:10.1029/2006JD007337.

Xu, Q. (2001), Abrupt change of the mid-summer climate in central east China by the influence of atmospheric pollution, *Atmos. Environ*., 35, 5029–5040.

Yu, R., B. Wang, and T. Zhou (2004), Tropospheric cooling and summer monsoon weakening trend over East Asia, *Geophys. Res. Lett.*, *31*, L22212, DOI:10.1029/2004GL021270.

Yu, R., and T. Zhou (2007), Seasonality and three dimensional structure of the interdecadal change in East Asian monsoon, *J. Climate*, *20*, 5344–5355.

Yuan, T., Z. Li, R. Zhang, J. Fan (2008), Increase of cloud droplet size with aerosol optical depth: An observation and modeling study, *J. Geophy. Res.*, 113, D04201, doi: 10.1029/2007JD008632.

Zhang, G. Z., L. G. Bian, J. Z. Wang, Y. Q. Yang, W. Q. Yao, and X. D. Xu (2005), The boundary layer characteristics in the heavy fog formation process over Beijing and its adjacent areas, *SCIENCE IN CHINA SERIES D: EARTH SCIENCES*, *48*, 88-101.

Zhang, R., G. Li, J. Fan, D. L. Wu, and M. J. Molina (2007), Intensification of Pacific storm track linked to Asian pollution, *Proc. Natl. Acad. Sci.*, 104, 5295– 5299, doi:10.1073/pnas.0700618104.

Zhang, X.Y., H.Y. Lu, R. Arimoto, and S.L. Gong (2002), Atmospheric dust loadings and their relationship to rapid oscillations of the Asian winter monsoon climate: two 250-kyr loess records. *Earth Planet. Sci. Lett.*, 202, 637–643.

Zhang, Y., K. R. Sperber, and J. S. Boyle (1997), Climatology and interannual variation of the East Asia winter monsoon: Results from the 1979-95 NCEP/NCAR reanalysis, *Mon. Wea. Rev.*, *125*, 2605–2619.

Zhao, F., and Z. Li (2007), Estimation of aerosol single scattering albedo from solar direct spectral radiance and total broadband irradiances measured in China, *J. Geophys. Res.*, *112*, D22S03, doi:10.1029/2006JD007384.

Zhu, J., and S. Wang (2002), 80 yr oscillation of summer rainfall over North China and East Asian Summer Monsoon, *Geophys. Res. Lett.*, *14*, 1672, DOI:10.1029/2001GL013997.